Aqueous alteration in CM chondrites: Implications for early processes and environments of the CM parent bodies

Maeda, Makoto

(Degree)
博士（理学）

(Date of Degree)
2010-03-25

(Date of Publication)
2016-01-14

(Resource Type)
doctoral thesis

(Report Number)
甲4915

(URL)
https://hdl.handle.net/20.500.14094/D1004915

Doctoral Dissertation

Aqueous alteration in CM chondrites: Implications for early processes and environments of the CM parent bodies

January 2010

Graduate School of Science, Kobe University

Makoto Maeda

Contents

Preface

Among the various processes that have affected the evolution of solar system materials, it has been widely recognized that water played a significant role by modifying the primary chemical and mineralogical characteristics of pristine nebular material. In fact, most of primitive extraterrestrial material (e.g. chondrite and interplanetary dust particles) exhibit many evidences of aqueous alteration with various degrees. In particular, carbonaceous chondrites, which have been widely recognized as the most primitive material with an elemental composition probably similar to solar abundances, show abundant and strong evidences of aqueous alteration (e.g. McSween, 1979; Tomeoka and Buseck, 1985; Zolensky et al., 1993; Brearley, 2005). Even thermally metamorphosed ordinary chondrites, which were extremely dry meteorites, show evidence that they have been affected by water. In addition to direct observations of meteorites, spectral analyses using astronomical telescopes also support the existence of hydrous minerals on various asteroids surfaces, which would be formed by aqueous alteration (e.g., Vilas and Gaffey 1989; Vilas et al., 1993, 1994).

These observations show that aqueous alteration has been extremely common and important process in the early solar systems. A detailed study of aqueous altered textures (commonly which appear in a micrometer scale) in carbonaceous chondrite essentially give constraints on when, where and how aqueous alteration occurred, thereby providing a clue to reveal the process of material evolution in the early solar system. A number of previous workers (e.g., DuFresne and Anders, 1962; Kerridge et al., 1979; McSween., 1979; Tomeoka and Buseck, 1985, 1988; Metzler et al., 1992; Brearley., 1993; Weisberg et al., 1993, 1995; Noguchi., 1995; Browning et al., 1996; Bischoff, 1998; Grossman et al., 2000, 2002; Hanowski and Brearley, 2001; Jones and

Brearley, 2006; Chizmadia and Brearley, 2008; Maeda et al., 2009) discussed the mechanism, condition and location of aqueous alteration in the primitive meteorites. However, most of these studies focused on the unique chondrite, and seem to lack systematic and thorough observations of a series of chondrites.

CM chondrites are the most abundant group of carbonaceous chondrite. They are characterized by their constituent texture (chondrule, chondrule rim and matrix) having been partially to completely replaced by hydrous phyllosilicates. The degree of aqueous alteration experienced by CM chondrites varies widely (McSween, 1979; Browning et al., 1996). CM chondrites are, therefore, the best samples to reveal process of aqueous alteration. In this paper, I will report and discuss aqueous alteration process from extensive survey of many CM chondrites.

Part I

General petrological and mineralogical characteristics in the seven CM carbonaceous chondrites

Chapter 1

Introduction

Where did the aqueous alteration occur?

In order to understand chemical and physical evolution of the early solar materials, aqueous alteration is one of the most important issues. A number of previous workers (e.g., Tomeoka and Buseck, 1985; Metzler et al., 1992; Browning et al., 1996; Bischoff, 1998; Hanowski and Brearley, 2001; Jones and Brearley, 2006; Chizmadia and Brearley, 2008) discussed the mechanism, condition and location of aqueous alteration in the CM chondrites. However, the entire picture of aqueous alteration in CM chondrites is still left unsettled because CM chondrites group shows wide mineralogical and petrological variations including brecciation, terrestrial weathering, aqueous alteration so on. The most significant issue of aqueous alteration in the CM chondrites is how to pick out only the evidence of aqueous alteration from a complex texture. In fact, many previous workers (e.g. McSween, 1979; Browning et al., 1996, Rubin et al., 2007) proposed that various parameters for determining the degree of aqueous alteration in CM chondrites.

In generally, meteorites have experienced aqueous alteration on different conditions (e.g. temperature, pressure, oxidized condition, duration time). Also, it is likely that the influences of aqueous alteration are different by the components and textures of the meteorites. Thus, in this part (Part I), I investigated each component (e.g. chondrule, chondrule rim and matrix) of CM chondrites in detail. Moreover, I estimated how change was provided to original textures in the CM chondrites by aqueous alteration.

In the early solar system, it is widely believed that many CM chondrites have

experienced extensive brecciation on their parent body (bodies). As a result of the brecciation, CM chondrites commonly consist of various lithologies, which have experienced different degrees of aqueous alteration on different places. Moreover, primitive and significant textures (e.g. chondrule rims) may have been lost by brecciation in the most CM chondrites. Nonetheless, many previous workers have not paid attention to whether the sample has experienced brecciation or not. An investigation of CM chondrites without brecciation is the most useful to reveal process of aqueous alteration. Moreover, even if a CM chondrite has experienced the brecciation, a careful distinction of the lithologies would make it possible to examine an evidence of aqueous alteration in each lithology. In the present part, seven CM chondrites, Murchison, Murray, Mighei, QUE97990, Y791198, Cold Bokkeveld and Nogoya have been studied. Although the former three chondrites (Murchison, Murray and Mighei) have obviously experienced brecciation, the three meteorites have been investigated in order to counterpoint a brecciated texture. The latter two (Cold Bokkeveld and Nogoya) chondrites also show apparent brecciation(s), but these contain relatively large regions with single lithology. Through an extensive survey of above CM chondrites, I will discuss a systematic effect of aqueous alteration in CM chondrites.

If we elucidate the effect of aqueous alteration on mineralogical textures, a following question will justly arise: where did the aqueous alteration occur? Generally, extensive aqueous alteration on the parent bodies probably overwrote or erased the earlier alteration history. Therefore, it is still controversial whether the aqueous alteration occurred in the solar nebula (e.g., Metzler et al., 1992; Bischoff, 1998) or on the meteorite parent bodies (e.g., Browning et al., 1996; Chizmadia and Brearley, 2008). To unravel the earliest alteration process, it is indispensable to investigate meteorites

that have experienced aqueous alteration as recognizably little as possible. The Yamato 791198 (Y791198) CM chondrite has been described by Metzler et al. (1992) as "a primary accretionary rock, obviously unaltered by secondary parent body processes such as aqueous alteration or brecciation." Since then, Y791198 has been recognized as the most primitive CM chondrite. Recently, however, Rubin et al. (2007) studied many CM chondrites, including Y791198, and estimated that the degree of aqueous alteration of a more recently described CM chondrite—Queen Alexandra Range 97990 (QUE97990) is lower than that of Y791198 based on Fe-Ni metal abundance. Fortunately, QUE97990 has already been reported as non-brecciation CM chondrites (e.g. Rubin et al., 2008). If this is the case, there is a possibility that QUE97990 gives us new insight into the early aqueous alteration process of the CM chondrites.

Chapter 2

2.1 Samples

Even if a chondrite shows no evidence of brecciation, it must be ultimately inhomogeneous at least in micro-meter scale. It is, therefore, important to establish criteria whether the observed region consist of single lithology or not. In the present study, objects satisfying the following three criteria regard as a single lithology.

1. The value of [number of chondrules surrounded rims / number of total chondrules] is more than 0.8.
2. The boundaries between chondrules and rims are clear.
3. Most of (> 90%) PCPs (described in detail in chapter 3.1.3) is more than 10 μm in size.

In order to find the sample (or regions in that) having a single lithology according to above requirements, seven CM chondrites (Murchison, Murray, Mighei, QUE97990, Yamato 791198, Cold Bokkeveld and Nogoya) were observed. The samples used for this study are two polished thin sections of Murchison (Figs. 2-1a, b), a polished thin section of Murray (Fig. 2-1c) and Mighei (Fig. 2-1d), a polished thin section of QUE97990 (Fig. 2-1e) from NASA, two polished thin sections of Yamato 791198 (Fig.2-1f, g) from NIPR and Cold Bokkeveld (Figs. 2-1h, i), a polished thin section of Nogoya (Fig. 2-1j).

2.2 METHODS

In this study, I studied the samples using a scanning electron microscope (SEM)

equipped with an energy-dispersive X-ray spectrometer (EDS), an electron probe microanalyzer (EPMA) equipped with wavelength-dispersive X-ray spectrometers (WDS), transmission electron microscope (TEM) (JEOL JEM-2010) equipped with an energy dispersive X-ray spectrometer (EDS) and synchrotron X-ray diffraction (SR-XRD).

SEM-EDS and EPMA-WDS

The micro-textural observation and semi-quantitative chemical analysis were carried out using an SEM-EDS system (JEOL JSM-6480LVII). For most observations, backscattered electron (BSE) imaging was mainly used. EDS chemical analyses were obtained by a ZAF matrix correction routine at 15 KV and a beam current 0.6 nA. For the quantitative analyses, EPMA-WDS system (JEOL JXA-8900) were performed at 15 KV and 12 nA in which data correction was made by the a Bence-Albee method. Well-characterized natural and synthetic minerals were used as chemical standards as follows: albite (Na), periclase (Mg), corundum (Al), quartz (Si), sanidine (K), fluorite (Ca), rutile (Ti), hematite (Fe), eskolaite (Cr), mangonosite (Mn), nickel oxide (NiO), potassium titanium phosphate (P) and pyrite (S).

TEM

Micro-structural analyses and electron diffraction were undertaken using a TEM-EDS system (JEOL JEM-2010 and Noran System SIX) equipped with a LAB6 cathode operating at 200 KV. TEM specimens were prepared from petrographic thin sections by further polishing on both sides by Ar ion milling. TEM images were collected by imaging plate (IP, Fuji FDL-UR-V).

SR-XRD

SR-XRD measurements were carried out on beamline BL10XU at SPring-8 in

Hyogo, Japan. The incident X-ray beam was monochromatized to a wavelength of 0.4153 Å and collimated to 20 μm in diameter; the diffracted beam was defected using a flat imaging plate (IP, Rigaku R-AXIS IV). The two-dimensional X-ray diffraction patterns were converted to the conventional 2theta-intensity profiles.

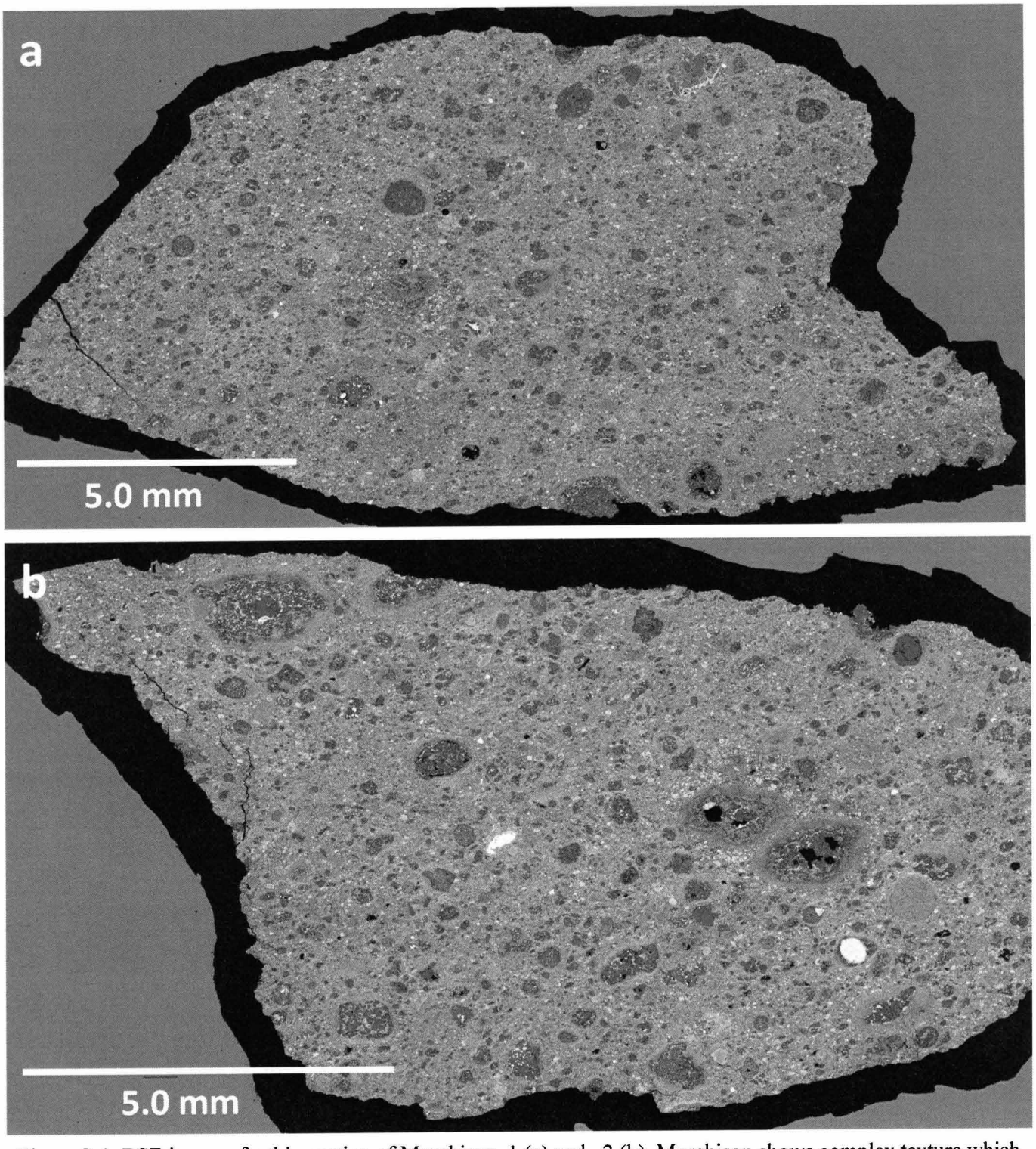

Figure 2-1. BSE image of a thin section of Murchison_1 (a) and _2 (b). Murchison shows complex texture which coexist brecciated and unbrecciated regions with less than 100 in order. Most of the regions of Murchison has experienced brecciation.

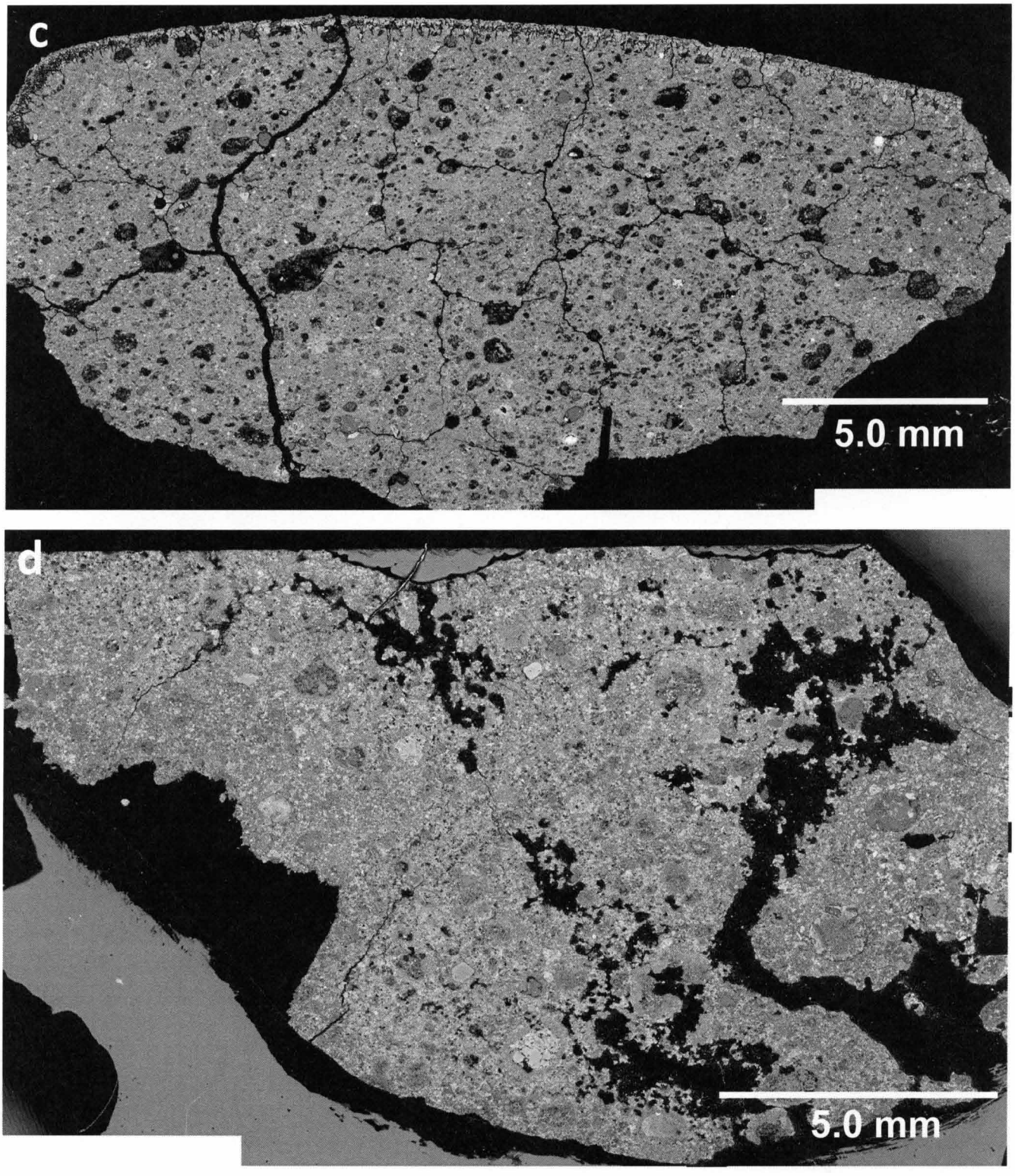

Figure 2-1. BSE image of thin sections of Murray (c) and Mighei (d). Murray and Mighei show complex texture that coexist brecciated and unbrecciated regions with less than 100 μm in order. Most of the regions in Murray and Mighei has experienced brecciation.

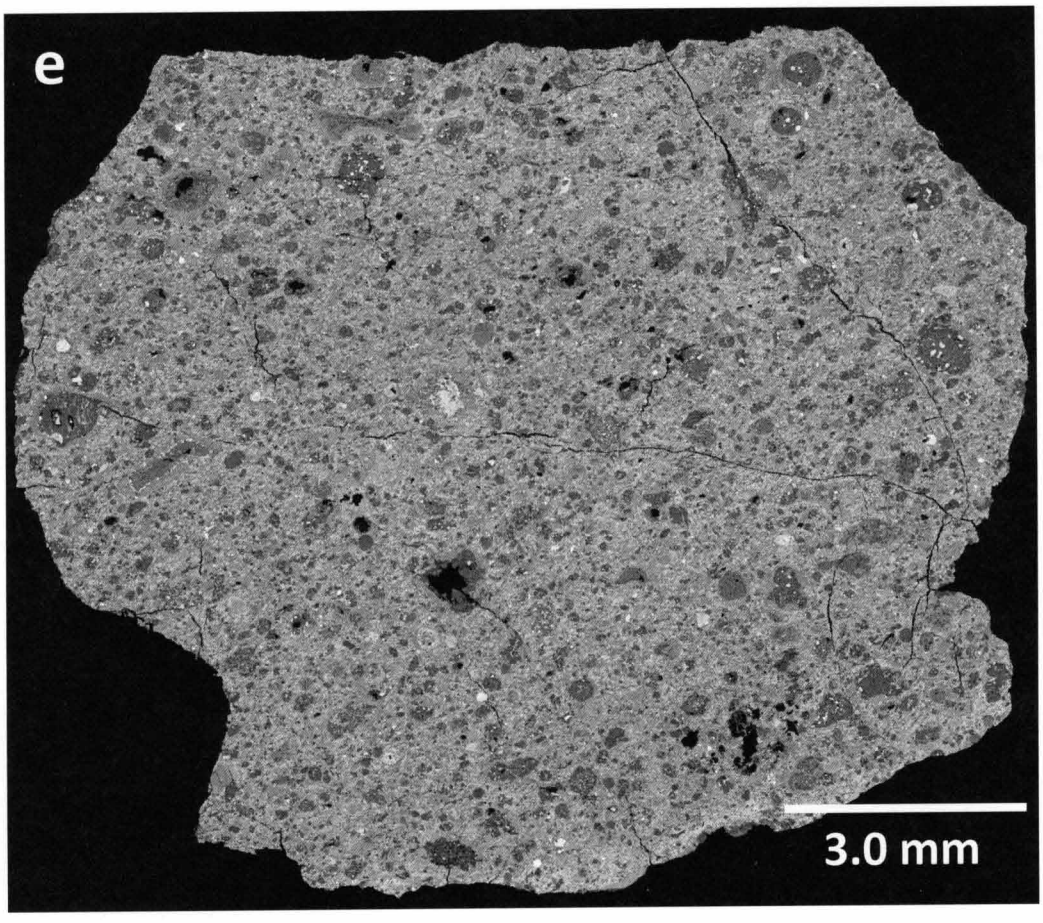

Figure 2-1 (e) BSE image of a thin section of QUE97990. QUE97990 is an unbrecciated CM chondrite.

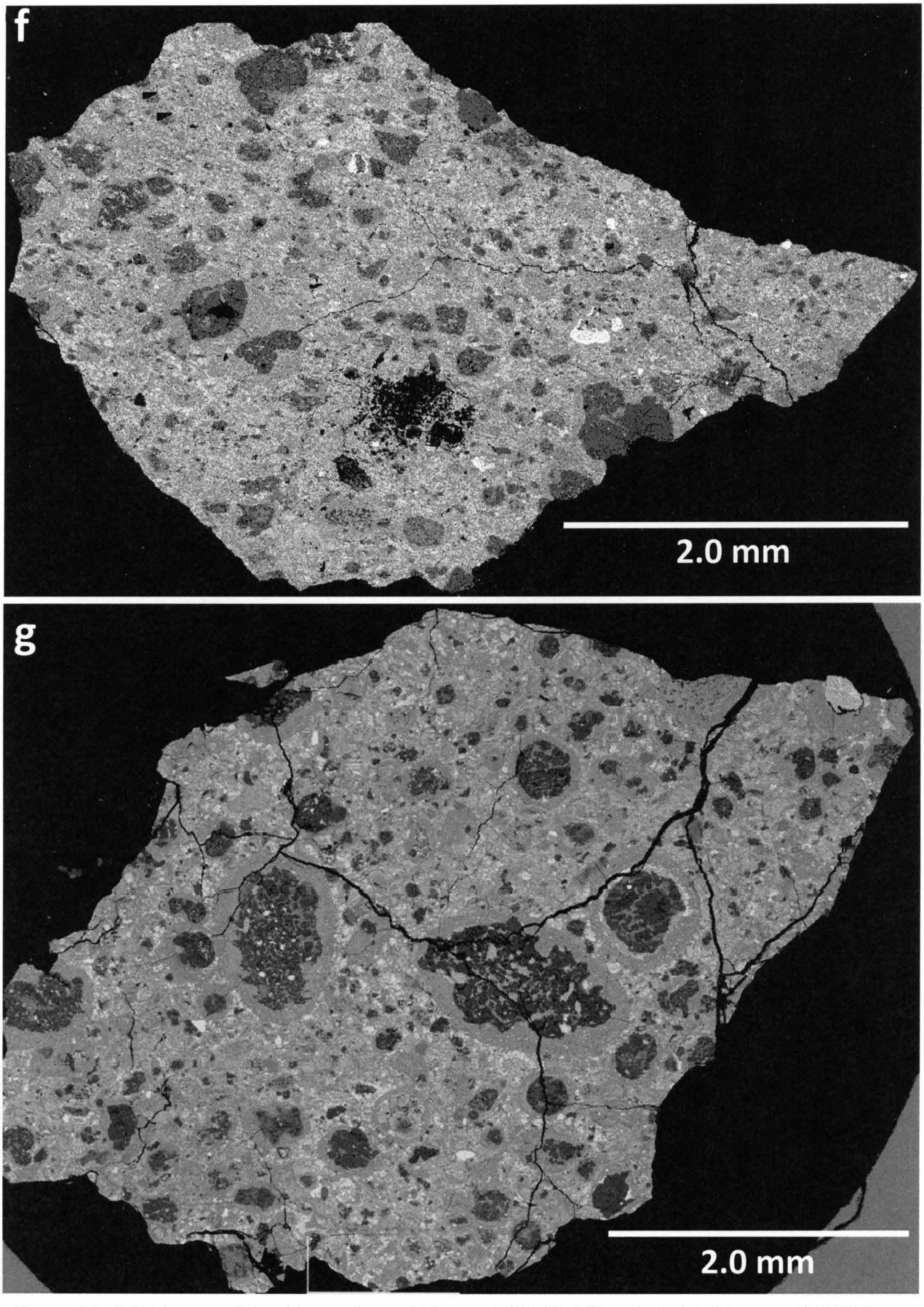

Figure 2-1. BSE image of the thin sections of Yamato 791198_1(f) and _2 (g). Yamato 791198 is an unbrecciated CM chondrite.

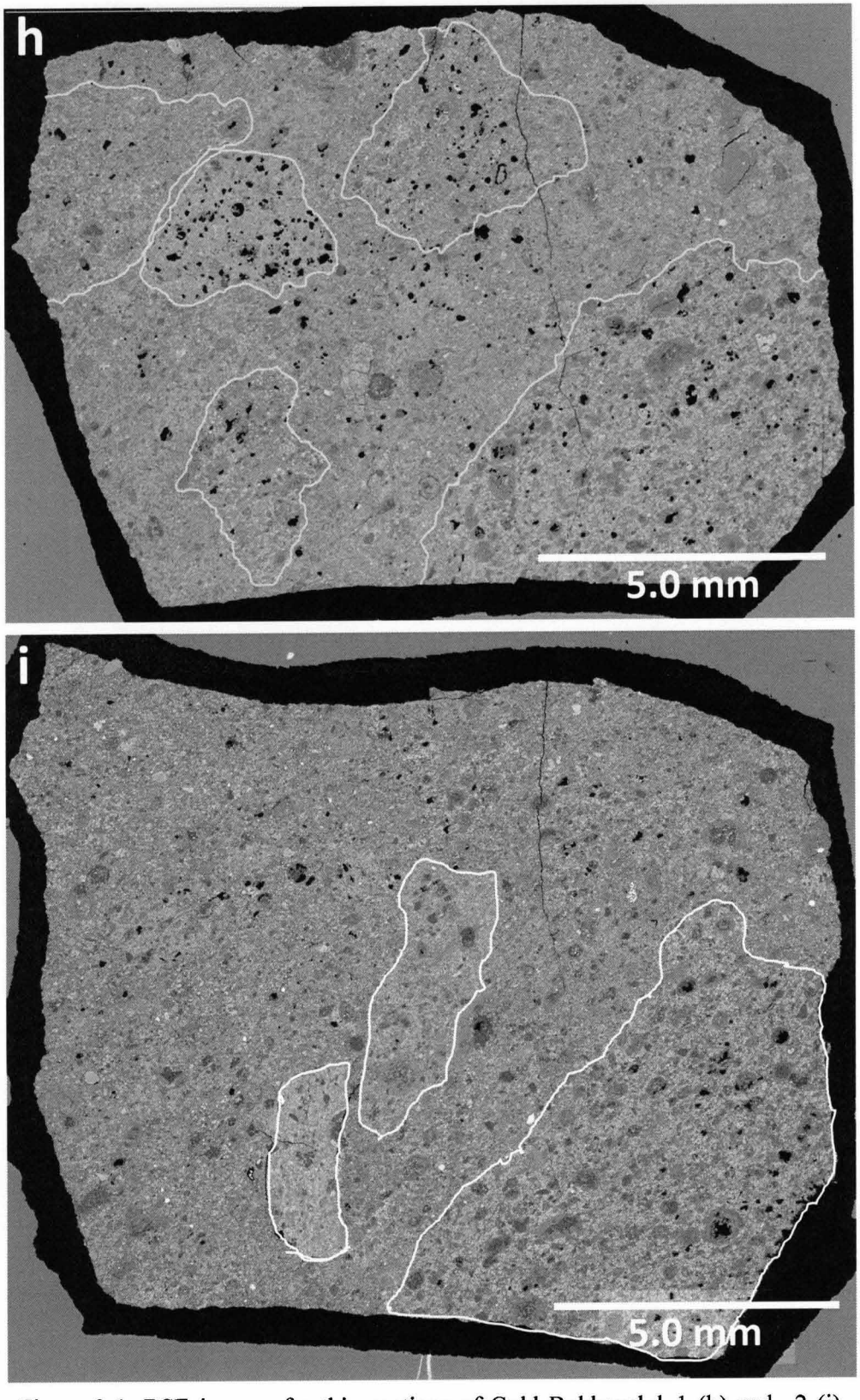

Figure 2-1. BSE image of a thin sections of Cold Bokkevekd_1 (h) and _2 (i). Cold Bokkeveld consists of brecciated and unbrecciated regions. The regions, which are surrounded by white line, are non-brecciation regions. I studied only the non-brecciation regions.

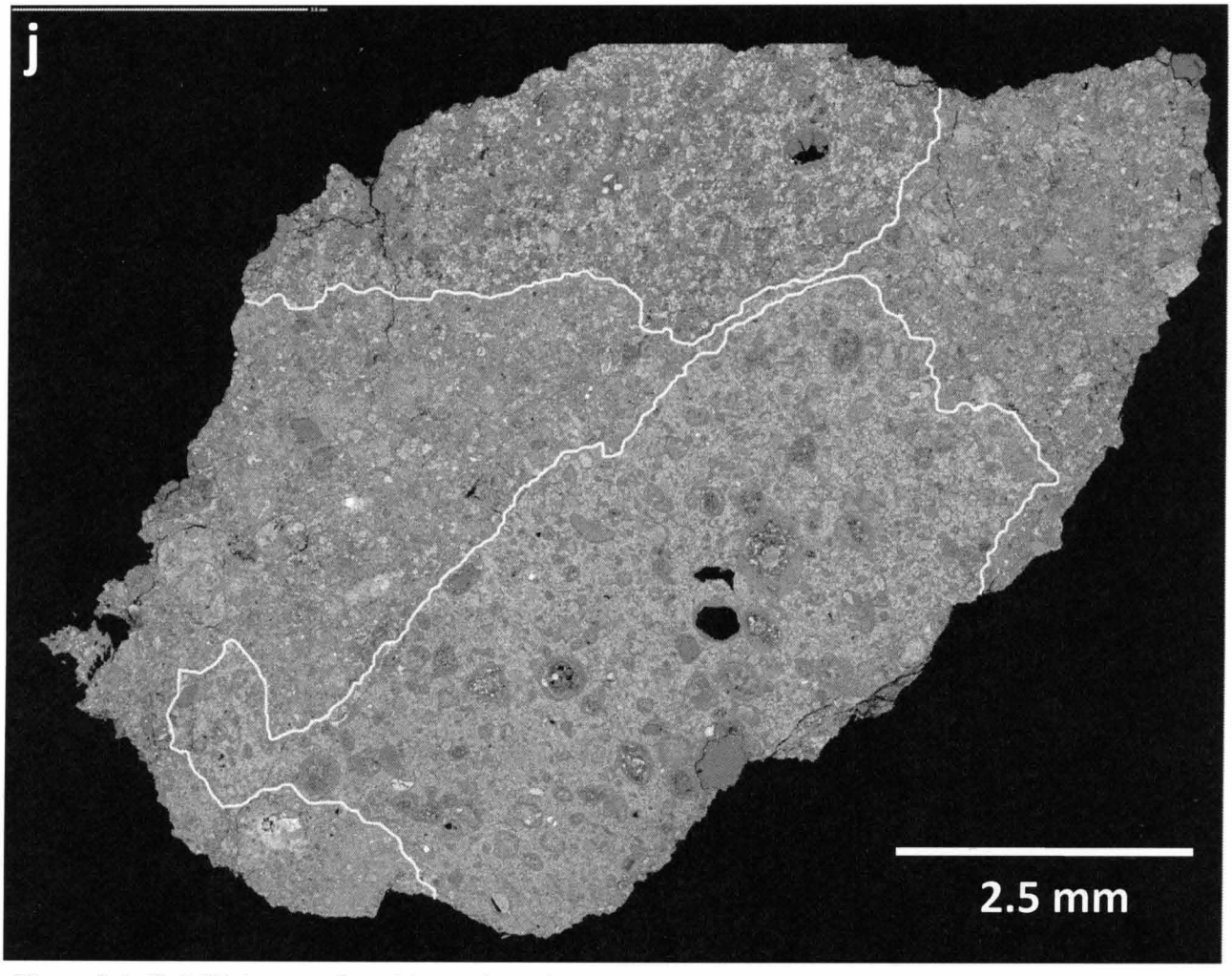

Figure 2-1 (j) BSE image of a thin section of Nogoya. Nogoya consist of brecciated and unbrecciated regions. The regions, which are surround by white line, are non brecciated regions.

Chapter3

Results: General petrological and mineralogical characteristics in seven CM carbonaceous chondrites

3.1. General petrology

All studied meteorites consists of chondrules, chondrule rims, CAIs (Ca-Al-rich inclusion), AOAs (amoeboid olivine aggregates), fine-grained aggregate (*Note:* this term means the aggregate of fine-grained minerals with diameter in less than several μm irrespective of mineral species) and matrices (Figs. 3-1a-c). Total abundance of CAIs, AOAs and fine grained aggregate in all studied meteorites are less than 1 vol %. Cold Bokkeveld and Nogoya mainly consist of two lithologies (host rock and large clasts) (Figs. 3-2a-d). As shown in Table 1, modal abundance (vol %) of major components in all studied meteorites appears to vary a great deal depending on degree of aqueous alteration and extent of brecciation (e.g. chondrule = 4 to 25 vol %). Contents of chondrules and rims in the host rocks of Cold Bokkeveld and Nogoya are smaller than that of large clasts (Table 1). Moreover, most of (> 80 %) chondrules in the host rocks of Cold Bokkeveld and Nogoya are not surrounded by fine-grained rims (Figs. 3-2a-d). These results suggest that the host rock of Cold Bokkeveld and Nogoya have experienced extensively brecciation. In order to investigate non-brecciated meteorites or regions, I focusing on large clasts in Cold Bokkeveld and Nogoya rather than the host rocks.

3.2 Chondrules

Chondrules in all studied meteorites mainly consist of phenocrysts of olivine and enstatite, with minor amount of diopside, and mesostases. Most of chondrules (> 90 %) in Murchison, Murray, Mighei, QUE97990 and Y791198 include opaque nodules (Murchison, Murray, Mighei: 30–200 μm in diameter; QUE97990, Y791198: 10—150 μm in diameter) that consist of Fe-Ni metal (both kamacite and taenite) and troilite, most of which have been partially replaced by tochilinite and cronstedtite (Figs. 3-3a-d). About a half of chondrules in Cold Bokkeveld (16/34) and Nogoya (19/36) include opaque nodules (10—100 μm in diameter), most of (> 90 %) which have been commonly replaced by tochilinite and cronstedtite (Figs. 3-3e-f). Chondrules in all studied meteorites are sub-rounded or irregular shape with 100-900 μm in diameter (Table 2). Average diameter of chondrules in Murray (322 μm) and Mighei (308 μm) are larger than that of the other studied meteorites (Murchison is 194 μm, QUE97990 is 205 μm, Y791198 is 193 μm, Cold Bokkeveld is 214 μm, Nogoya is 158 μm) (Table 2). Figs. 3-4a-g shows distribution of diameter of chondrules in the studied meteorites. About 50 % of chondrules in Murchison, QUE97990, Y791198 and Cold Bokkeveld ranges in diameter from 100 to 200 μm (Figs. 3-4a-g).

I investigated phenocrysts in chondrules with a diameter of more than 100 μm (Number of chondrules; Murchison = 36, Murray = 57, Mighei = 18, QUE97990 = 34, Y791198 = 39, Cold Bokkeveld = 34, Nogoya = 36). The phenocrysts of olivine and enstatite in Murchison, Mighei, Murray, QUE97990 and Y791198 show no evidence of replacement by phyllosilicates (Figs. 3-5a-d). It has been reported that in many other CM chondrites, the enstatite phenocrysts have been partially replaced by phyllosilicates

(e.g., Hanowski and Brearley, 2001; Rubin et al., 2007). Thus the observation suggests that the degrees of aqueous alteration of these meteorites are relatively low in the CM chondrite group. In contrast, the phenocrysts in Cold Bokkeveld (13/34) and Nogoya (22/36) show evidence of altered by aqueous alteration (Figs. 3-6a, b). These results show that a degree of aqueous alteration in Cold Bokkeveld and Nogoya is higher than that of the other studied meteorites (Figs.3-6c, d). Moreover, pseudomorphs are found in the chondrules in Cold Bokkeveld and Nogoya. In Cold Bokkeveld, most of (> 80 %) pseudomorphs show round shape (Figs. 3-6a, b). The size and shape of the pseudomorphs are similar to that of opaque nodules in the chondrules. Moreover, Fe-Ni metal is rarely survived inside the pseudomorphs, while minor of pseudomorphs shows a shape of short prism (Fig. 3-6b). These results suggest that round shaped pseudomorphs were formed by altered opaque nodule. On the other hand, pseudomorphs in Nogoya show shape of short prismatic (Figs. 3-6c, d). Moreover, Ca-carbonate and Ca-sulfate as phenocrysts are found in the chondrules of Nogoya (Fig. 3-7b).

3.3 Chondrule mesostases

Chondrule mesostases have been largely altered to Mg-Fe serpentine (Figs. 3-8a, b). Backscattered image of the mesostases in QUE97990, Y791198 and Cold Bokkeveld show a significant contrast of two regions; an iron-rich region (FeO = about 15-25 wt%) and an iron-poor region (FeO = about 25-35 wt%) (Figs. 3-9a-c). Fe-rich region and Fe-poor region mainly consist of Mg-Fe serpentine. The boundary between Fe-rich and Fe-poor regions is clearer than that of Y791198 and Cold Bokkeveld (Figs. 3-9a-c).

These results imply that chemical compositions of the entire mesostases in QUE97990 are more heterogeneous than that of the other studied meteorites. Table 3 shows chemical compositions of the mesostases. The contents of Al_2O_3 in the mesostases of Murchison, Murray, Mighei, QUE97990 and Y791198 are more abundant than that of Cold Bokkeveld and Nogoya. Figs. 3-10a-g show distribution of FeO contents in the mesostases. The FeO contents of the mesostases in Murchison, Murray and QUE97990 are relatively heterogeneous, while those of Mighei, Y791198, Cold Bokkeveld and Nogoya are relatively homogeneous in at least 10 μm scale.

The mesostases in QUE97990 shows unique texture which is not found in the other studied meteorites. 14 (~ 41 %) of the 34 chondrule mesostases studied contain dense arrays of parallel, thin lath-shaped crystallites (~ 1 μm in width) of diopside (Figs. 3-11a, b), which are primary quenched products formed during chondrule formation.

3.4 Chondrule margins

I found that the chondrules in all studied meteorites often show a depression texture on their surfaces (Figs. 3-12, 13, 14, 15). I refer to these depressions as embayments. Especially, embayments in QUE97990 show unique textures. 25 (~ 73 %) of the 34 chondrules in QUE97990 studied show topographic depressions on their surfaces (Figs. 3-13a-c and 3-14a-c). The size and shape of the embayments are comparable to those of opaque nodules contained within the chondrules (see Figs. 3-13a and 3-14a for example). The inside of the embayments commonly consists of one to all of three materials: (1) Fe-Ni metal, (2) tochilinite-rich, and (3) cronstedtite-rich (Figs. 3-13b, c, 3-14b, c, and Table 4); the identification of materials (2) and (3) is based on

their compositional similarities to tochilinite and cronstedtite, respectively (see Table 2 in Tomeoka and Buseck (1985)). The tochilinite-rich material is distinctly richer in Fe, Ni and S, and the cronstedtite-rich material is richer in Fe than the rims (Table 4); thus these materials appear brighter than the rims in BSE images. In many embayments, Fe-Ni metal commonly occurs at the bottom and the tochilinite-rich material and the cronstedtite-rich material occur toward the outside, thus exhibiting a zonal texture (Figs. 3-13b, c). Figures 3-14b and 3-14c show that the cronstedtite-rich material occurs in not only the inside but also the outside of an embayment.

In the other studied meteorites, most of (> 80 %) chondrules also show embayments on their surfaces (Figs. 3-12a-f). However, Fe-Ni metal, tochilinite and cronstedtite are rare, and the inside of the embayments is largely composed of the Mg-Fe serpentine-rich material that is indistinguishable from the surrounding rims (Table 4). These characteristics of embayments on their surfaces are different from that in QUE97990.

3.5 Chondrule rims

3.5.1 Thickness and shape

In Murchison, Murray and Mighei, chondrule with fine-grained rims is rare. Only relatively large chondrules in the three meteorites (> 200 μm in diameter) are surrounded by fine-grained rims which are typically 40 to 120 μm in thickness (Figs. 3-16a-g), although the boundaries between the rims and matrices are unclear (Fig. 3-17a). These characteristics of the three meteorites suggest that they have experienced extensive brecciations. In contrast, most of (> 90 %) chondrules in QUE97990,

Y791198, Cold Bokkeveld and Nogoya are surrounded by-fine grained rims which are typically 20 to 120 μm in thickness (Figs. 3-17c, e). Moreover, most of boundaries between the rims and matrices are clear. A part of the rims in Nogoya shows boundaries between chondrules and the rims which are unclear (Figs. 3-18a, b). These results suggest that these meteorites (including the clasts) are unbrecciated. Thickness of the rims in QUE97990, Y791198, Cold Bokkeveld (large clasts) and Nogoya (large clasts) increases with increasing diameter of the chondrules. The chondrules with 100 to 200 in diameter are surrounded by the rims with about 20 μm in thickness, while the chondrules with 200 to 300μm is surrounded by about 30 μm thick rims.

3.5.2 Major constituent mineral

The rims in all studied meteorites mainly consist of Mg-Fe serpentine with minor amount of Ca-carbonate, various anhydrous silicates and opaque minerals (Figs. 3-17b, d, f). Minor amounts of tochilinite and fine grains (< 5 μm in size) of olivine, enstatite, diopside, Ca-carbonate, troilite, pentlandite, and Fe-Ni metal are found in the rims in Murchison, Murray, Mighei, QUE97990 and Y791198 (Table 5, Table 6, Figs 3-17d, f). Previous workers (e.g., Metzler et al., 1992; Hanowski and Brearley, 2001) reported that Fe-Ni metal is rare in rims of CM chondrites because of its high susceptibly to aqueous alteration. However, Fe-Ni metal is common in the rims of the above five meteorites which suggests that degrees of aqueous alteration of Murchison, Murray, Mighei, Y791198 and QUE97990 are relatively low in the CM group. Fig. 3-19 shows the modal abundance of opaque minerals including Fe-Ni metal in the rims. The contents of Fe-Ni metal in the rims in QUE97990 are more abundant than that of the other studied meteorites. This result suggests that a degree of aqueous alteration in QUE97990 is

lower than that of the other studied meteorites. The contents of Fe-sulfide in Cold Bokkeveld and Nogoya are less abundant than that of the other studied meteorites. In all studied meteorites, tochilinite commonly occurs as PCPs (Poorly-characterized-phase) which are intergrowth, on a submicron scale, of serpentine and tochilinite. PCPs are typically less than 10 μm diameter.

Fig. 3-20 shows the abundance of anhydrous silicates minerals in the rims. Previous workers (e.g., Hanowski and Brearley, 2001) reported that in anhydrous silicates composing CM chondrite, enstatite is relatively susceptible to aqueous alteration. The enstatite in the rims in Murray and QUE97990 are more abundant than that of Murchison, Mighei, Y791198, Cold Bokkeveld and Nogoya. In Cold Bokkeveld and Nogoya, moreover, Fe-Ni metal and anhydrous silicates are not found in the rims. These results suggest that aqueous alteration increases as following order; Murray, QUE97990 < Murchison, Mighei, Y791198 < Cold Bokkeveld, Nogoya. As shown in table 5, the rims include minor minerals of various species (e.g. magnetite, chromite, barringerite). Table 7 shows chemical compositions of the minor minerals.

3.5.3 Chemical compositions

Table 8 shows chemical compositions of the rims. The contents of FeO and S in Murchison, Murray, QUE97990 and Y791198 are more abundant than that of Cold Bokkeveld and Nogoya. This result suggests that contents of Fe-sulfide in Cold Bokkeveld and Nogoya are less abundant than that of the other studied meteorites.

3.6 Matrix

3.6.1 Mineralogy

The matrices in the studied meteorites mainly consist of Mg-Fe serpentine and PCPs, Ca-carbonate with minor amount of various anhydrous silicates and Fe-rich minerals. Minor amounts of fine grains (< 5 μm in size) of olivine, enstatite, diopside, troilite, pentlandite, and Fe-Ni metal are found in the matrices of all studied meteorites expect for Cold Bokkeveld and Nogoya (Table 5, Table 6, Figs. 3-21a-f).The existence of Fe-Ni metal and enstatite, which are susceptible to aqueous alteration, suggests that degrees of aqueous alteration of these meteorites are relatively low in the studied meteorites (Figs. 3-22, 3-23). In contrast, Fe-Ni metal and anhydrous silicates are not found in the rims in Cold Bokkeveld and Nogoya (Figs. 3-22, 3-23). This result shows that degrees of aqueous alteration in Cold Bokkeveld and Nogoya are relatively high in the studied meteorites.

In the all studied meteorites, PCPs commonly occurs in the matrices. PCPs in Murchison, Murray and Mighei are typically less than 10 μm in diameter (Fig. 3-21b). In contrast, PCPs in QUE97990, Y791198, Cold Bokkeveld and Nogoya are typically 20 to 150 μm in diameter (Figs 3-21d, f). These results suggest that Murchison, Murray and Mighei have experienced extensively brecciation. Moreover, contents of the PCPs in QUE97990, Y791198, Cold Bokkeveld and Nogoya are more abundant than that of Murchison, Murray and Mighei (Figs. 3-21a, c, f). PCPs in QUE97990 and Y791198 show massive texture (Figs. 3-24a, b). On the other hand, PCPs in Cold Bokkeveld and Nogoya show fibrous texture (Fig. 3-24c). Ca-carbonate (calcite) in QUE97990, Y791198, Cold Bokkeveld and Nogoya) is surrounded by PCPs (Figs. 3-25a-c). As shown in table 5, the rims include minor minerals of various species (e.g. magnetite, chromite, barringerite). Table 7 shows chemical compositions of the minor minerals.

3.6.2 Chemical compositions

Table 9 shows chemical compositions of the serpentine in the matrices of the studied meteorites. The contents of FeO in Murchison, Murray, QUE97990 and Y791198 are more abundant than that of Mighei, Cold Bokkeveld and Nogoya. This result is consistent with that of the rims. Moreover, the chemical compositions of serpentine in each studied meteorite are similar to that of the rims in each studied meteorite.

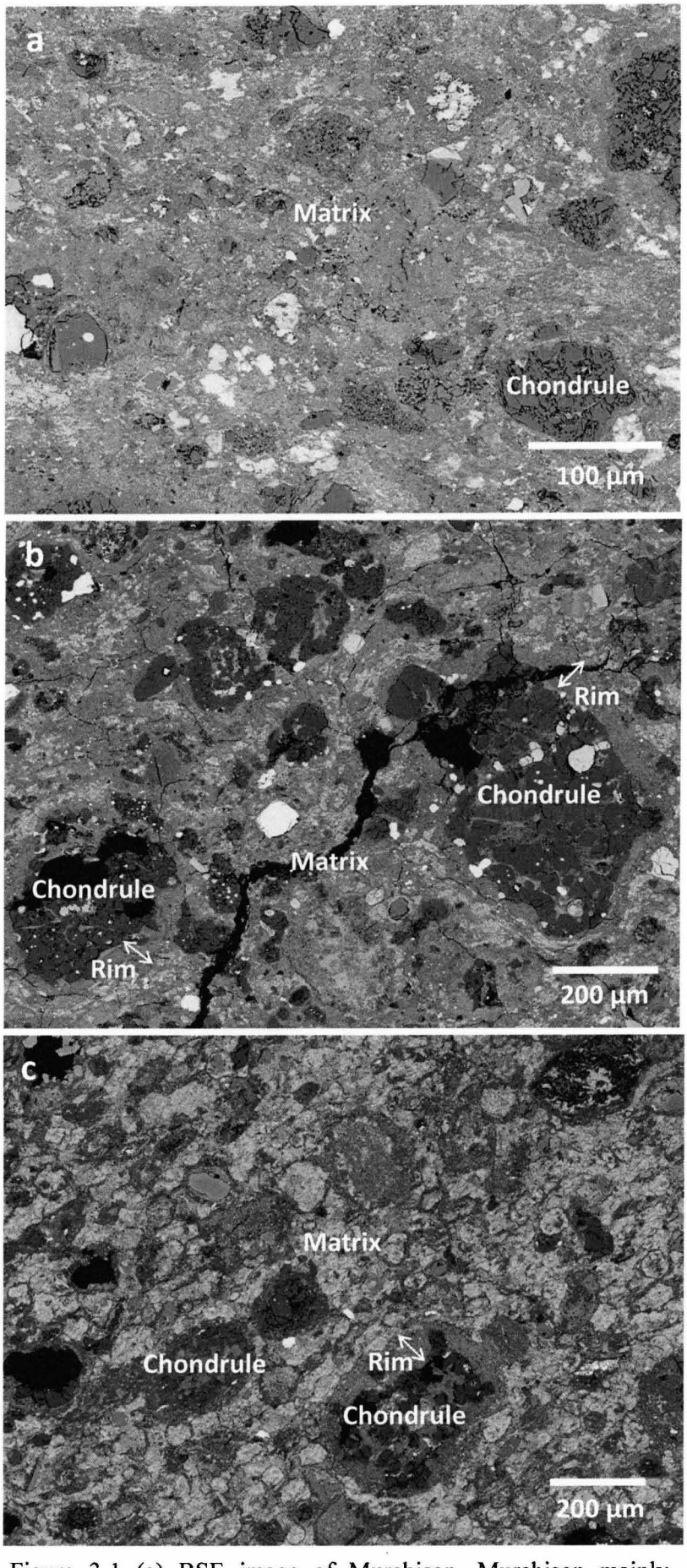

Figure 3-1 (a) BSE image of Murchison. Murchison mainly consists of chondrules and matrix. (b) (c) BSE images of QUE97990 and Cold Bokkeveld. These meteorites mainly consist of chondrules, chondrule rims and matrices.

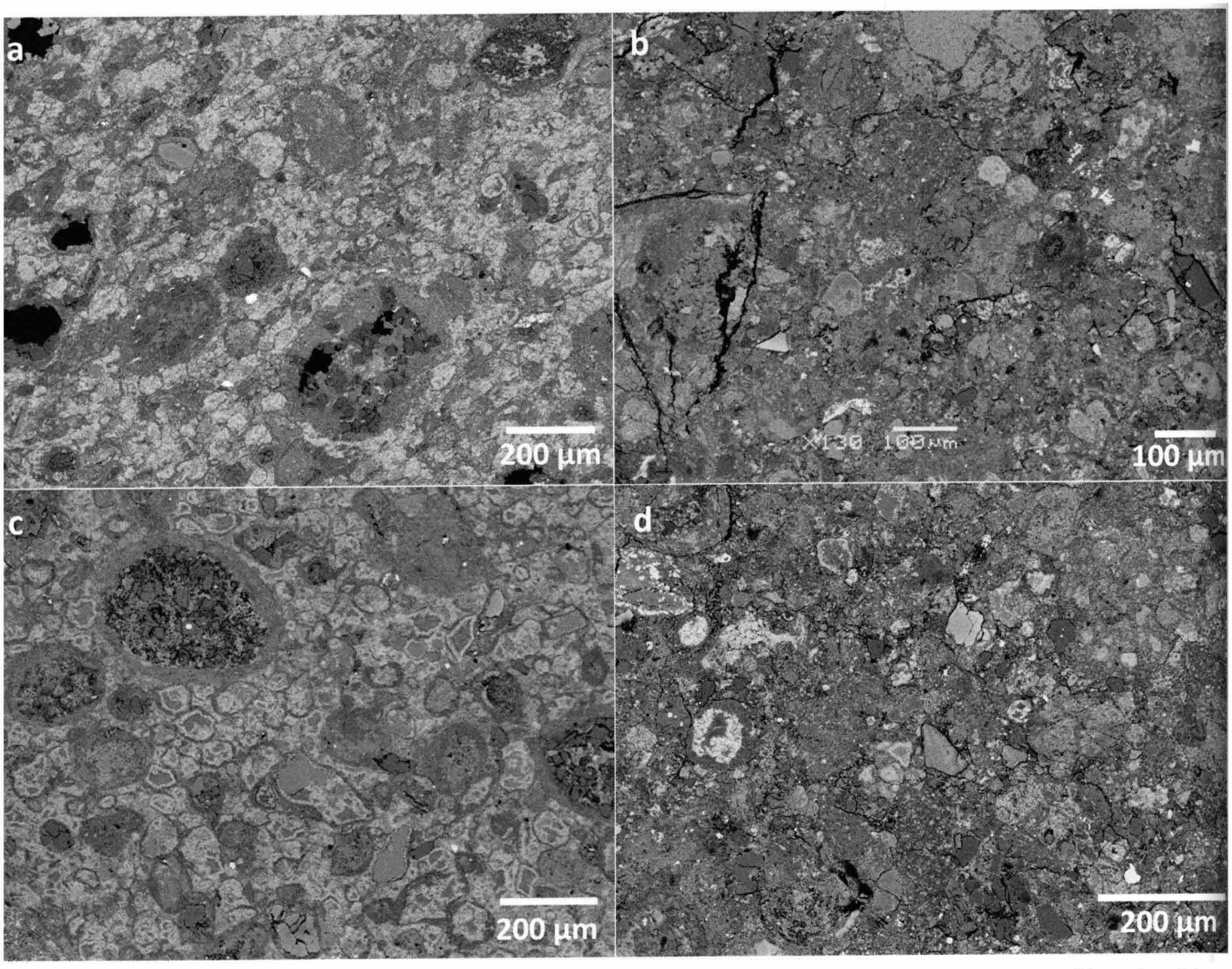

Figure 3-2 BSE images of Cold Bokkeveld (a, b) and Nogoya (c, d). Cold Bokkeveld and Nogoya consist of brecciated (a, c) regions and unbrecciated (b, d) regions.

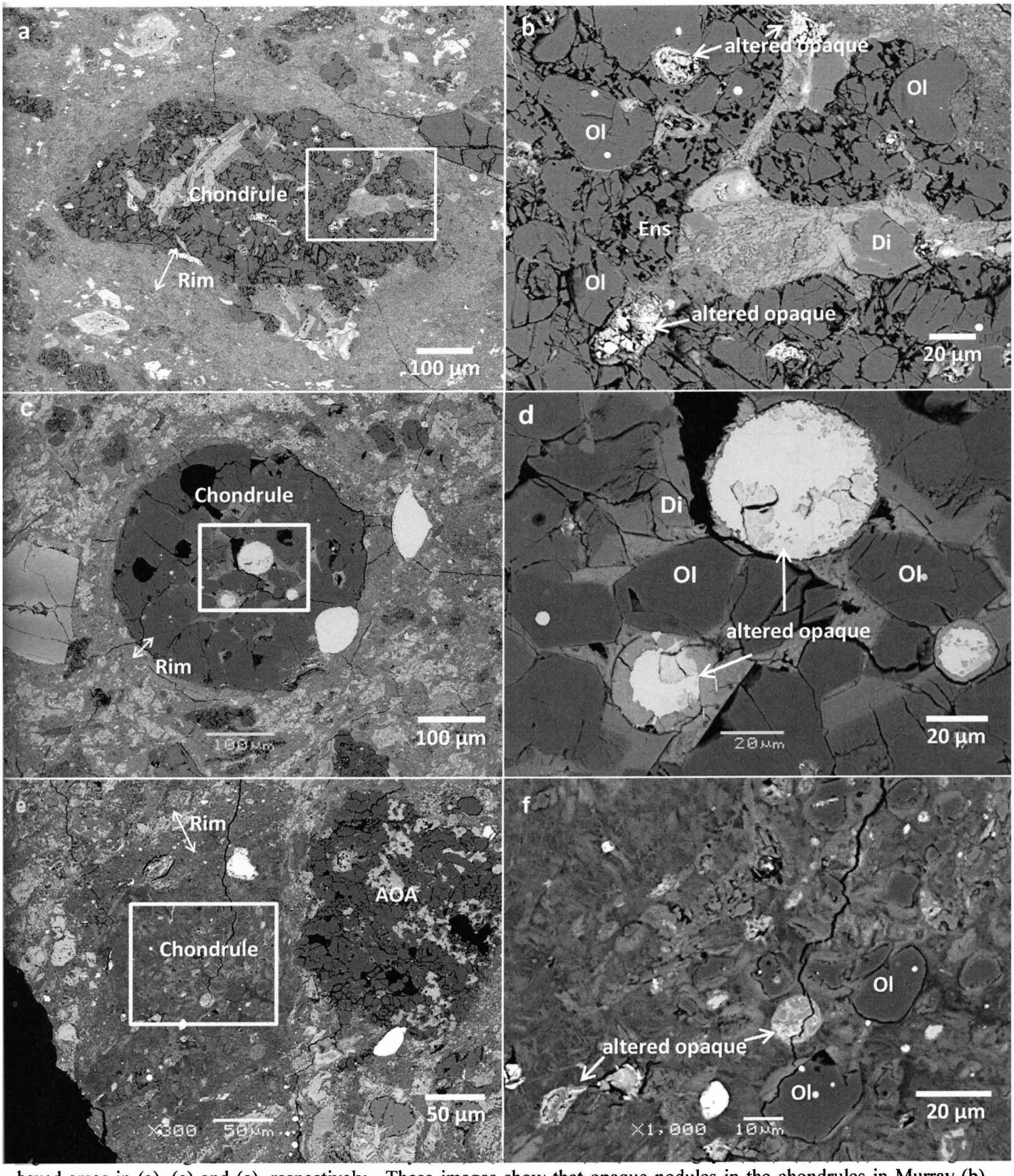

boxed areas in (a), (c) and (e), respectively. These images show that opaque nodules in the chondrules in Murray (b), QUE97990 (d) and Nogoya (f) have been partially replaced to cronstedtite and tochilinite.

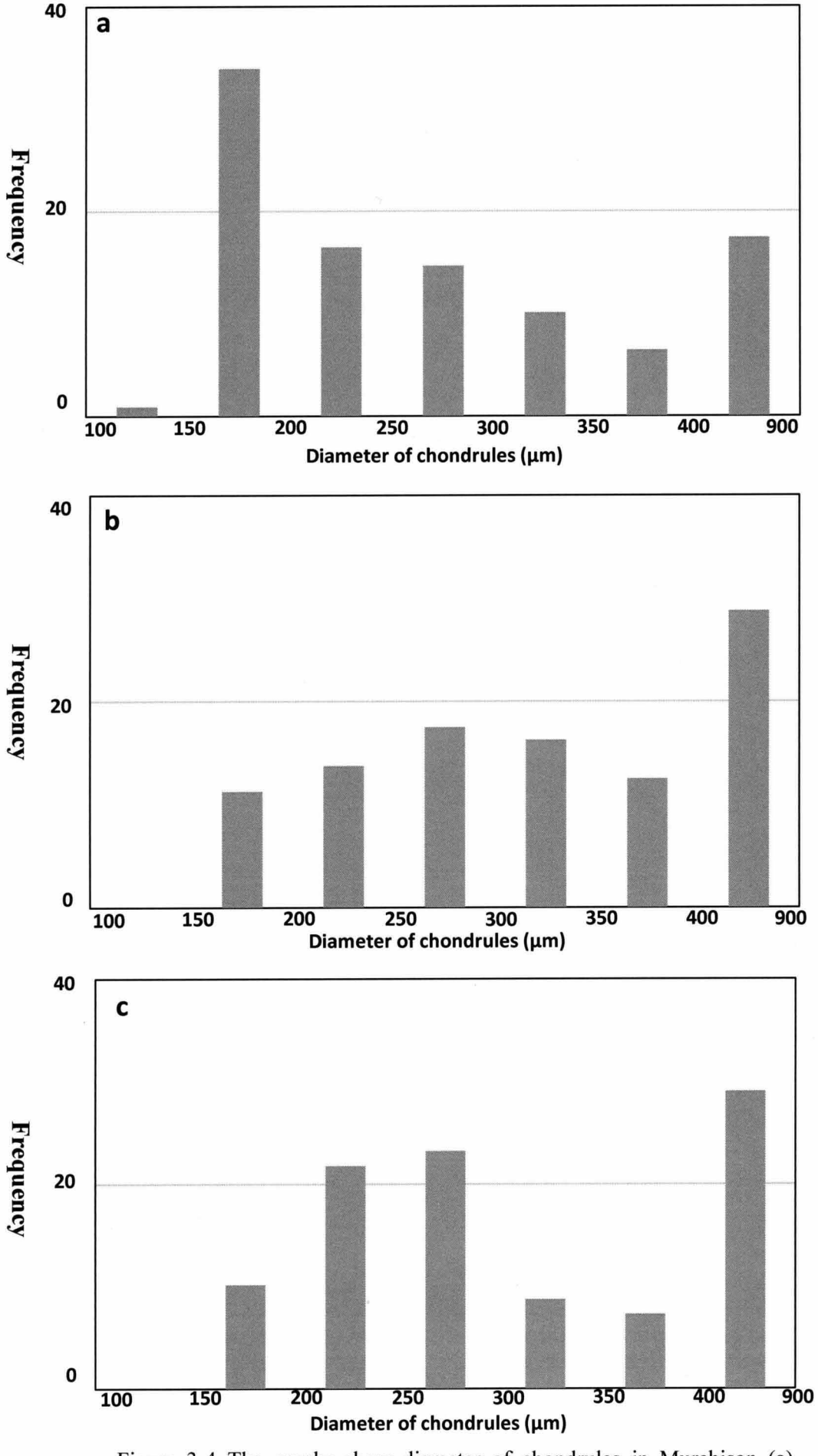

Figure 3-4 The graphs show diameter of chondrules in Murchison (a), Murray (b) and Mighei (c).

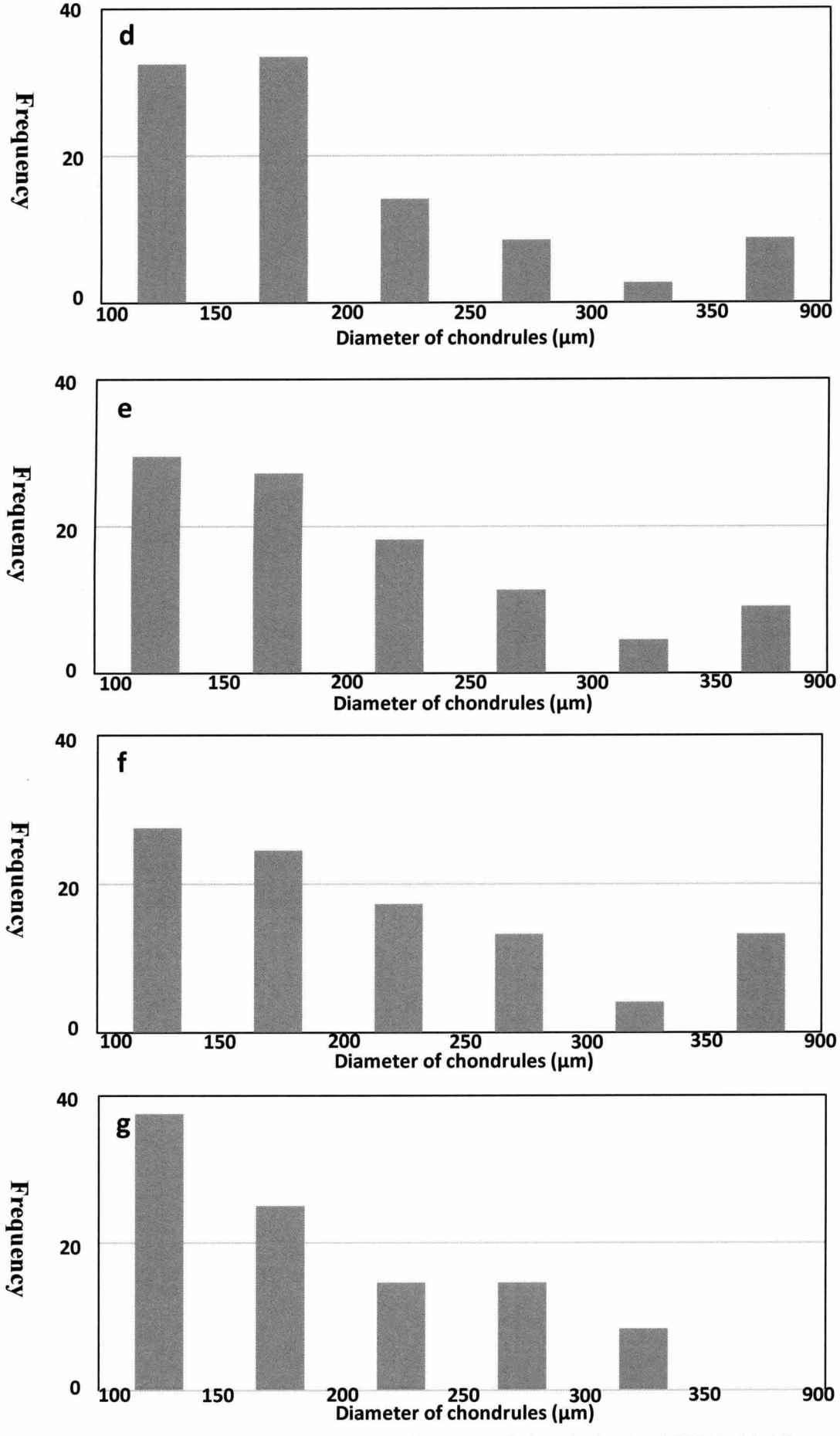

Figure 3-4. The graphs shows diameter of chondrules in QUE97990 (d), Y791198 (e), Cold Bokkeveld (f) and Nogoya (g).

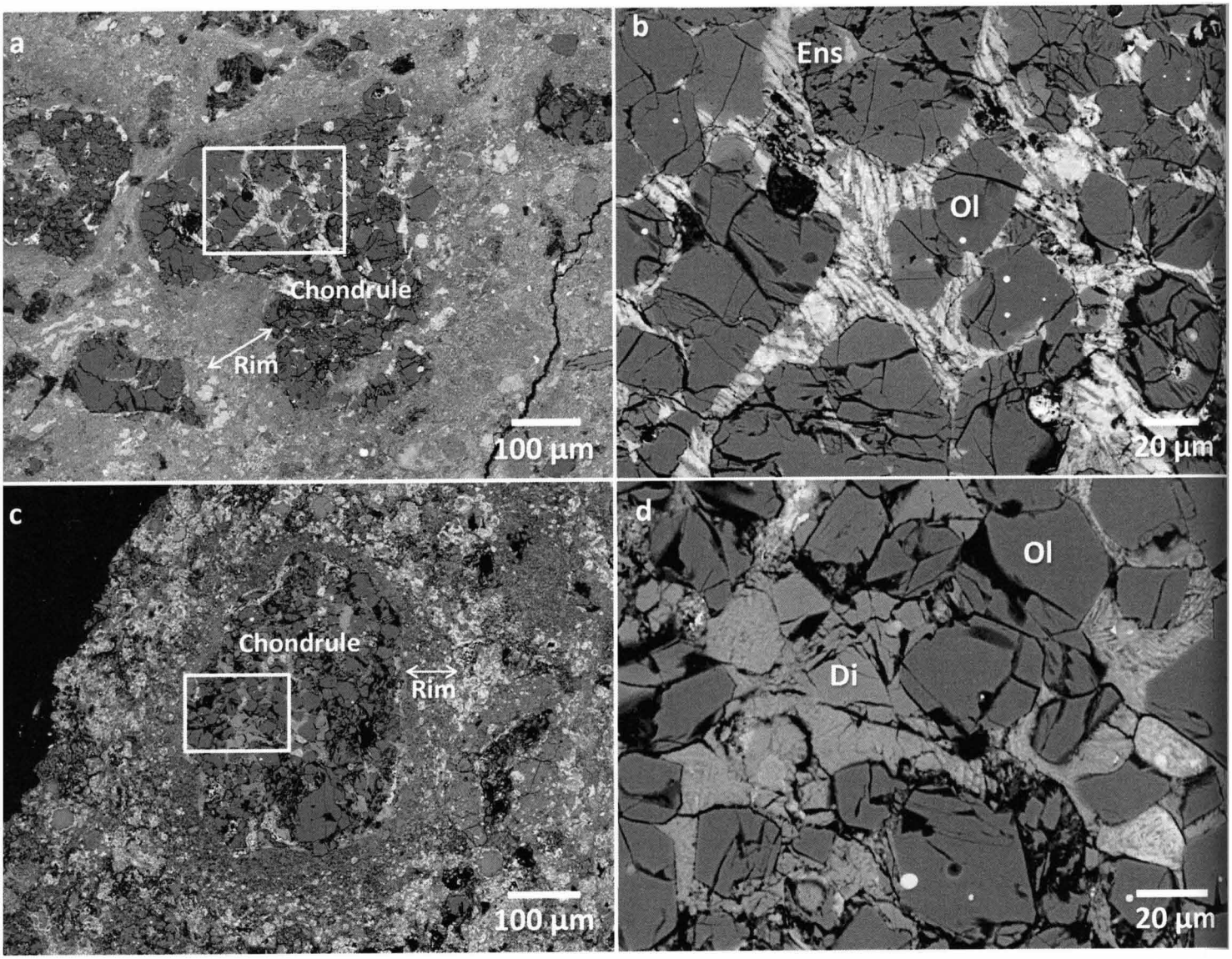

Figure 3-5. BSE image of a chondrule in Murray (a) and Mighei (c). (b) (d) Image of boxed area in (a) and (c), respectively. These images show phenocrysts not replacing to phyllosilicates.

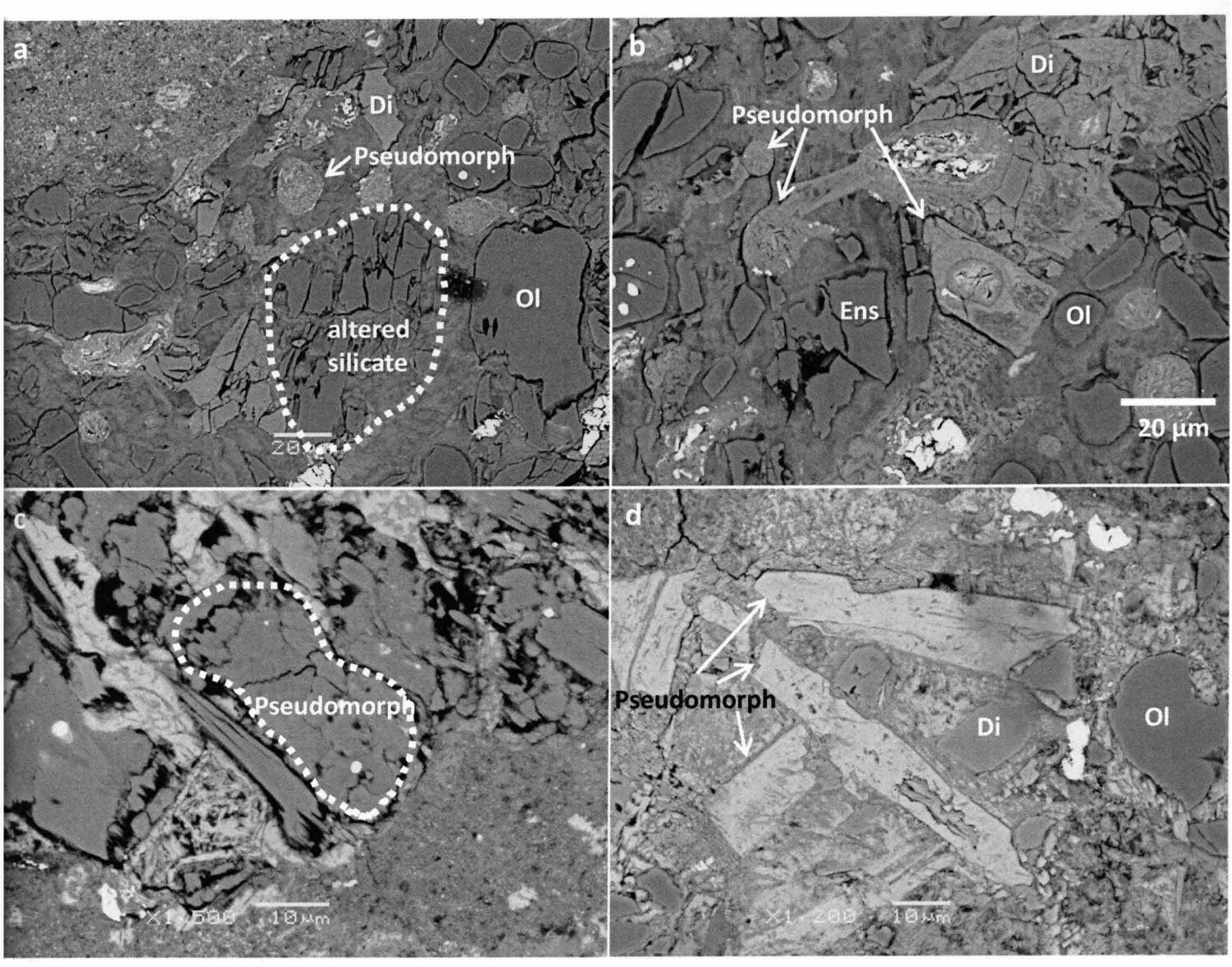

Figure 3-6. BSE image of altered phenocrysts and pseudomorphs in Cold Bokkeveld (a, b) and Nogoya (c, d). Most of pseudomorph in Cold Bokkeveld shows round shape. On the other hand, most of pseudomorphs in Nogoya show shape of short prismatic.

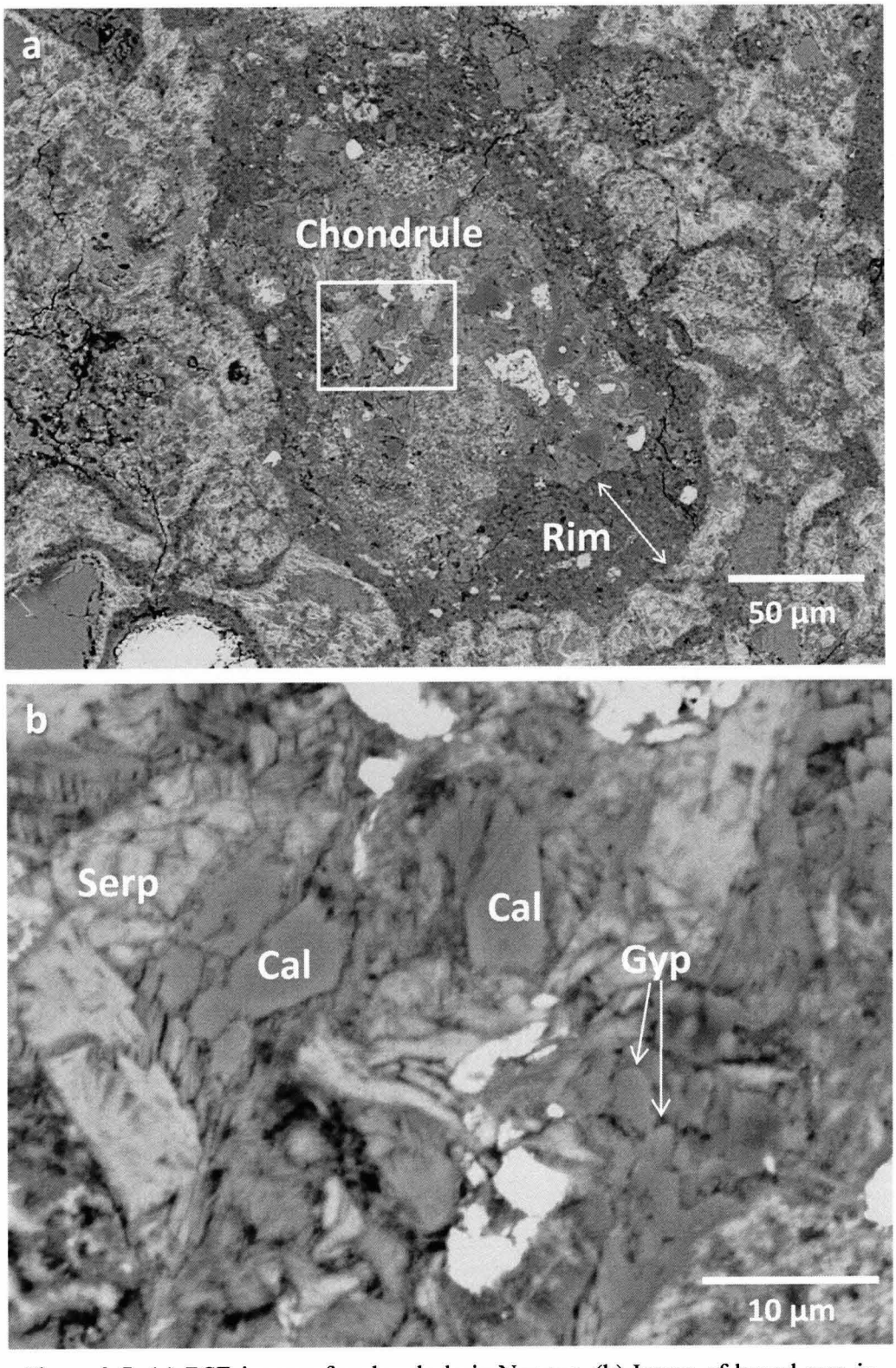

Figure 3-7. (a) BSE image of a chondrule in Nogoya. (b) Image of boxed area in (a), showing calcite and gypsum as phenocrysts in the chondrule.

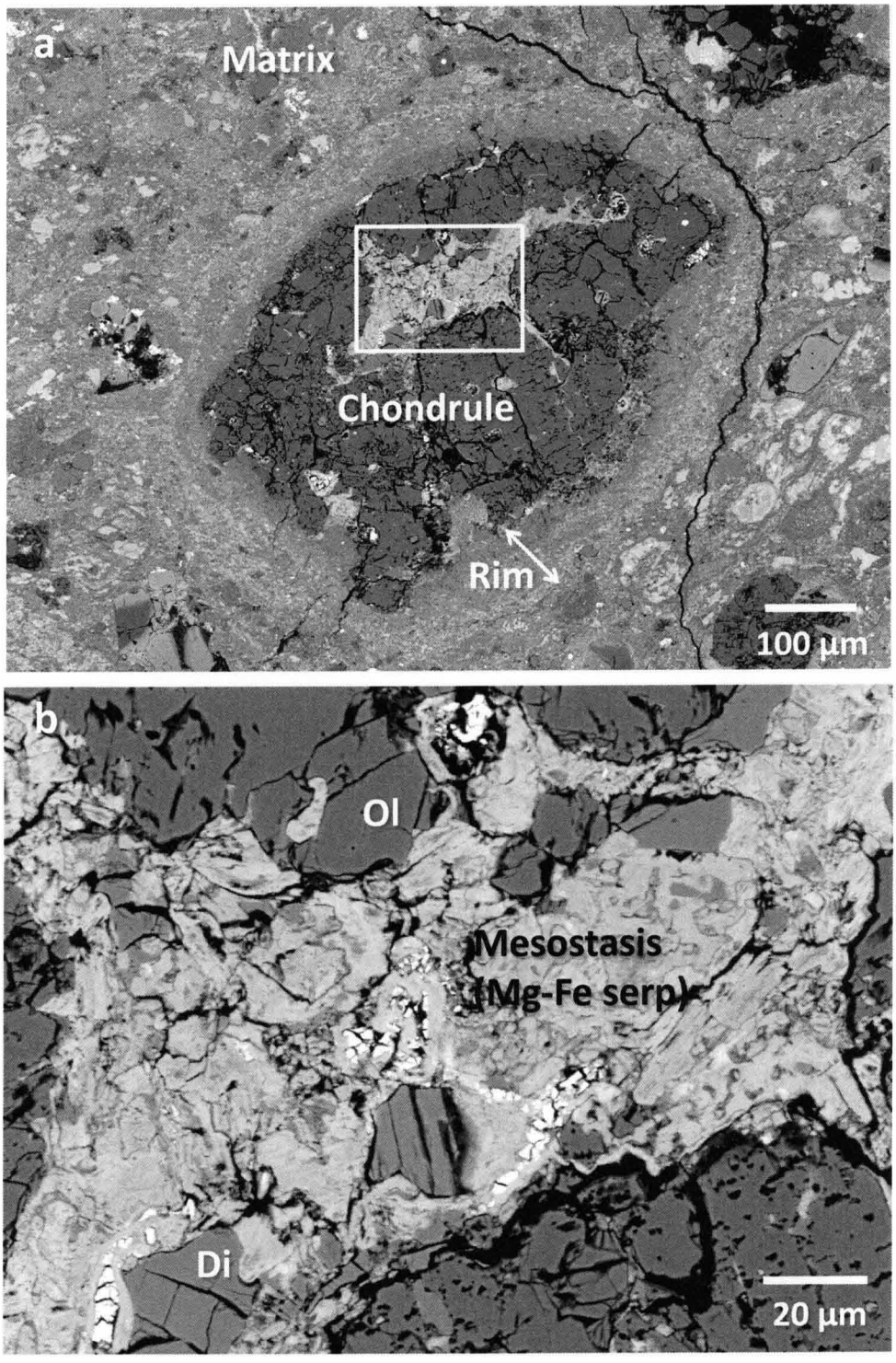

Figure 3-8. (a) BSE image of a chondrule in Murray. (b) Image of boxed area in (a), showing the mesostasis that has been largely altered to Mg-Fe. The mesostases in all studied meteorites have been largely altered to Mg-Fe serpentine.

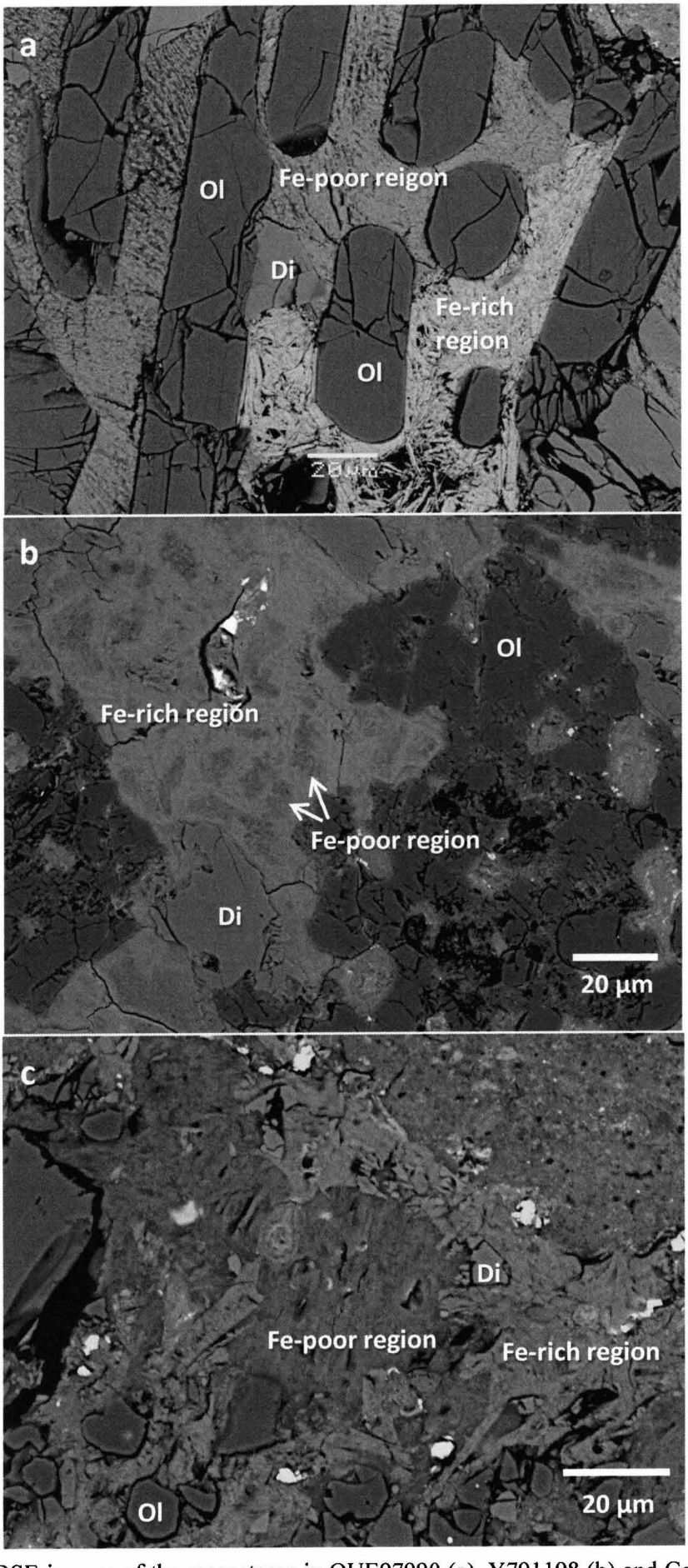

Figure 3-9. BSE images of the mesostases in QUE97990 (a), Y791198 (b) and Cold Bokkeveld (c). These mesostases show a significant contrast of two regions; iron-rich regions (FeO = about 15-25 wt%) and iron-poor regions (FeO = about 25-35 wt%).

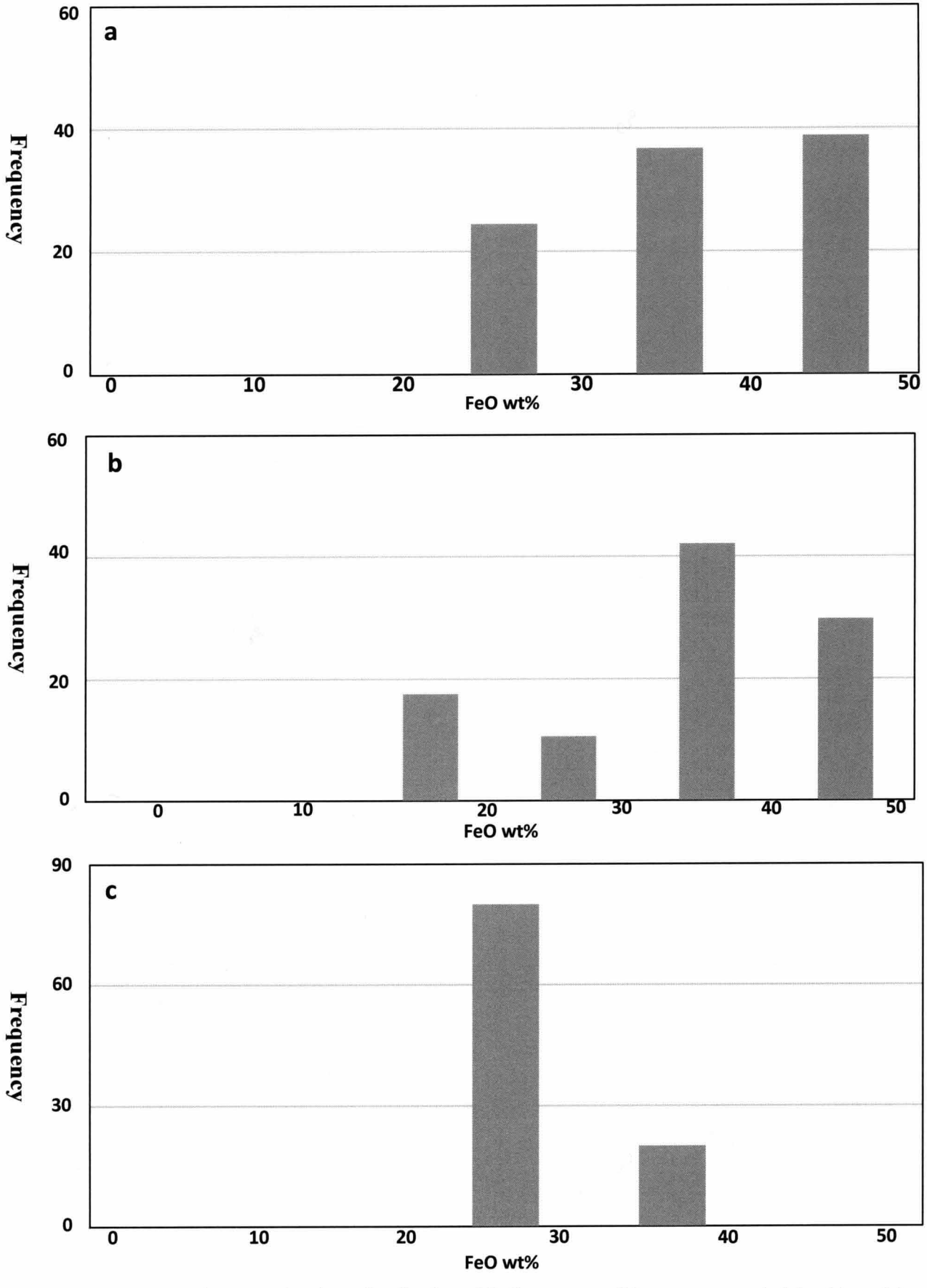

Figure 3-10. These graphs show distribution of FeO contents of the mesostases in Murchison (a), Murray (b) and Mighei (c). The analyses were performed by using defocused beam (~5 μm in diameter).

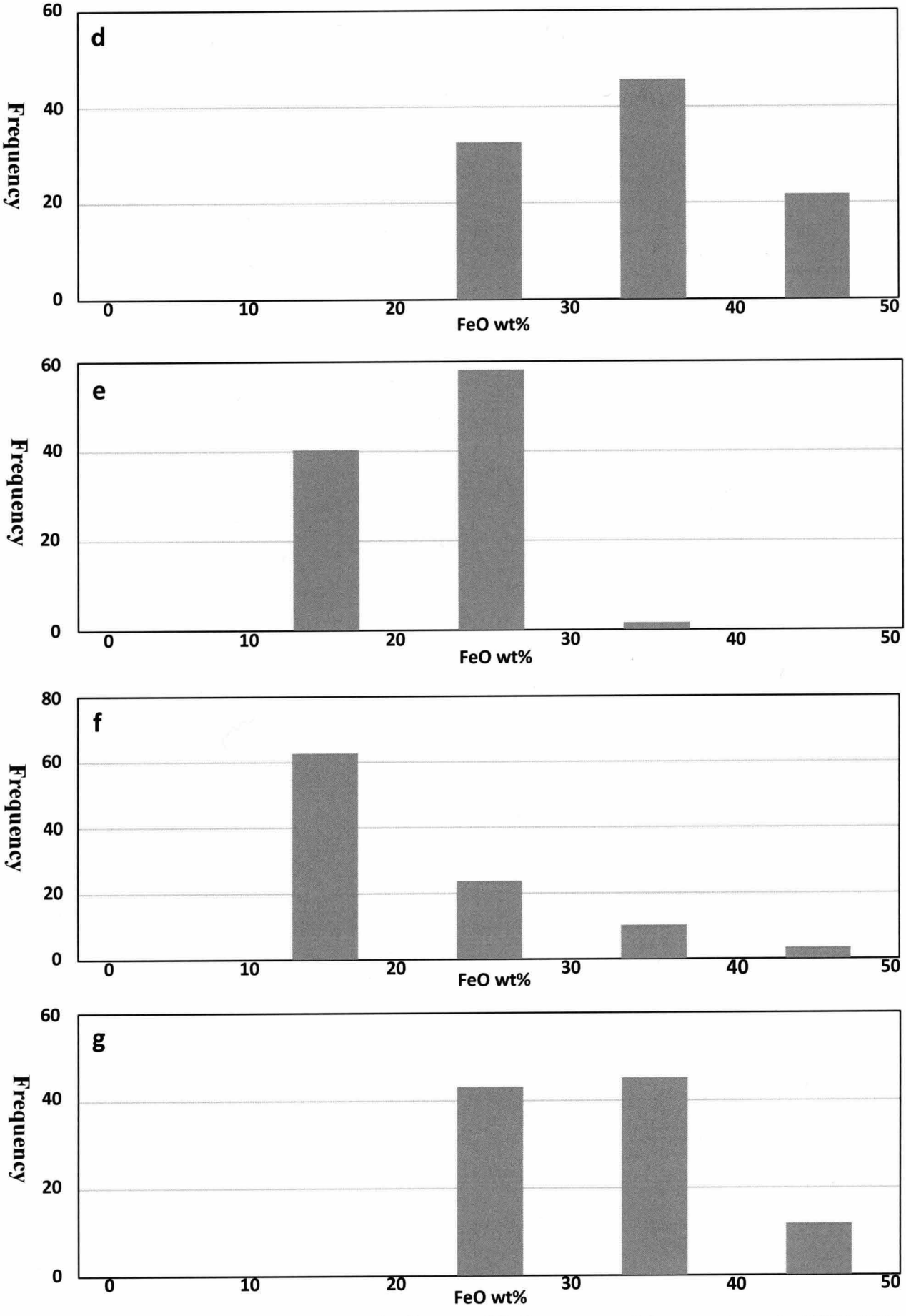

Figure 3-10. These graphs show distribution of FeO contents of the mesostases in QUE97990 (d), Y791198 (e), Cold Bokkeveld (f) and Nogoya (g). The analyses were performed by using defocused beam (~5 μm in diameter).

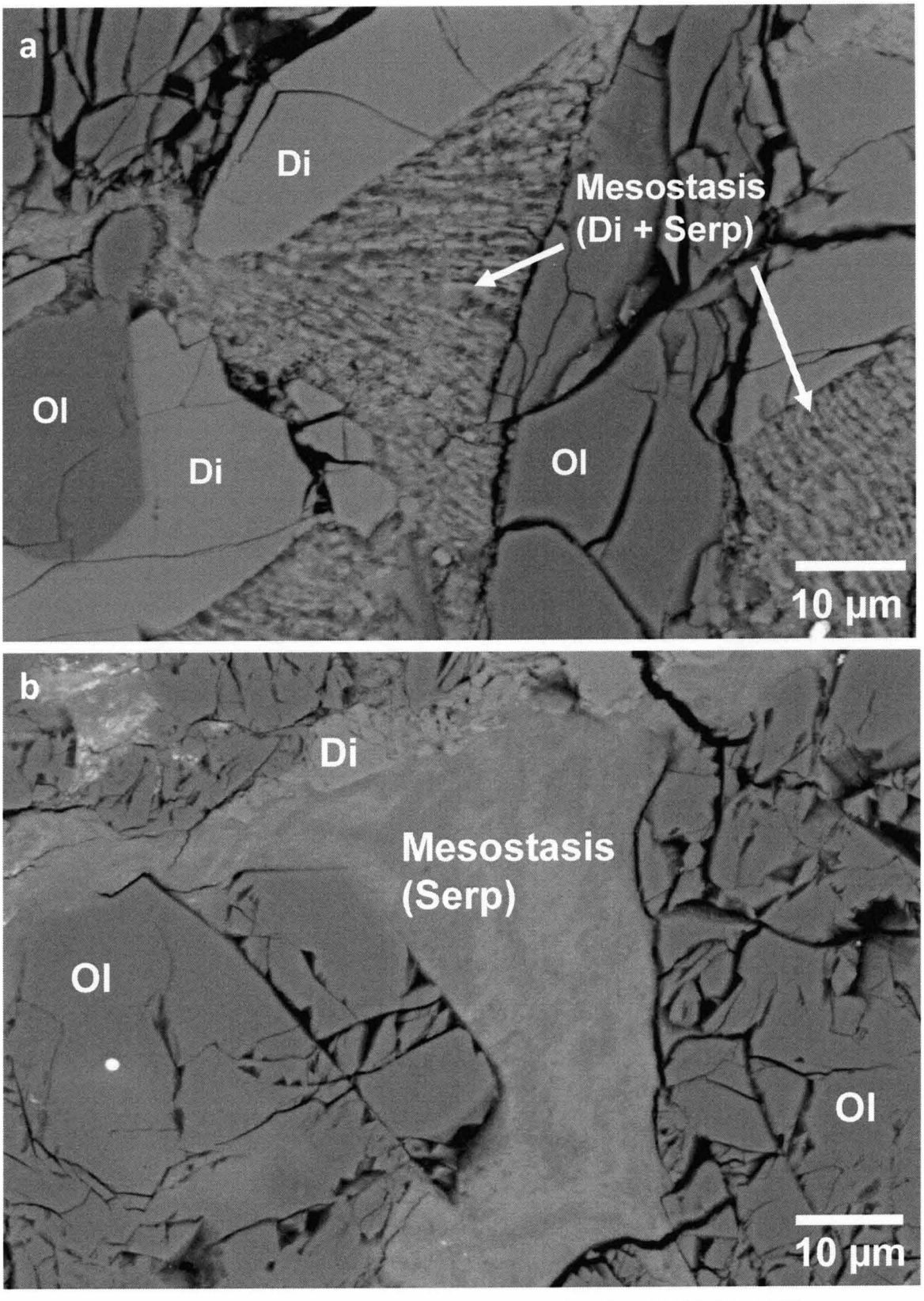

Figure 3-11. BSE images of the mesostases in QUE97990 (a) and Y791198 (b). (a) The mesostasis in QUE97990 shows quenched texture. The quenched texture in the mesostases does not occur in the all studied meteorites including Y791198 that was reported as the lowest altered CM chondrite by Metzler (1992).

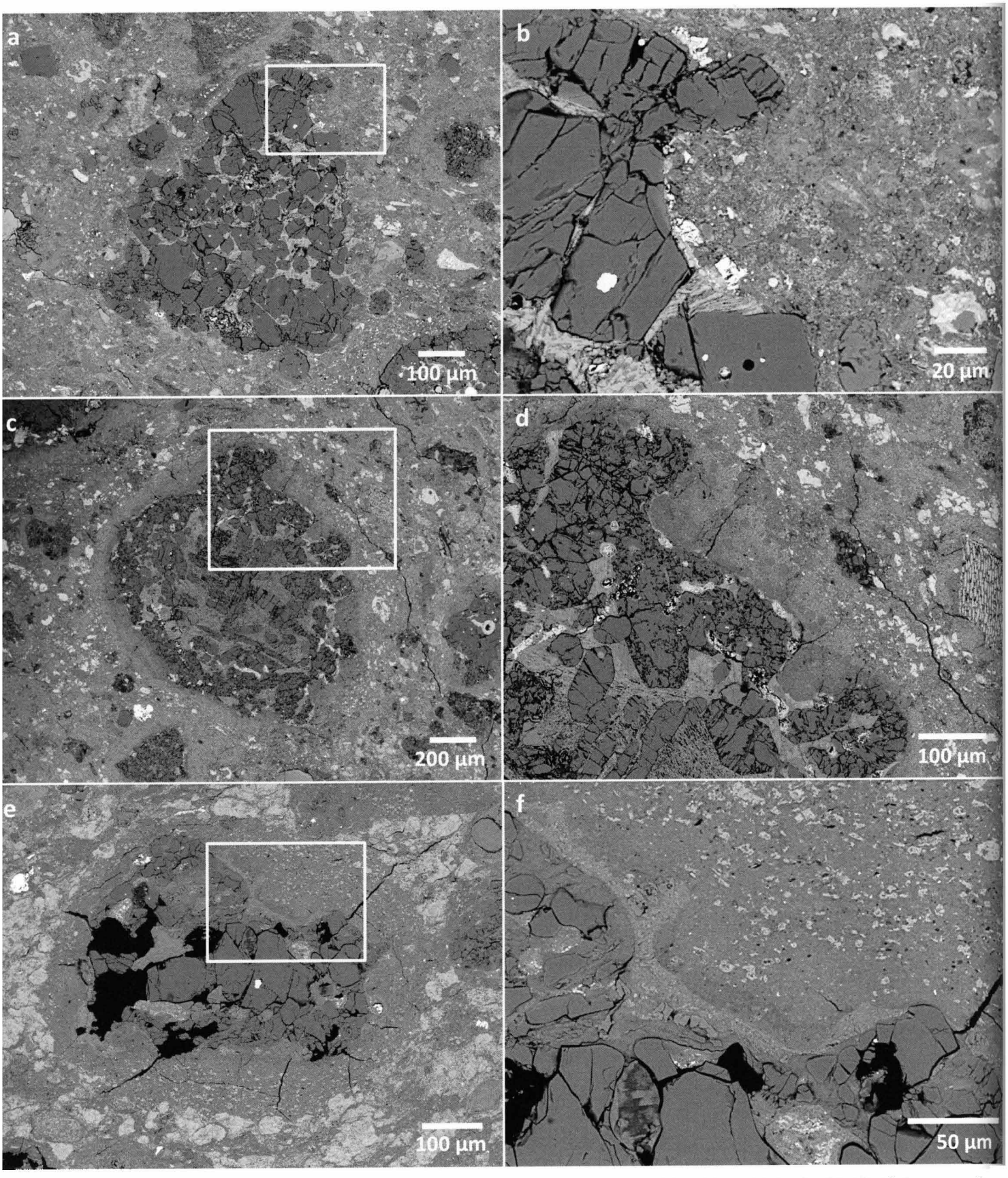

Figure 3-12 BSE images of chondrules in Murchison (a, b), Murray (c, d) and Cold Bokkeveld (e, f). (b) (d) (f) Images of boxes area in (a), (c) and (e), respectively, showing embayments on chondrule surfaces. The embayments is largely composed of the Mg-Fe serpentine-rich material that is indistinguishable from the surrounding rims. The characteristics in the embayments are similar to that of all studied meteorites expect for QUE97990.

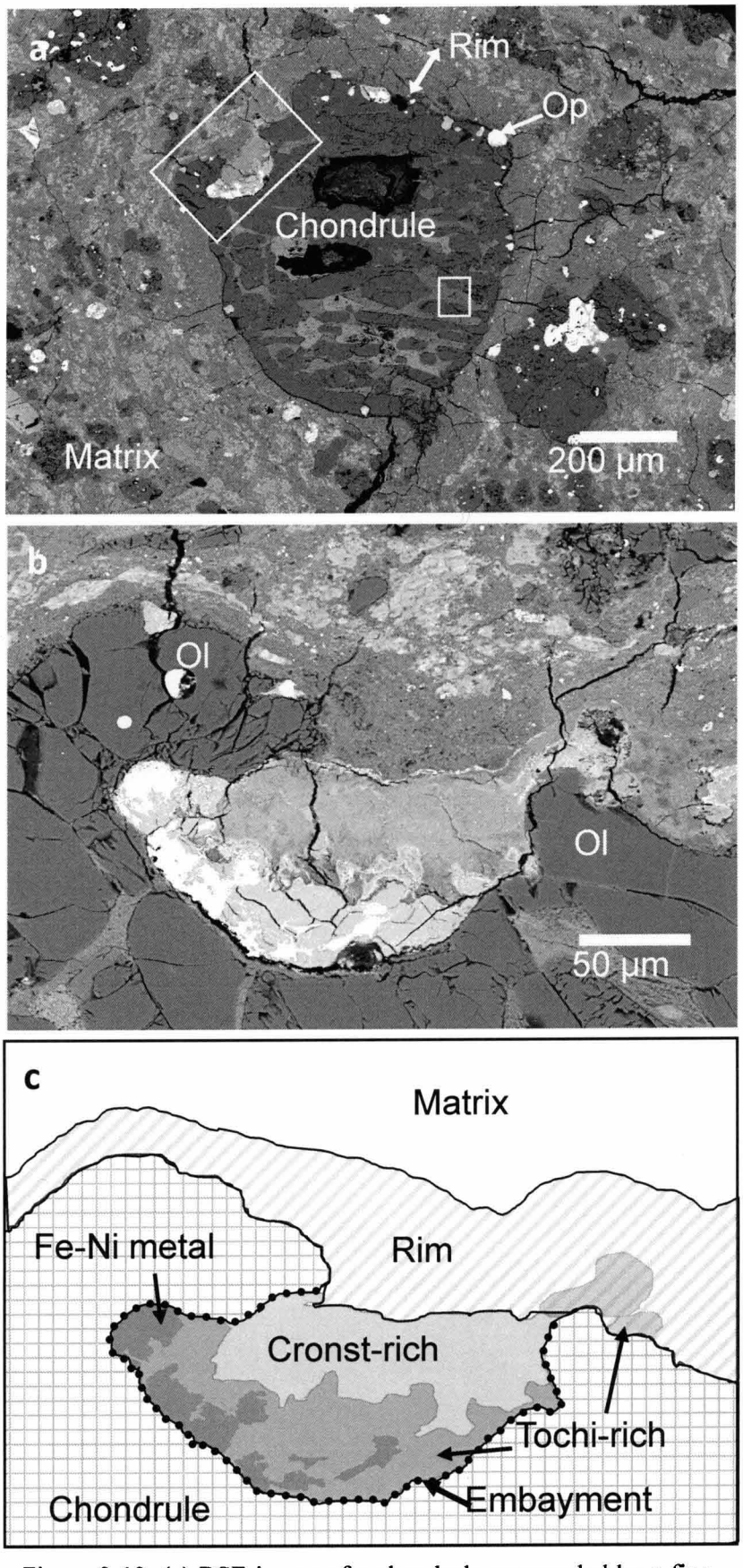

Figure 3-13. (a) BSE image of a chondrule surrounded by a fine-grained rim in QUE97990. (b) Image of the boxed area in (a), showing embayments on chondrule surface. (c) Illustration of (b) showing three zones, (1) Fe-Ni metal, (2) tochilinite-rich (Tochi-rich), (3) cronstedtite-rich (Cronst-rich), in the embayment.

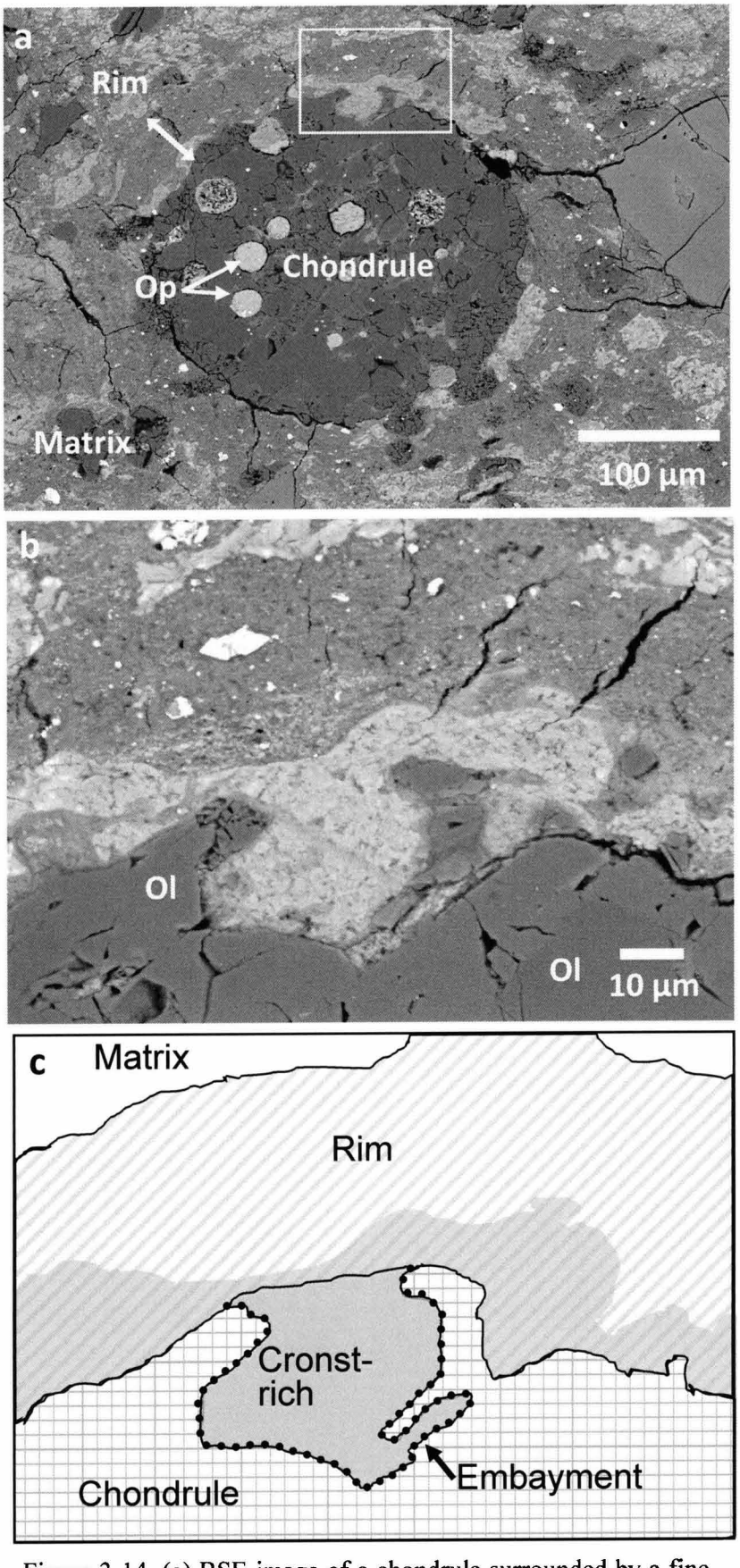

Figure 3-14. (a) BSE image of a chondrule surrounded by a fine-grained rim in QUE97990. (b) Image of the boxed area in (a), showing an embayment on chondrule surface. (c) Illustration of (b) showing the cronstedtite-rich (Cronst-rich) material not only fills the embayment but also extend to the outside of the embayments.

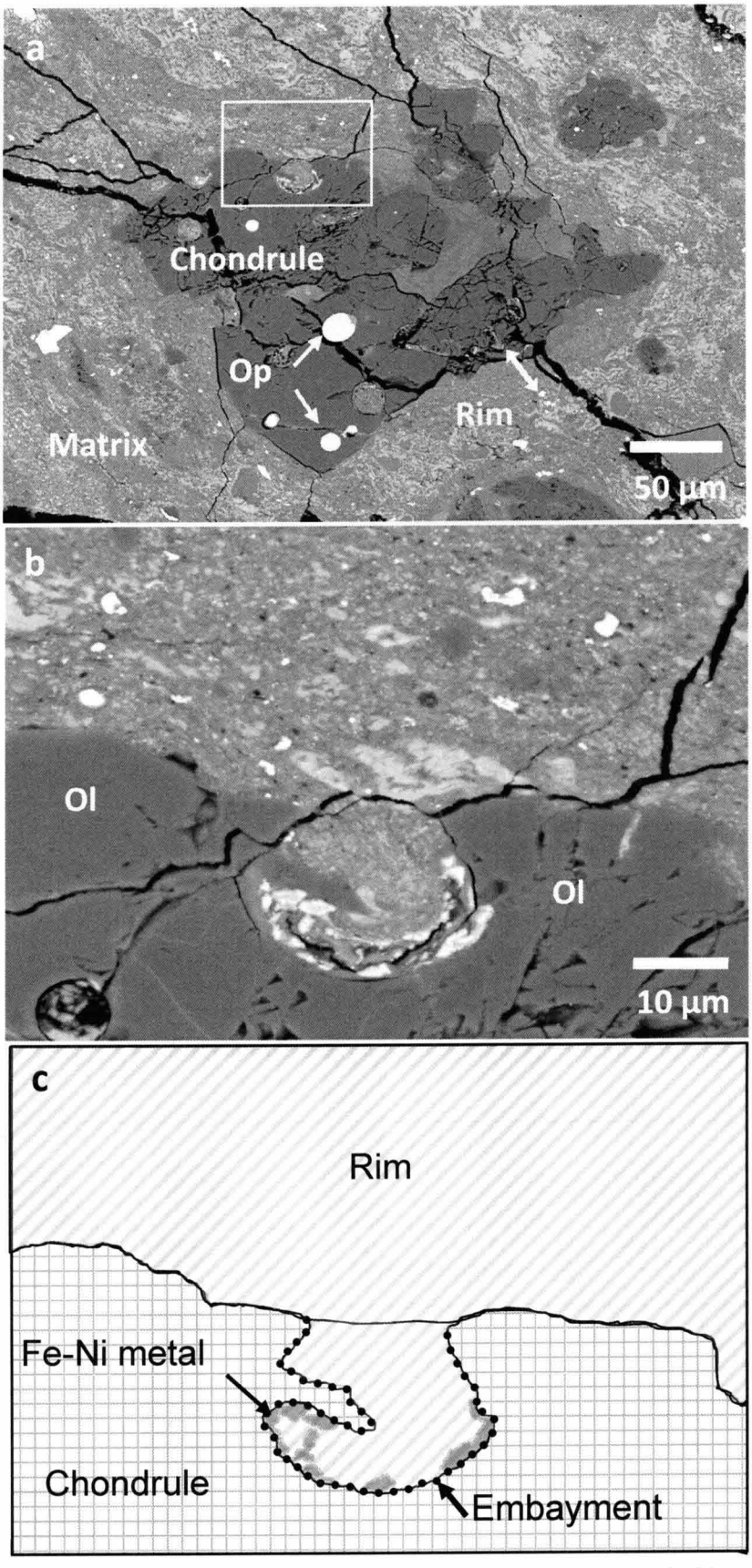

Figure 3-15. (a) BSE image of a chondrule surrounded by a fine-grained rim in Yamato 791198_1. (b) Image of the boxed area in (a), showing an embayment on the chondrule surface. (c) Illustration of (b) showing that the embayment is filled with the material that is distinguishable from the rim.

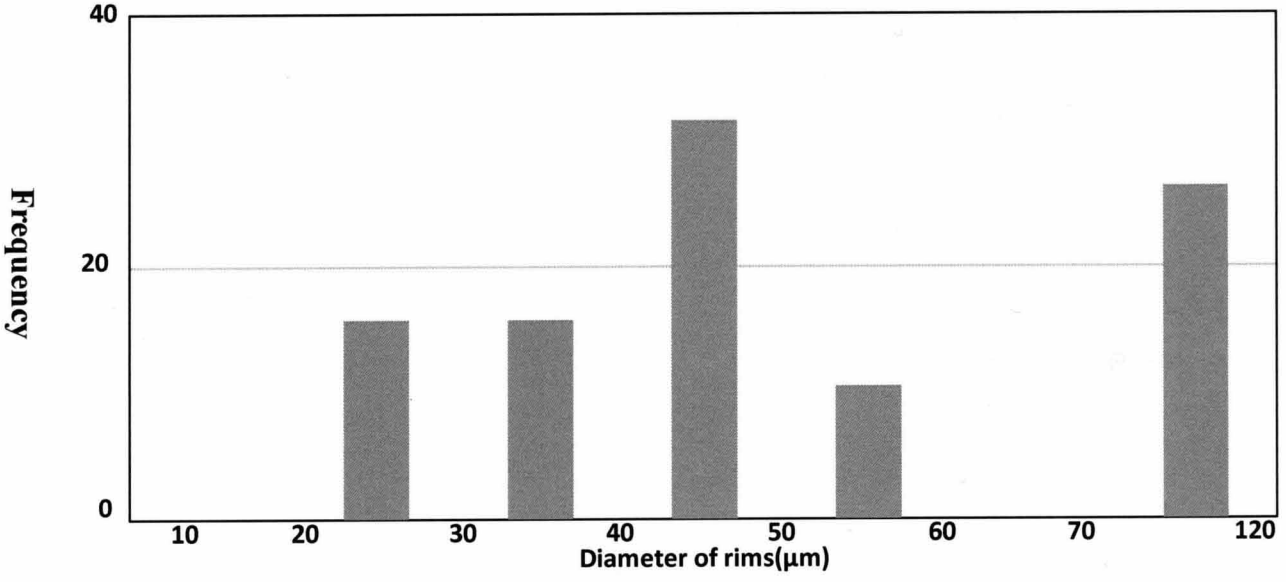

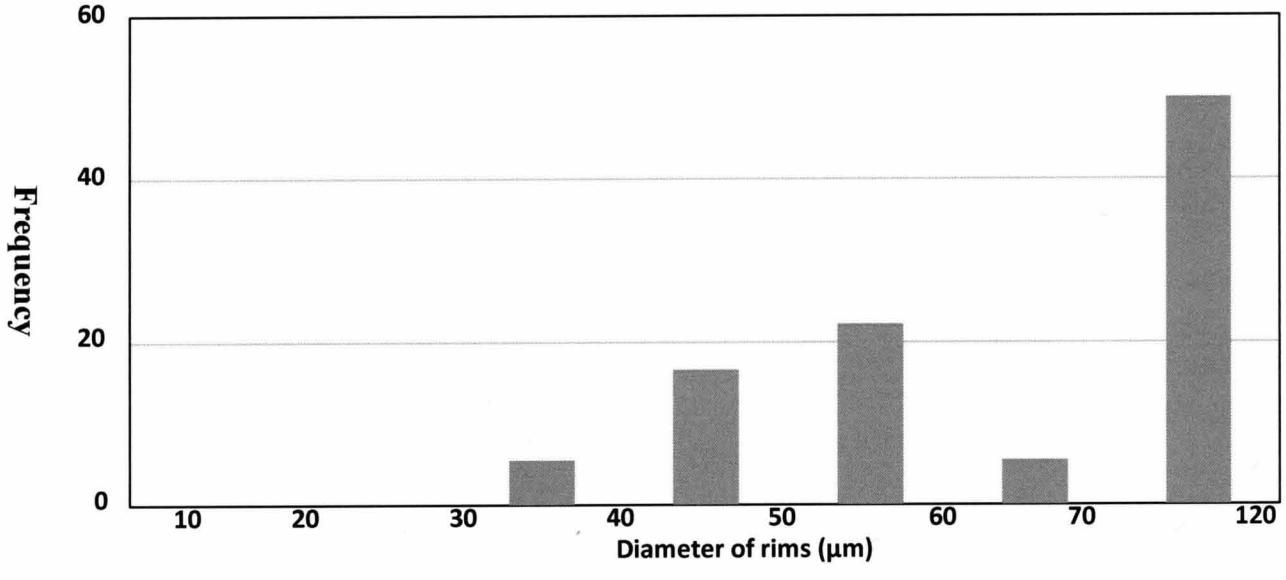

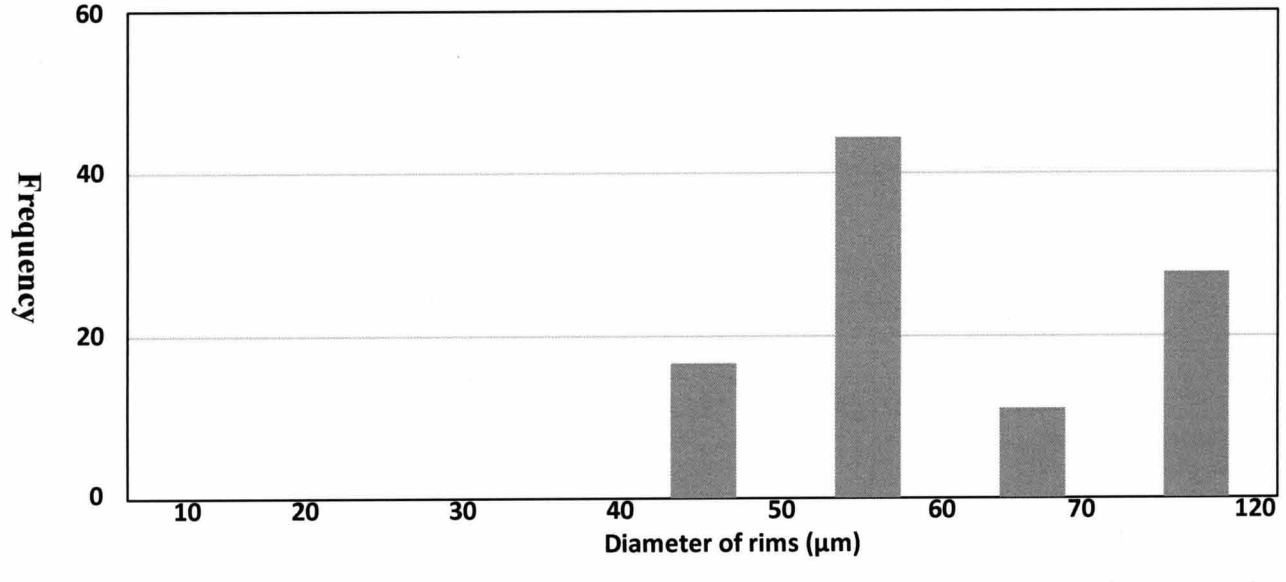

Figure 3-16. The thickness of rims was measured as an average of measured randomly selected 10 areas in a chondrule in Murchison (a), Murray (b) and Mighei (c).

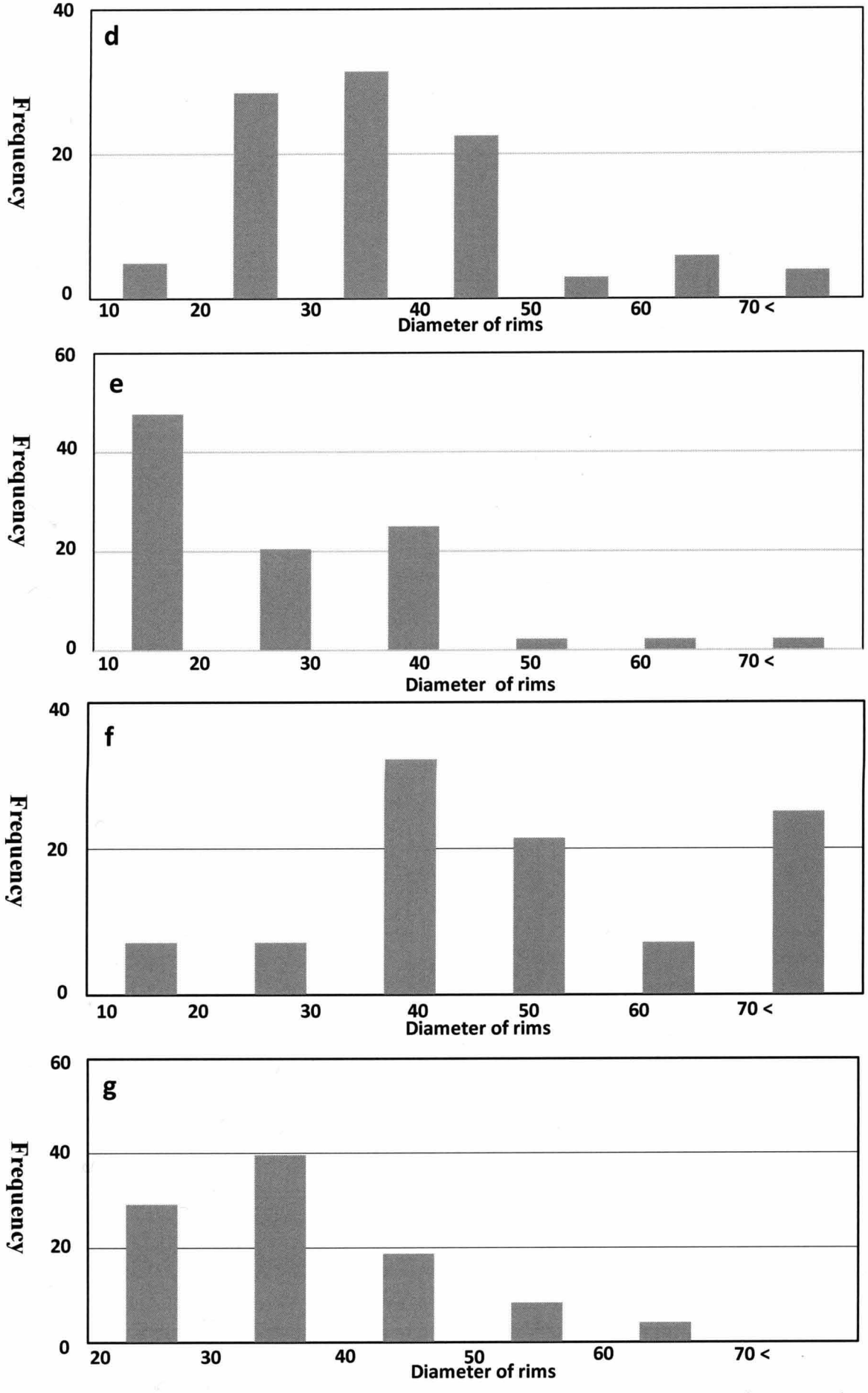

Figure 3-16. The thickness of rims was measured as an average of measured randomly selected 10 areas in a chondrule in QUE97990 (d), Y791198 (e), Cold Bokkeveld (f) and Nogoya (g).

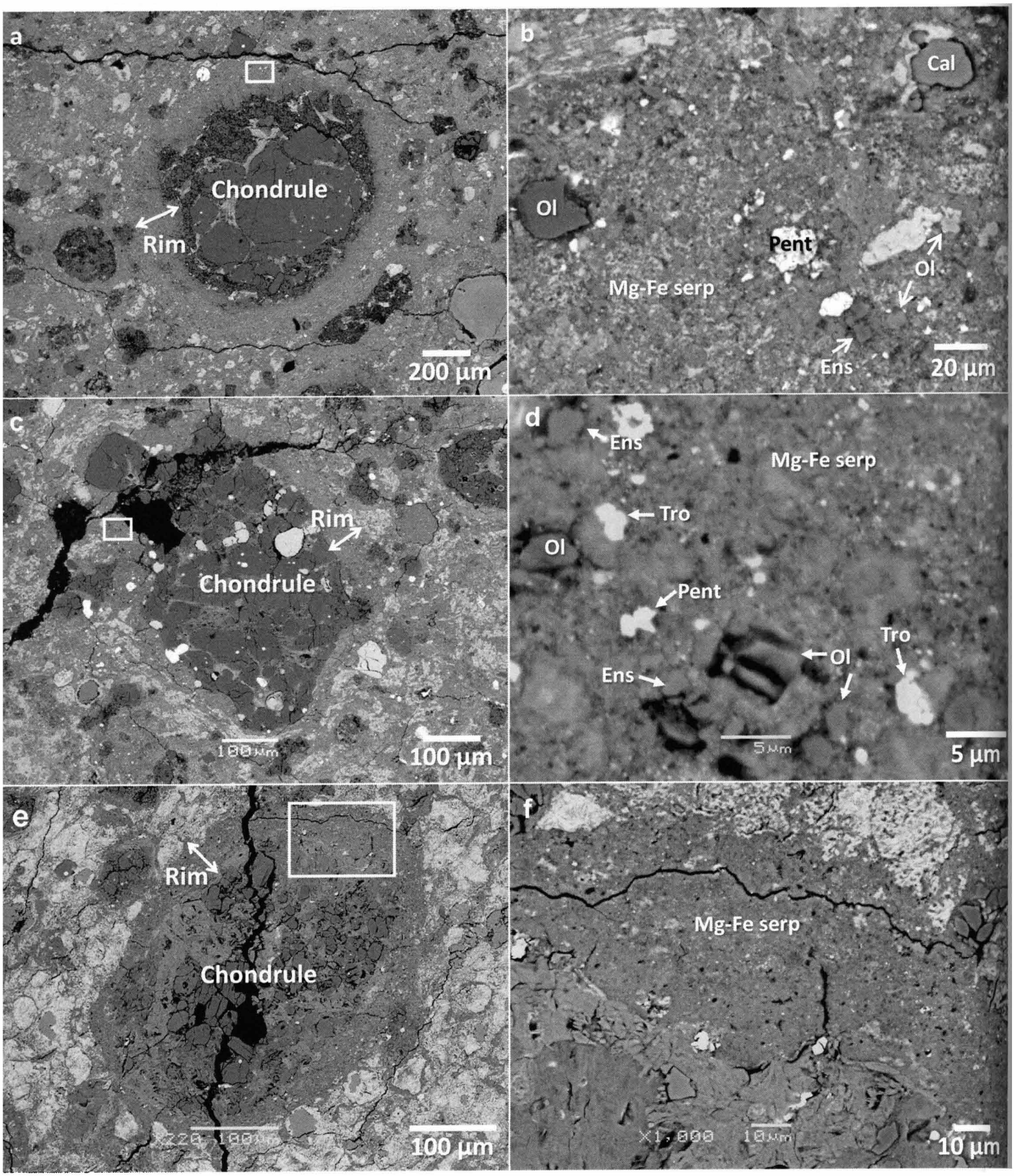

Figure 3-17. BSE images of the chondrule rims in Murray (a, b), QUE97990 (c, d) and Cold Bokkeveld (e, f). (b) (d) (f) Images of boxed areas in (a), (c) and (e), respectively. The boundary between in the rim and matrix in Murray is not clear. On the other hand, those of QUE97990 and Cold Bokkeveld are clear. The rims in Murray and QUE97990 consist of Mg-Fe serpentine, Fe-sulfide and anhydrous silicates. On the other hand, the rim in Cold Bokkeveld mainly consist of Mg-Fe serpentine.

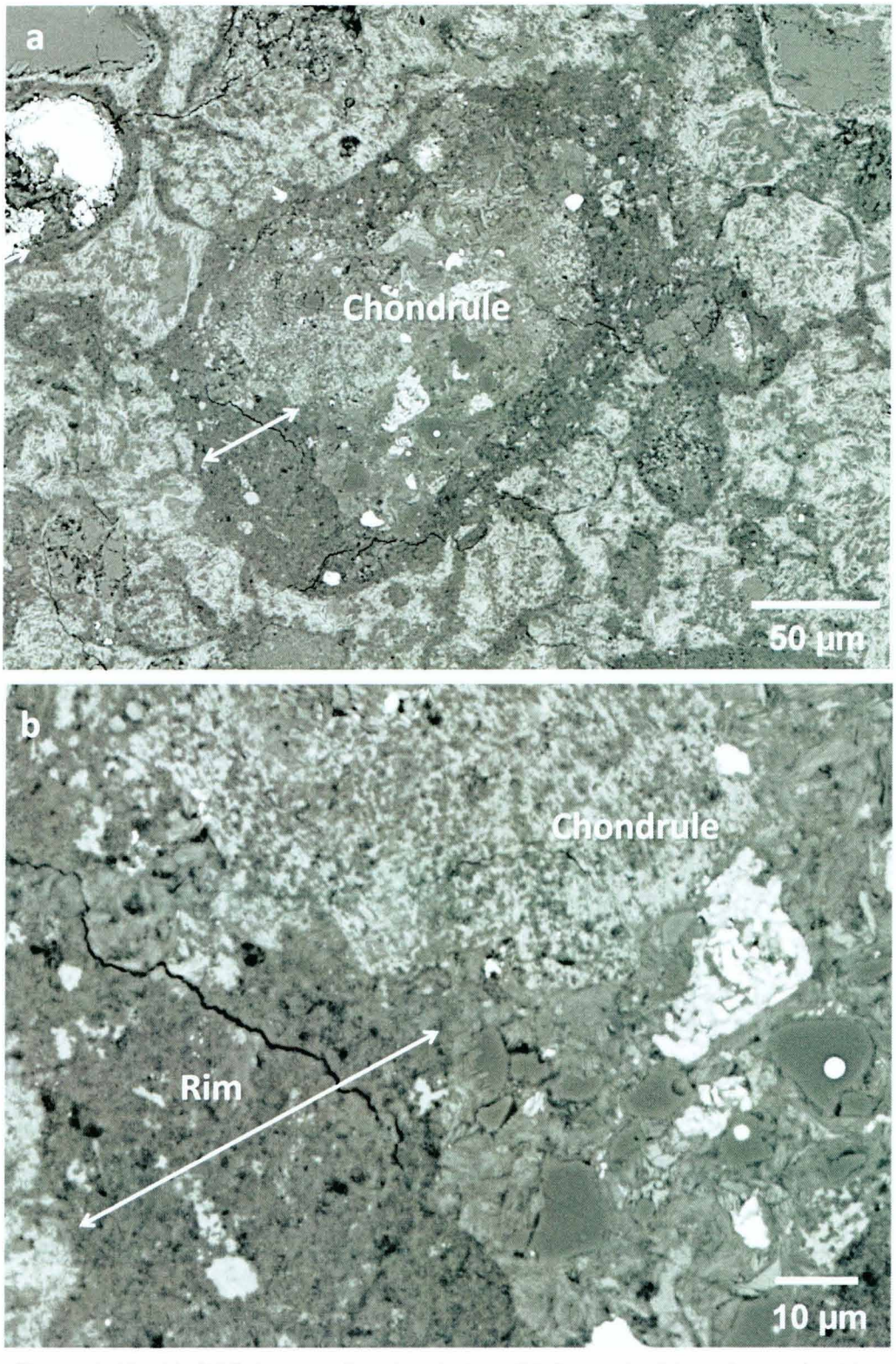

Figure 3-18. (a) BSE image of a chondrules. (b) Imaged of boxed area in (a), showing a boundary between a chondrule and matrix. The boundary is not clear.

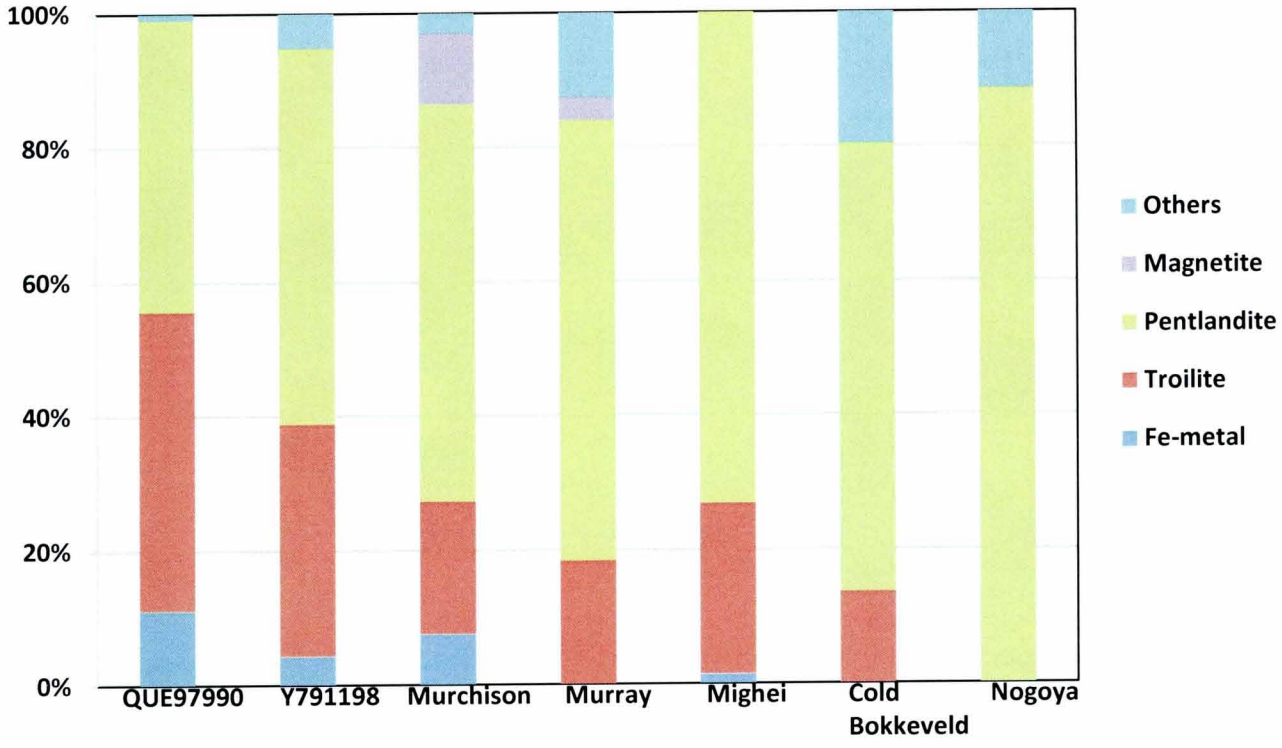

Figure 3-19. This graph shows existence ratio of opaque minerals in the rims in the studied meteorites. I analyzed randomly selected opaque mineral (more than 50 grains) in the rims.

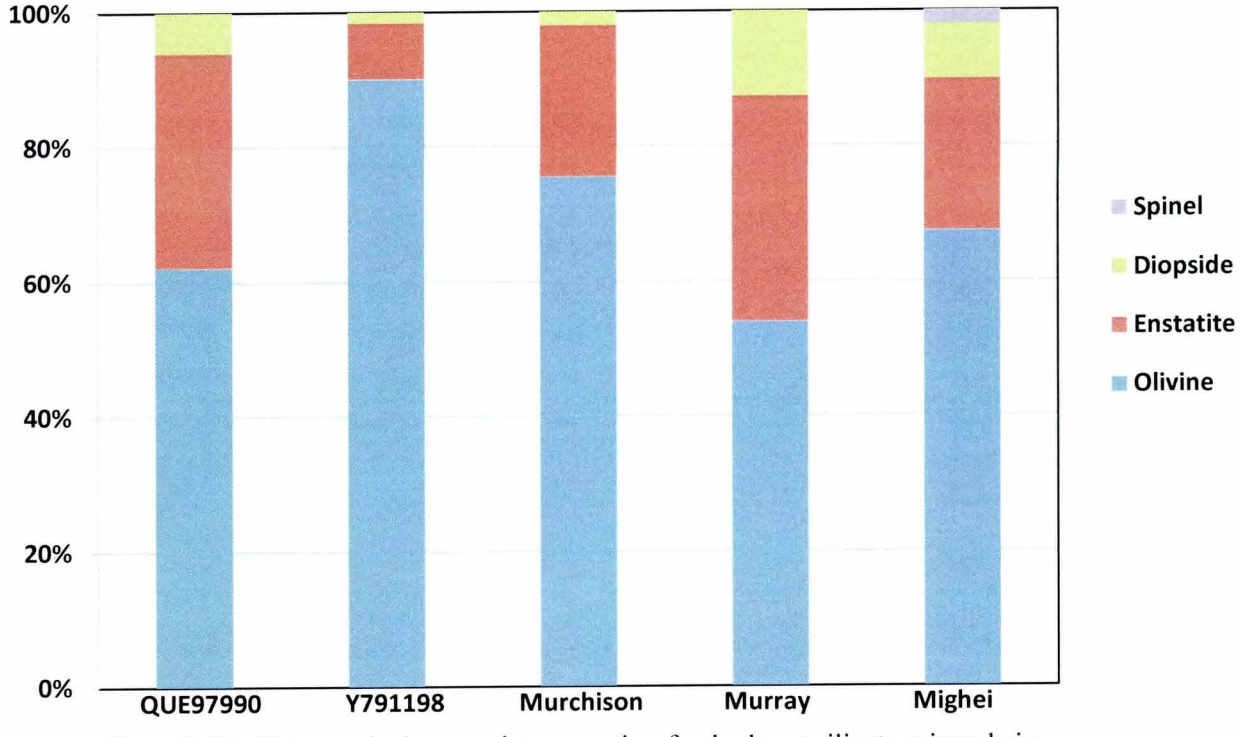

Figure 3-20. This graph shows existence ratio of anhydrous silicate minerals in the rims in the studied CM chondrites. I analyzed randomly selected anhydrous silicate mineral (more than 50 grains) in the rims.

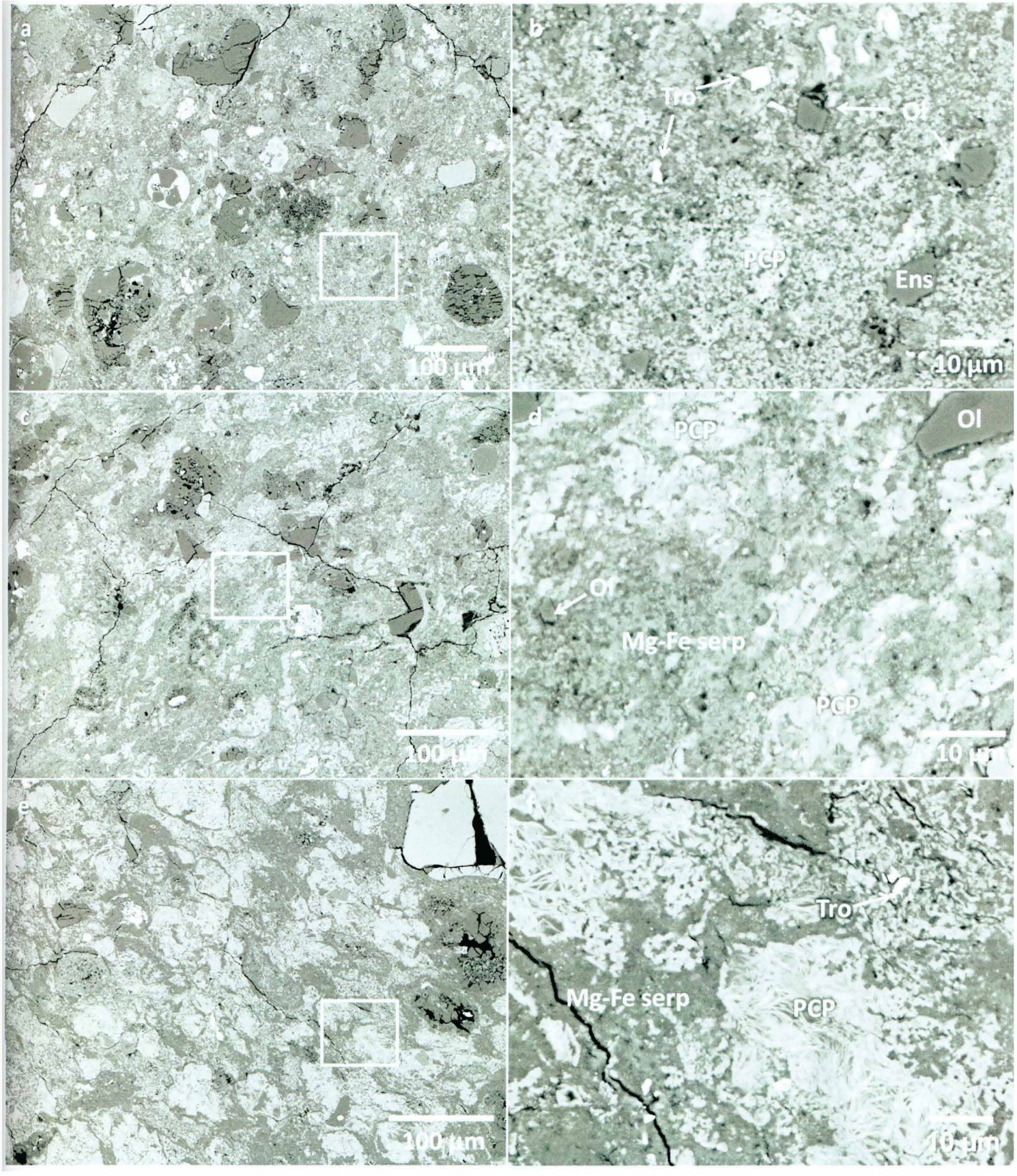

Figure 3-21 BSE images of matrices in Murchison (a, b), QUE97990 (c, d) and Cold Bokkeveld (e, f). (b) (d) (f) Images of boxed areas in (a), (c) and (e), respectively. (b) The matrix in Murchison mainly consist of Mg-Fe serpentine and fine-grained PCPs with minor amount of Fe-sulfide and anhydrous silicates. (d) The matrix in QUE mainly consist of Mg-Fe serpentine and PCPs with minor amount of Fe-sulfide and anhydrous silicates. (f) The matrix in Murchison mainly consist of Mg-Fe serpentine and PCPs with minor amount of Fe-sulfide.

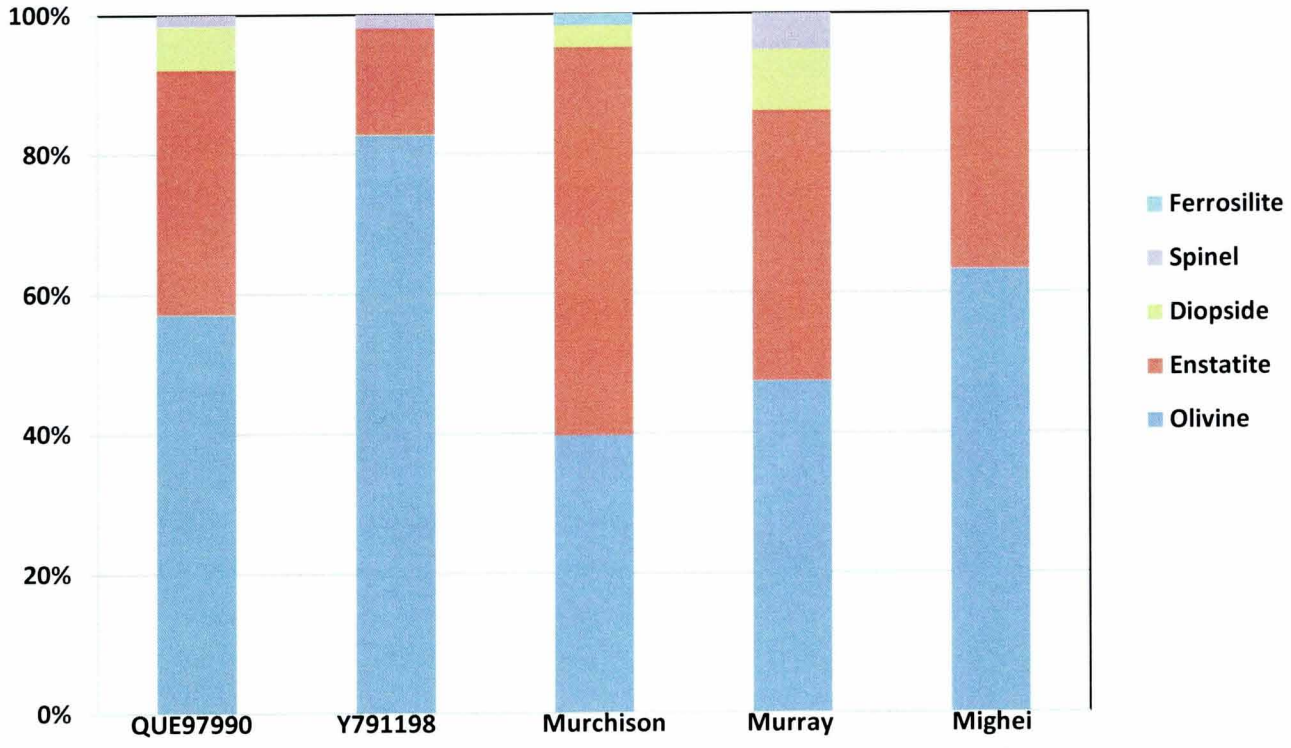

Figure 3-22. This graph shows existence ratio of anhydrous silicate minerals in the matrices in the studied CM chondrites. I analyzed randomly selected anhydrous silicate minerals (more than 50 grains) in the matrices.

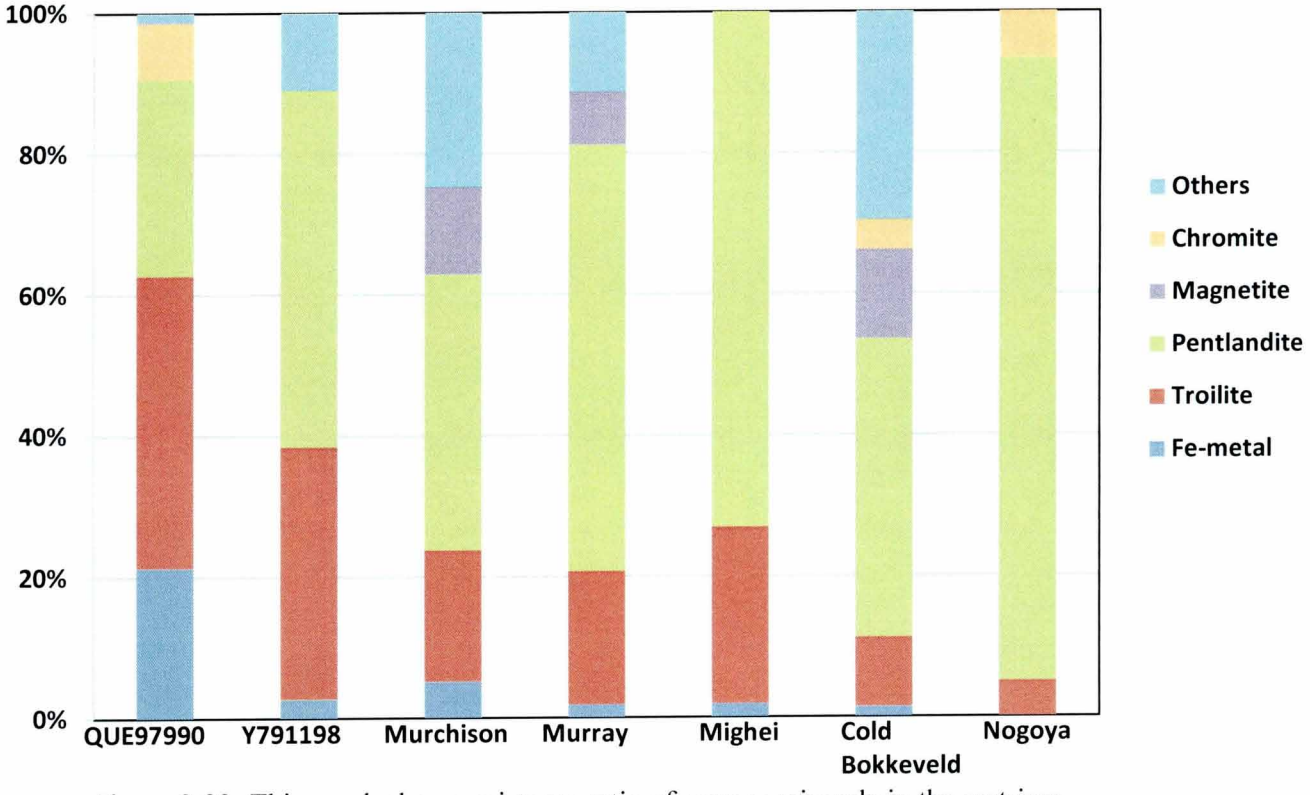

Figure 3-23. This graph shows existence ratio of opaque minerals in the matrices in the studied CM chondrites. I analyzed randomly selected opaque minerals (more than 50 grains) in the matrices.

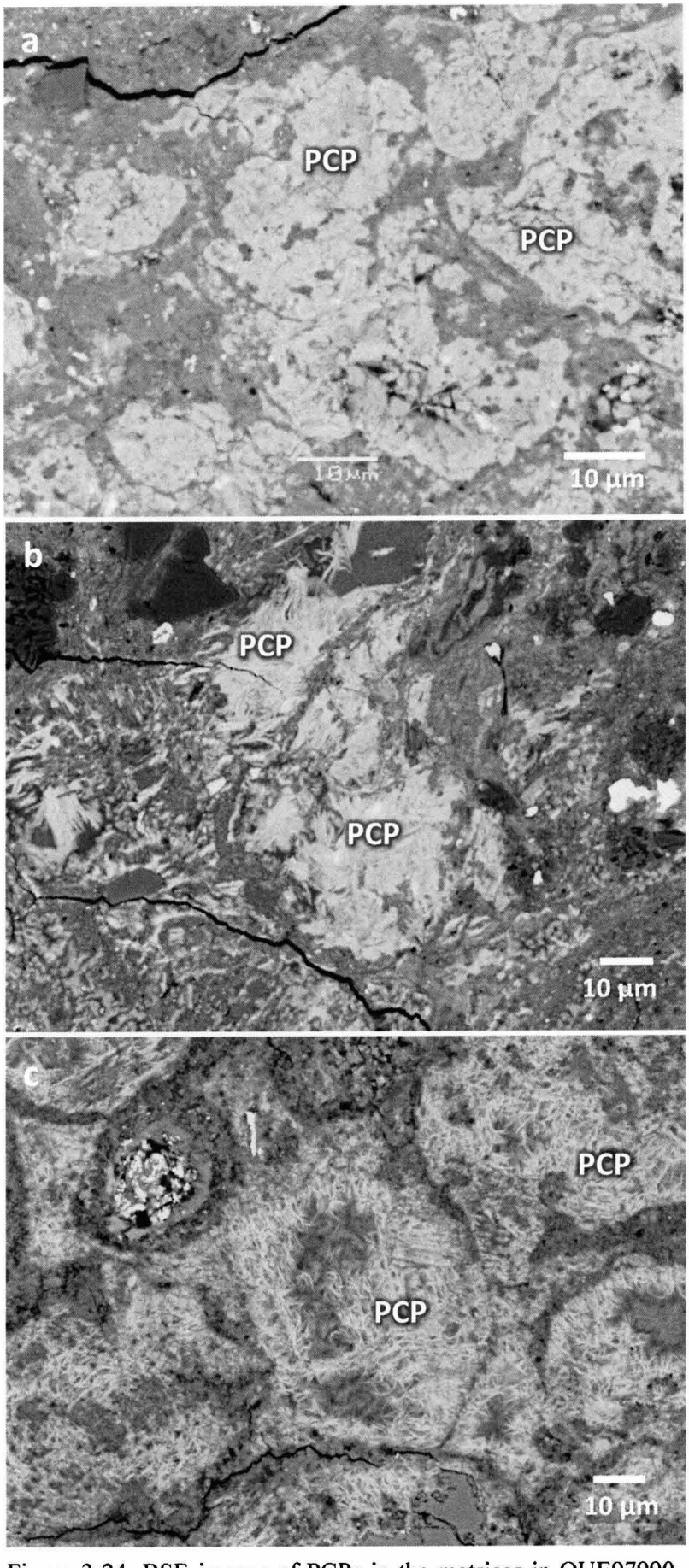

Figure 3-24. BSE images of PCPs in the matrices in QUE97990 (a), Y791198 (b) and Nogoya (c). PCPs in QUE 97990 and Y791198 commonly show massive texture. On the other hand, PCPs in Cold Bokkeveld show fibrous texture.

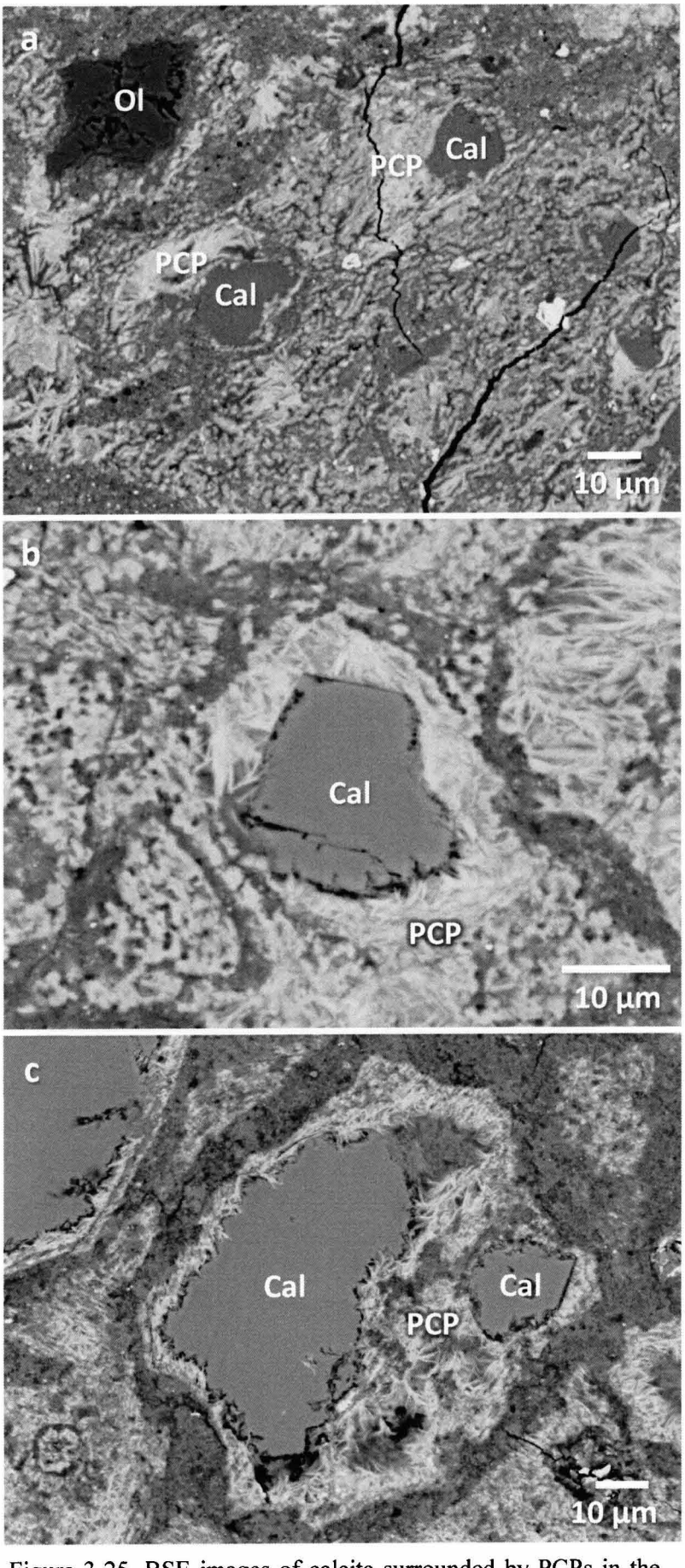

Figure 3-25. BSE images of calcite surrounded by PCPs in the matrices in QUE97990 (a), Cold Bokkeveld (b) and Nogoya (c).

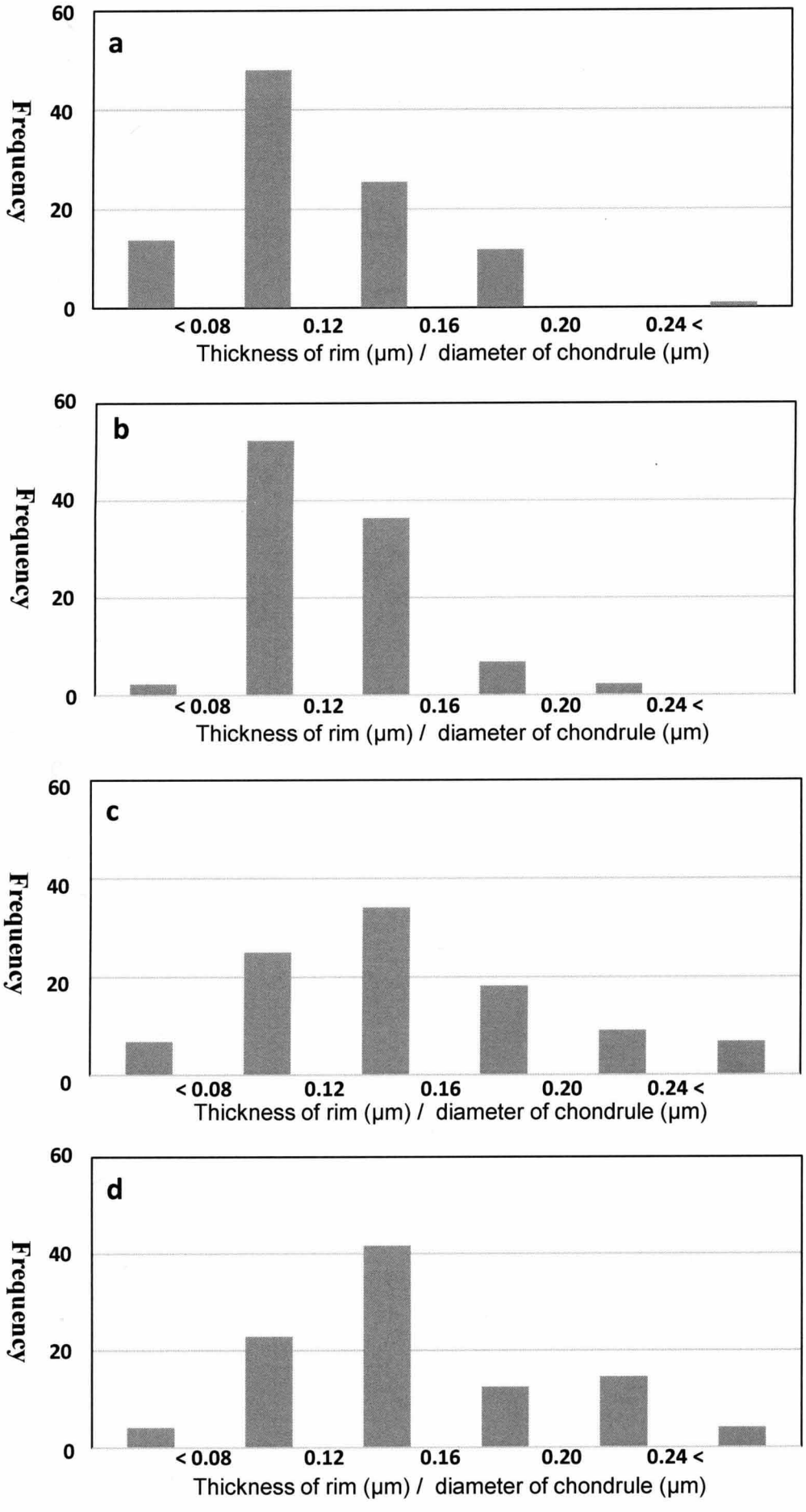

Figure 3-25. These graphs show distribution of thickness of the rims / diameter of the surrounded chondrules in QUE97990 (a), Y791198 (b), Cold Bokkeveld (c) and Nogoya (d).

Table1 Modal compositions of major components

	Murchison	Murray	Mighei	QUE97990	Yamato 791198	Cold Bokkeveld		Nogoya	
	Host	Host	Host	Host	Host	Host	Clast	Host	Clast
Chondrule	14	7	4	25	22	8	14	6	9
Chondrule rim	3	4	2	14	17	5	11	1	8
Matix	83	89	94	61	61	87	75	93	83

Table 2 Diameter of chondrules

	Murchison	Murray	Mighei	QUE97990	Yamato 791198	Cold Bokkeveld	Nogoya
Range (μm)	80-800	100-700	100-900	100-850	100-400	150-900	80-500
Average (μm)	194	322	308	205	193	214	158

Table 3 EDS analyses of chondrule mesostases

	Chondrule mesostases				
	Murchison	Murray	Mighei	QUE97990	Yamato791198
SiO_2 (wt%)	22.60 (± 2.32)*	21.88 (± 4.00)	27.62 (± 1.70)	20.88 (± 3.52)	28.70 (± 2.58)
TiO_2	0.25 (± 0.15)	0.18 (± 0.16)	0.26 (± 0.11)	0.23 (± 0.58)	0.30 (± 0.57)
$Al2O_3$	5.11 (± 2.63)	4.43 (± 1.71)	5.18 (± 2.10)	5.77 (± 1.73)	5.58 (± 1.16)
Cr_2O_3	0.47 (± 0.38)	0.32 (± 0.24)	0.51 (± 0.28)	0.39 (± 0.43)	0.52 (± 0.36)
FeO	37.00 (± 7.88)	43.09 (± 9.29)	28.30 (± 3.19)	34.71 (± 6.16)	21.26 (± 3.30)
NiO	0.65 (± 1.31)	0.41 (± 0.37)	0.42 (± 0.26)	0.52 (± 0.48)	0.46 (± 0.50)
MnO	0.18 (± 0.13)	0.23 (± 0.17)	0.22 (± 0.14)	0.26 (± 0.17)	0.23 (± 0.15)
MgO	8.66 (± 2.50)	8.15 (± 4.62)	17.31 (± 3.06)	11.24 (± 2.07)	20.78 (± 2.87)
CaO	1.27 (± 1.20)	0.80 (± 0.95)	0.43 (± 0.43)	1.4 (± 1.29)	0.69 (± 0.90)
Na_2O	0.37 (± 0.21)	0.29 (± 0.21)	0.24 (± 0.20)	0.34 (± 0.21)	0.19 (± 0.13)
S	0.51 (± 0.66)	0.61 (± 0.58)	0.64 (± 0.36)	1.47 (± 0.58)	0.72 (± 0.13)
Total	76.43	80.45	80.74	76.75	79.00

	chondrule mesostases	
	Cold Bokkeveld	Nogoya
SiO_2 (wt%)	30.00 (± 3.66)	24.34 (± 1.25)
TiO_2	0.17 (± 0.11)	0.18 (± 0.12)
$Al2O_3$	3.26 (± 2.19)	4.03 (± 0.29)
Cr_2O_3	0.52 (± 0.30)	0.40 (± 0.23)
FeO	20.82 (± 7.60)	32.19 (± 5.74)
NiO	0.71 (± 0.46)	0.32 (± 0.33)
MnO	0.23 (± 0.14)	0.20 (± 0.14)
MgO	19.76 (± 3.66)	12.24 (± 2.07)
CaO	0.44 (± 0.61)	0.48 (± 1.01)
Na_2O	0.22 (± 0.14)	0.21 (± 0.14)
S	0.67 (± 0.14)	0.60 (± 0.70)
Total	76.52	74.72

The analyses were peformed by using a defocused beam (~5 μm in diameter).
Fe contents are calculated as FeO, but part pf Fe is probably contributed from Fe sulfide
*Standard deviation.

Table 4 EDS analyses of materials in the chondrule embayment and rims

	QUE97990			Y791198	
	Embayment		Rim	Embayment	Rim
	Tochilinite-rich	Cronstedtite-rich	Mg-Fe serpentine-rich	Mg-Fe serpentine-rich	Mg-Fe serpentine-rich
No. of analyses	20	21	40	35	40
SiO_2 (wt%)	3.47 (± 0.99)*	20.3 (± 3.3)	24.3 (± 1.9)	26.8 (± 1.2)	28.4 (± 1.2)
TiO_2	0.14 (± 0.05)	0.11 (± 0.09)	0.11 (± 0.09)	0.2 (± 0.10)	0.13 (± 0.10)
$Al2O_3$	0.55 (± 0.14)	3.98 (± 0.87)	2.87 (± 0.48)	2.58 (± 0.61)	2.21 (± 0.22)
Cr_2O_3	1.78 (± 1.09)	0.61 (± 0.92)	0.44 (± 0.17)	0.53 (± 0.24)	0.48 (± 0.24)
FeO	46.1 (± 2.9)	40.6 (± 11.4)	25.2 (± 1.7)	29.0 (± 2.5)	27.78 (± 1.9)
NiO	11.1 (± 1.7)	2.09 (± 1.62)	2.59 (± 0.54)	2.20 (± 0.65)	2.46 (± 0.44)
MnO	1.15 (± 0.33)	1.00 (± 0.39)	0.18 (± 0.21)	0.86 (± 0.13)	0.84 (± 0.21)
MgO	3.83 (± 0.47)	8.91 (± 2.93)	14.4 (± 1.8)	14.4 (± 1.6)	15.6 (± 1.7)
CaO	0.73 (± 0.17)	0.50 (± 0.50)	1.03 (± 0.28)	0.65 (± 0.11)	0.31 (± 0.12)
Na_2O	0.13 (± 0.07)	0.36 (± 0.23)	0.16 (± 0.12)	0.21 (± 0.10)	0.19 (± 0.12)
S	15.6 (± 1.1)	2.92 (± 1.48)	4.08 (± 0.70)	3.49 (± 0.88)	3.53 (± 0.73)
Total	84.6	81.4	75.4	80.9	81.9

The analyses were performed by using a defoucused beam (~5 μm in diameter).
Fe contents are calculated as FeO, but part pf Fe is probably contributed from Fe sulfide
*Standard deviation.

Table 5 Existence ration of anhydrous silicate minerals in the rims and matrices

	Murchison			Murray		Mighei		QUE97990			Y791198		Cold Bokkeveld
	Rim	Matrix	Mag-clast	Rim	Matrix	Rim	Matrix	Rim	Matrix	Mag-calst	Rim	Matrix	Mag-clast
Olivine	37	25	15	34	27	33	38	51	36	0	54	43	37
Enstatite	11	35	25	21	22	11	22	26	22	0	5	8	7
Diopside	1	2	7	8	5	4	1	5	4	2	1	1	0
Spinel	0	0	0	0	3	1	0	0	1	0	0	1	0
Ferrosilite	0	1	0	0	0	0	0	0	0	0	0	0	0
Other	0	0	0	0	0	0	1	0	0	0	0	0	0
Total (Nmber)	49	63	47	63	57	49	62	82	63	2	60	53	44

The analyses were performed randomly selected opaque minerals (< 50 grains) in the rims in each meteorites.
Mag-clast = Magnetite-rich clast

Table 6 Existence ration of opaque minerals in the rims and matrices

	Murchison			Murray		Mighei	
	Rim	Matrix	Mag-clast	Rim	Matrix	Rim	Matrix
Fe-metal	5	5	0	1	1	1	1
Troilite	13	18	2	16	10	18	13
Pentlandite	39	38	4	57	32	52	38
Fe-Ni-S-P	1	16	0	10	3	0	0
Magnetite	7	12	50	3	4	0	0
Fe-Ni-P	0	5	0	0	3	0	0
Chromite	0	0	0	1	0	0	0
Fe-Cr-S	0	1	0	0	0	0	0
Fe-Mn-Ni-S	0	0	0	0	0	0	0
Fe-Cr-S-O	1	0	0	0	0	0	0
Fe-Cr-Ni-P	0	0	0	0	0	0	0
Others	1	0	0	0	0	0	0
Total (Number)	67	95	56	88	53	71	52

	QUE97990			Y791198		Cold Bokkeveld			Nogoya	
	Rim	Matrix	Mag-clast	Rims	Matrix	Rim	Matix	Mag-clast	Rim	Matrix
Fe-metal	12	16	1	5	2	0	1	1	0	0
Troilite	48	31	2	40	26	9	7	8	0	3
Pentlandite	47	21	5	66	37	44	30	11	46	53
Fe-Ni-S-P	0	0	0	3	8	8	13	0	0	0
Magnetite	0	0	29	0	0	0	9	102	0	0
Fe-Ni-P	1	1	0	1	0	3	7	0	0	0
Chromite	0	6	0	1	0	0	3	0	4	4
Fe-Cr-S	0	0	0	0	0	0	1	0	0	0
Fe-Mn-Ni-S	0	0	0	0	0	2	0	0	0	0
Fe-Cr-S-O	0	0	0	0	0	0	0	0	0	0
Fe-Cr-Ni-P	0	0	0	0	0	0	0	0	2	0
Others	0	0	0	0	0	0	0	1	0	0
Total (Number)	108	75	37	116	73	66	71	123	52	60

The analyses were performed randomly selected opaque minerals (< 50 grains) in the rims in each meteorites.

Table 7 EDS analyses of minor minerals in the rims and matrices

	Rim		
	Fe-Ni-P-S ric materials	Fe-Ni-P rich materials	Fe-Mn-Ni-S rich materials
SiO_2 (wt%)	0.75 (± 0.65)*	1.45 (± 0.95)*	2.67 (± 1.98)
TiO_2	0.21 (± 0.12)	0.12 (± 0.17)	---
Al_2O_3	0.23 (± 0.15)	0.21 (± 0.04)	0.13 (± 0.11)
MgO	0.45 (± 0.44)	0.91 (± 0.39)	1.86 (± 1.25)
CaO	0.47 (± 0.68)	0.17 (± 0.11)	0.46 (± 0.45)
Na_2O	0.89 (± 0.68)	0.39 (± 0.01)	0.03 (± 0.04)
Fe	29.47 (± 1.45)	54.09 (± 9.19)	21.24 (± 9.73)
Ni	30.76 (± 3.03)	30.42 (± 8.88)	16.40 (± 3.52)
Mn	0.20 0.12)	---	9.16 (± 8.82)
Cr	0.63 (± 0.81)	0.16 (± 0.07)	0.81 (± 0.21)
P	6.25 (± 2.11)	19.70 (± 7.68)	---
S	24.47 (± 3.05)	0.33 (± 0.24)	33.59 (± 1.45)
Total	94.55	104.97	103.33

	Rim
	Fe-Cr-Ni-P rich materials
SiO_2 (wt%)	1.17
TiO_2	---
Al_2O_3	0.09
MgO	0.29
CaO	0.23
Na_2O	---
Fe	46.39
Ni	8.35
Mn	---
Cr	21.04
P	17.42
S	---
Total	94.98

	Matrix		
	Fe-Ni-P-S ric materials	Fe-Ni-P rich materials	Fe-Cr-S rich materials
SiO_2 (wt%)	0.75 (± 0.65)*	1.45 (± 0.95)	2.67 (± 1.98)
TiO_2	0.21 (± 0.12)	0.12 (± 0.17)	---
Al_2O_3	0.23 (± 0.15)	0.21 (± 0.04)	0.13 (± 0.11)
MgO	0.45 (± 0.44)	0.91 (± 0.39)	1.86 (± 1.25)
CaO	0.47 (± 0.68)	0.17 (± 0.11)	0.46 (± 0.45)
Na_2O	0.89 (± 0.68)	0.39 (± 0.01)	0.03 (± 0.04)
Fe	29.47 (± 1.45)	54.09 (± 9.19)	21.24 (± 9.73)
Ni	30.76 (± 3.03)	30.42 (± 8.88)	16.40 (± 3.52)
Mn	0.20 0.12)	---	9.16 (± 8.82)
Cr	0.63 (± 0.81)	0.16 (± 0.07)	0.81 (± 0.21)
P	6.25 (± 2.11)	19.70 (± 7.68)	---
S	24.47 (± 3.05)	0.33 (± 0.24)	33.59 (± 1.45)
Total	94.55	104.97	103.33

The analyses were peformed by using a defocused beam (~5 μm in diameter).
Fe contents are calculated as FeO, but part pf Fe is probably contributed from Fe sulfide
The Fe-Cr-Ni-P rich material is only one grain.
*Standard deviation.

Table 8 EDS analyses of chondrule rims

	Chondrule rims			
	Murchison	Murray	Mighei	QUE97990
SiO_2 (wt%)	23.37 (± 1.70)*	24.26 (± 2.62)	24.01 (± 1.36)	23.92 (± 2.55)
TiO_2	0.14 (± 0.09)	0.13 (± 0.08)	0.13 (± 0.09)	0.12 (± 0.06)
$Al2O_3$	2.08 (± 0.39)	2.54 (± 0.50)	2.64 (± 0.51)	2.75 (± 0.35)
Cr_2O_3	0.39 (± 0.19)	0.43 (± 0.17)	0.53 (± 0.12)	0.46 (± 0.10)
FeO	24.72 (± 3.32)	28.01 (± 6.11)	20.68 (± 3.37)	25.97 (± 2.00)
NiO	1.76 (± 0.41)	1.83 (± 0.46)	2.00 (± 0.53)	2.33 (± 0.40)
MnO	0.18 (± 0.15)	0.26 (± 0.17)	0.23 (± 0.14)	0.20 (± 0.08)
MgO	13.77 (± 1.46)	13.98 (± 2.18)	13.84 (± 1.02)	14.10 (± 1.92)
CaO	0.69 (± 0.29)	0.73 (± 0.50)	0.75 (± 0.31)	0.96 (± 0.28)
Na_2O	0.60 (± 0.19)	0.39 (± 0.23)	0.70 (± 0.21)	0.58 (± 0.14)
S	2.64 (± 0.59)	2.73 (± 1.02)	2.70 (± 0.23)	3.48 (± 0.74)
Total	70.20	75.00	68.40	75.46

	Chondrule rims		
	Yamato791198	Cold Bokkeveld	Nogoya
SiO_2 (wt%)	27.00 (± 1.05)	29.35 (± 2.00)	28.12 (± 1.47)
TiO_2	0.38 (± 0.18)	0.11 (± 0.07)	0.16 (± 0.06)
$Al2O_3$	2.24 (± 0.25)	1.95 (± 0.20)	2.02 (± 0.18)
Cr_2O_3	0.31 (± 0.14)	0.54 (± 0.16)	0.57 (± 0.11)
FeO	27.33 (± 1.12)	20.97 (± 3.25)	18.48 (± 1.38)
NiO	2.20 (± 0.23)	1.79 (± 0.31)	1.82 (± 0.30)
MnO	0.32 (± 0.14)	0.20 (± 0.13)	0.16 (± 0.09)
MgO	15.49 (± 0.87)	18.05 (± 0.99)	17.84 (± 1.47)
CaO	0.22 (± 0.13)	0.73 (± 0.37)	0.80 (± 0.53)
Na_2O	0.17 (± 0.05)	0.12 (± 0.09)	0.72 (± 0.11)
S	4.64 (± 0.43)	1.41 (± 1.48)	2.23 (± 0.41)
Total	79.87	74.19	72.82

The analyses were peformed by using a defocused beam (~5 μm in diameter).
Fe contents are calculated as FeO, but part pf Fe is probably contributed from Fe sulfide
*Standard deviation.

Table 9 EDS analyses of matrices

	Matrix			
	Murchison	Murray	Mighei	QUE97990
SiO_2 (wt%)	23.76 (± 2.23)*	26.02 (± 2.26)	24.15 (± 2.27)	24.47 (± 2.04)
TiO_2	0.09 (± 0.08)	0.14 (± 0.11)	0.15 (± 0.23)	0.19 (± 0.17)
$Al2O_3$	2.26 (± 0.48)	2.84 (± 0.57)	2.54 (± 0.69)	2.60 (± 0.67)
Cr_2O_3	0.34 (± 0.15)	0.38 (± 0.17)	0.42 (± 0.18)	0.45 (± 0.20)
FeO	26.56 (± 3.56)	28.25 (± 4.44)	20.94 (± 2.14)	25.86 (± 2.20)
NiO	1.67 (± 0.46)	1.47 (± 0.50)	1.60 (± 0.50)	2.30 (± 0.51)
MnO	0.34 (± 0.30)	0.20 (± 0.12)	0.18 (± 0.12)	0.18 (± 0.17)
MgO	13.52 (± 2.15)	14.45 (± 2.19)	13.96 (± 1.69)	13.94 (± 1.79)
CaO	0.77 (± 0.44)	0.81 (± 0.78)	0.52 (± 0.62)	0.97 (± 0.93)
Na_2O	0.61 (± 0.16)	0.20 (± 0.11)	0.53 (± 0.20)	0.57 (± 0.19)
S	2.47 (± 0.62)	2.34 (± 0.59)	2.35 (± 0.56)	3.69 (± 0.71)
Total	72.15	76.90	67.15	74.96

	Matrix		
	Yamato791198	Cold Bokkeveld	Nogoya
SiO_2 (wt%)	27.54 (± 1.13)	31.82 (± 2.14)	30.35 (± 1.76)
TiO_2	0.29 (± 0.22)	0.12 (± 0.11)	0.14 (± 0.11)
$Al2O_3$	2.15 (± 0.37)	1.85 (± 0.31)	2.05 (± 0.34)
Cr_2O_3	0.40 (± 0.18)	0.50 (± 0.19)	0.32 (± 0.24)
FeO	26.68 (± 1.92)	18.93 (± 2.45)	20.09 (± 2.54)
NiO	2.16 0.48	1.79 (± 0.39)	1.69 (± 0.44)
MnO	0.21 (± 0.15)	0.20 (± 0.16)	0.40 (± 0.23)
MgO	15.34 (± 0.81)	18.89 (± 1.84)	18.35 (± 2.29)
CaO	0.28 (± 0.21)	0.69 (± 0.43)	0.21 (± 0.19)
Na_2O	0.20 (± 0.14)	0.14 (± 0.12)	0.72 (± 0.19)
S	3.31 (± 0.55)	1.28 (± 0.42)	2.25 (± 0.50)
Total	78.25	78.81	76.31

The analyses were peformed by using a defocused beam (~5 μm in diameter).
Fe contents are calculated as FeO, but part pf Fe is probably contributed from Fe sulfide
*Standard deviation.

Table 10 Modal compositions of major components in host meteorites and Magnetite-rich clasts

	QUE97990		Murchison		Cold Bokkeveld	
	host	clast	host	clast	host	clast
Chondrule	25	17	13	10	14	0
Chondrule rim	14	0	4	0	16	0
Matrix	61	83	83	90	70	100

Table 11 EDS analyses of phyllosilicates in host matrices and clast matirces

	QUE97990				Cold Bokkeveld			
	matrices		clasts matrices		matrices		clasts matrices	
No. of analyses	56		11		47		27	
SiO_2	24.47	(± 2.04)	33.12	(± 0.53)	31.82	(± 2.14)	31.04	(± 2.68)
TiO_2	0.19	(± 0.17)	0.07	(± 0.06)	0.12	(± 0.11)	0.09	(± 0.06)
Al_2O_3	2.60	(± 0.67)	3.37	(± 0.31)	1.85	(± 0.31)	2.04	(± 0.21)
Cr2O3	0.45	(± 0.20)	0.30	(± 0.15)	0.50	(± 0.19)	0.38	(± 0.06)
FeO	25.86	(± 2.20)	19.80	(± 0.74)	18.93	(± 2.45)	17.28	(± 2.50)
NiO	2.30	(± 0.51)	1.26	(± 0.32)	1.79	(± 0.39)	1.35	(± 0.20)
MnO	0.18	(± 0.17)	0.38	(± 0.07)	0.20	(± 0.16)	0.18	(± 0.06)
MgO	13.94	(± 1.79)	21.59	(± 0.56)	18.89	(± 1.84)	17.81	(± 0.72)
CaO	0.97	(± 0.93)	0.45	(± 0.18)	0.69	(± 0.43)	0.38	(± 0.13)
Na_2O	0.57	(± 0.19)	0.10	(± 0.14)	0.14	(± 0.12)	0.14	(± 0.04)
S	3.69	(± 0.71)	1.17	(± 0.06)	1.28	(± 0.42)	1.49	(± 0.29)
total	74.96		81.45		78.81		72.18	

	Murchison			
	matrices		clasts matrices	
No. of analyses	40		13	
SiO_2	23.76	(± 2.23)	28.08	(± 1.91)
TiO_2	0.09	(± 0.08)	0.10	(± 0.07)
Al_2O_3	2.26	(± 0.48)	2.79	(± 0.28)
Cr2O3	0.34	(± 0.15)	0.37	(± 0.06)
FeO	26.56	(± 3.56)	18.85	(± 4.01)
NiO	1.67	(± 0.46)	1.72	(± 0.44)
MnO	0.34	(± 0.30)	0.25	(± 0.06)
MgO	13.52	(± 2.15)	17.28	(± 2.25)
CaO	0.77	(± 0.44)	1.04	(± 0.46)
Na_2O	0.61	(± 0.16)	0.60	(± 0.17)
S	2.47	(± 0.62)	3.20	(± 1.14)
total	72.15		74.27	

The analyses were peformed by using a defocused beam (~5 μm in diameter).
Fe contents are calculated as FeO, but part pf Fe is probably contributed from Fe sulfide
*Standard deviation.

Chapter 4

Discussion: Aqueous alteration process in the unbrecciated meteorites or regions of four CM chondrites

QUE97990 and Yamato 791198 are composed of the single and unique lithology through whole rocks. Cold Bokkeveld and Nogoya show brecciated textures, but they include the large clast sufficient to examine their alteration history of the clast (described in chapter 2). Although the other studied meteorites also include the clasts, these are too small to be studied. Based on these investigation, I particular paid attention to QUE97990, Yamato 791198, and a part of Cold Bokkeveld and Nogoya.

4.1 Degrees of aqueous alteration

Based on the observation of the major components, the degree of alteration increases as follows: QUE97990 < Y791198 < Cold Bokkeveld < Nogoya. In generally, CM chondrites have experienced not only aqueous alteration, but also brecciation in various degrees. The chondrites have complex petrologic textures produced by these processes. As demonstrated in the present study, however, a careful distinction of unbrecciated CM chondrites and a detailed observation of two or more major components made possible to estimate a degree of aqueous alteration with higher reliability than that of previous studies

The mesostases in QUE97990 include quenched crystallites of diopside, but the chondrule mesostases in the other meteorites studied include no such crystallites. Quenched crystallites of diopside are commonly observed in chondrule mesostases in anhydrous type 3 chondrites (e.g., Jones and Scott, 1989; Jones and Danielson, 1997), but have not been reported from any CM chondrites. These results suggest that QUE97990 is the lowest altered CM chondrites.

4.2 Petrological and mineralogical changes with advancing aqueous alteration

4.2.1 Chondrules

Components of chondrules are replaced to phyllosilicates with increasing alteration in the following order; glassy material in mesostases, opaque minerals (Fe-Ni metal and Fe-sulfide), enstatite, olivine. It is likely that first Fe and S components are provided for the mesostases with alteration of opaque minerals. As following, Mg and Si components would be provided for the mesostases with alteration of Mg-rich silicates. However, FeO contents in the mesostases of high altered meteorites (e.g. Nogoya) are more abundant than that of low altered meteorites (e.g. Y791198). This result suggests that Fe components were provided for the chondrules from outside (e.g. the rims) of chondrules.

4.2.2 Chondrule margins

The texture and mineralogy of the embayments on the chondrule surfaces suggest that they were formed by replacing opaque nodules, which were located near the

surfaces of their host chondrules, during aqueous alteration. The Fe-Ni metal at the bottom of the embayments is probably an unaltered residue of opaque nodules, and the tochilinite-rich and cronstedtite-rich materials are secondary products formed by replacing Fe-Ni metal and/or troilite in opaque nodules (Figs. 3-13b, c, 3-14b, c). In Y791198, Cold Bokkeveld and Nogoya, the inside of the embayments has probably been more extensively altered than in QUE97990, and thus has been largely replaced by the Mg-Fe serpentine-rich material (Figs. 3-12b, d, f and 3-15b). The texture of the chondrule embayments and rims in the four meteorites suggests that the alteration reaction took place after the chondrules acquired their own rims. The chondrule margins have probably been involved in extensive dissolution, and transportation and deposition of dissolved ions in the rims. These reaction and process most likely proceeded with the presence of aqueous solutions. Thus, aqueous alteration in the four meteorites would occur on their parent bodies.

4.2.3 Chondrule rims

Thickness of the rims / diameter of the chondrules increase with increasing alteration (Fig. 3-25a-d). This result is apparently inconsistent with the result of similar measurement by Metzler et al. (1992), in which they concluded that there are no relation between thickness of rims and a degree of alteration. Metzler et al., (1992) may not discriminate different lithologies in brecciated meteorites. Moreover, I found that with increasing alteration, both abundance and diameter of chondrules decrease. These results might show that a part of chondrules becomes chondrules rims as aqueous alteration proceeds. This hypothesis is consistent with investigation of embayments that suggest extensively interaction between chondrules and rims.

The rims in QUE97990 and Y791198 commonly consist of mixture of Fe-Mg serpentine, Fe-sulfide, olivine and enstatite. In contrast, those of Cold Bokkeveld and Nogoya consist of almost Mg-Fe serpentine. Moreover, chemical compositions of the rims become Fe-poorer with increasing alteration (Table 6). These results show that Fe components migrate into outside rims (chondrule and /or matrix).

4.2.4 Matrix

PCPs in low altered meteorites (e.g. QUE97990) show massive texture, while PCPs in high altered meteorites (e.g. Nogoya) show fibrous clustered texture. This result suggests that texture of PCPs changes by increasing alteration. Chemical compositions of the serpentine become Fe-poor with progression of aqueous alteration. This result is same as that of the rims.

4.3 Where did the aqueous alteration occur?

The all observed meteorites show various evidence of aqueous alteration in their constituent components. Nogoya shows the most extensive altered textures in whole rocks, followed by that of Cold Bokkeveld, Y791198 and QUE97990. Even focusing on any components (chondrules, chondrule rims, matrices), the same sequence is delivered, suggesting that the components in each meteorite would have experienced aqueous alteration with a same degree. In other words, aqueous alteration would have occurred after the accretion of the components to same place on the parent body. This conclusion is consistent with observation of embayment (above discussed in chapter 4.2.2). On the other hand, chondrule rims and matrices become poor in FeO content with increasing

alteration, while the mesostases become rich in FeO content with advancing alteration. This result implies that Fe components in the rims and matrices migrated into chondrules. These results suggest that the each component have experienced aqueous alteration on same place and at same time. Thus, aqueous alteration would occur on their parent body after accretion.

Conclusion of Part I

Based on my research, degrees of aqueous alteration increase in the following order; QUE97990, Yamato 791198, Cold Bokkeveld, Nogoya. Furthermore, interaction among chondrules, chondrule rims and matrices occurred during aqueous alteration. These results suggested that these components have experienced aqueous alteration on same place and at same time. Thus, CM chondrites would have experienced aqueous alteration on their parent body. Moreover, my research revealed that QUE97990 is the lowest altered CM chondrites. This result suggests that the lowest altered meteorite in the CM chondrites also have experienced extensively aqueous alteration on their parent body.

Part II

Magnetite-rich clasts in CM chondrites: Implications for environments of aqueous alteration

Chapter 5

Introduction

How conditions did aqueous alteration occur in the CM chondrites?

In part II, let us focus on under what environments aqueous alteration occurred on the parent body (or bodies) of the CM chondrites. Previous researchers (e.g. Brearley, 2005) revealed that alteration conditions (oxidized/reduced or temperature) strongly correspond the chemical types of chondrites. Such conditions are mainly estimated by species and abundance of secondary minerals by aqueous alteration. CM chondrites are considered to have experienced aqueous alteration on reduced condition (e.g. Brearley, 2005) because the chondrites contain abundant tochilinite and Fe-sulfide as secondary minerals, which assemblage are stable at the reduced condition. On the other hand, CI chondrite is believed to have experienced aqueous alteration at oxidized condition (Brearley, 2005). The other hydrous carbonaceous chondrites (e.g. CO, CV, CR chondrites) are also considered to have experienced aqueous alteration on oxide conditions by their secondary minerals. Although many researchers have been concerned with the environment where and how aqueous alteration of chondritic meteorites took place (e.g. McSween 1979; Tomeoka and Buseck, 1985; Rubin et al., 2008), a widely acceptable alteration scenario has not been established yet.

In the following chapters, I will show unique clasts in the three CM chondrites (QUE97990, Murchison and Cold Bokkeveld) which would be important key how environment aqueous alteration occurred in the CM chondrites. Although the three CM

chondrites show different mineralogy, these clasts have very similar characteristics. Moreover, the clasts show many mineralogical similarities to CI chondrites. I believe that the clasts give us new insight about condition during aqueous alteration in the CM chondrites.

Chapter 6

Results: Petrologic and mineralogical characteristics of magnetite-rich clasts and host meteorites

Because a detailed description of host meteorites of Murchison, QUE97990 and Cold Bokkeveld have already described (chapter 3), this chapter is focusing on the mineralogical and petrological differences between host rock and guest rock (i.e. clasts).

6.1 QUE97990

6.1.1 Magnetite-rich clasts

In the matrix of QUE97990, one unique clast was found: The clast (0.21 mm^2) shows irregular shape (Fig. 6-1a). The clast includes chondrules ("clast chondrule") and matrix ("clast matrix"). Table 10 shows modal abundance of major components as follows; chondrule is 17 vol%, matrix is 83 vol%. Chondrule rims are not found in the clast.

Clast chondrule

The chondrules mainly consist of phenocrysts of olivine and enstatite, with minor amount of diopside, and mesostasis. Most of phenocrysts are forsterite, and have been partly replaced by phyllosilicate (Fig. 6-2a). Such altered phenocrysts do not occur in

the host meteorite (described in chapter 3.4.2). Previous studies (e.g. Hanowski and Brearley, 2001) reported that forsterite is less susceptible to aqueous alteration relative to other silicates in the CM chondrites. Therefore, degree of aqueous alteration of the clasts can be considered to be higher than that in host meteorite.

Clast matrix

The clast matrix mainly consists of Mg-Fe-Si-Al-O rich materials, magnetite and minor amounts of fine-grained (< 10 μm in size) troilite, pentlandite, Fe-Ni metal, Ca-carbonate, diopside. Table 11 shows chemical compositions of Mg-Fe-Si-Al-O rich materials. The summations of Mg-Fe-Si-Al-O rich materials commonly range between 75 and 85 by weight. The missing portions may be water. Moreover, Mg-Fe-Si-Al-O rich materials show fibrous texture. Thus, I identified Mg-Fe-Al-O rich materials as phyllosilicates. The opaque minerals mainly consist of magnetite (about 80 % in abundance) (Fig. 6-4). Magnetite in the clast matrix appears as not only a granular crystal with several μm in diameter, but also as framboidal polycrystalline assemblage (Fig. 6-5a). Moreover, PCPs are completely absent in the clast matrix. Chemical compositions of phyllosilicate in the clast matrix are similar to those of mixture of serpentine and saponite (Fig. 6-6).

6.2 Murchison

6.2.1 Magnetite-rich clasts

In the matrix of Murchison, nine magnetite-rich clasts were found. Magnetite-rich clasts show irregular shape with 0.02 to 1.00 mm in diameter (Fig. 6-1b). The clasts consist of chondrules and matrix. Table 10 shows modal compositions of major

components as follows; chondrules are 10 vol%, matrix is 90 vol%.

Clast chondrule

Chondrules mainly consist of phenocrysts of olivine and enstatite, with minor amount of diopside, and mesostases. Chondrules are not surrounded by fine-grained rims. Phenocrysts of forsterite have been partly replaced by phyllosilicate (Fig. 6-2b). Such altered phenocrysts are not found in the host meteorite. These results show that degrees of aqueous alteration in the clasts are higher than that in host meteorite.

Clast matrix

The clast matrix mainly consists of Mg-Fe-Si-Al-O rich materials and magnetite with minor amounts of fine-grained (10 μm in size) troilite, pentlandite, Ca-carbonate, olivine, enstatite and diopside. The characteristics of Fe-Si-Al-O rich materials are similar to that of clast matrix in QUE97990. Thus, I identified Fe-Si-Al-O rich materials as phyllosilicates. The anhydrous silicate minerals mainly consist of enstatite (> 50 %) and olivine (> 30 %) (Fig. 6-3). The opaque minerals mainly consist of magnetite (> 80 %). Magnetite in the clast matrix develops not only granular euhedral shape, but also framboidal polycrystalline (Fig. 6-5a). PCPs are completely absent in the clast matrix. On the other hand, magnetite is rarely found (< 15 % of the opaque minerals in abundance) in the host matrix (Fig. 6-4). These results show that major opaque minerals are different between clast and host matrices. EDX analyses of phyllosilicate in the clasts and host matrices also show a small, but clear difference (Table 11, Fig. 6-6). Chemical compositions of phyllosilicate in the clast matrix are similar to mixing serpentine and saponite. These various characteristics of the clasts are similarities to that of QUE97990.

6.3 Cold Bokkeveld

6.3.1 Magnetite-rich clasts

In the matrix of Cold Bokkeveld, six magnetite-rich clasts were found: The clasts show irregular shape with 0.02 to 1.00 mm in diameter (Fig. 6-1c). The clasts mainly consist of matrix with minor amount of mineral fragments (< 1% in abundance). Chondrules rims are not found in the clasts.

Clast matrix

The clasts matrices mainly consist of Mg-Fe-Si-Al-O rich materials and magnetite with minor amounts of fine-grained (< 5 μm in size) troilite, pentlandite, Fe-Ni metal, Ca-carbonate, olivine and enstatite. The characteristics of Fe-Si-Al-O rich materials are similar to that of clast matrix in QUE97990 and Murchison. Thus, I identified Fe-Si-Al-O rich materials as phyllosilicates. The anhydrous silicates consist of olivine (> 80 %) and enstatite (< 20 %) (Fig. 6-3). The opaque minerals mainly consist of magnetite (> 80 %) (Fig. 6-4). Magnetite in the clast matrix develops not only granular euhedral shape, but also framboidal polycrystalline (Fig. 6-5c). PCPs are completely absent in the clast matrix. On the other hand, magnetite is rare in the host matrix (less than about 10 vol% of the opaque minerals in host matrix) (Fig. 6-4). These results show that major opaque minerals are different between clast and host matrix. EDX analyses of phyllosilicate in the clast matrix and host matrix also show a small, but clear difference (Fig. 6-6, Table 11). Chemical compositions of phyllosilicate in the clast matrix are similar to mixing serpentine and saponite (Fig. 6-7). Most of characteristics in the clasts are similarities to that of QUE97990 and Cold Bokkeveld.

6.4 TEM observation

In order to investigate difference between host and clast matrices with sub-micron scale, QUE97990, Murchison and Cold Bokkeveld were observed by TEM.

Host matrices in QUE97990 and Murchison

Fig. 6-8 shows that the host matrix in QUE97990 mainly consists of amorphous or nanocrystalline silicate materials and sulfide grains of various species are embedded within the amorphous silicate material. These characteristics of host matrix in QUE97990 are similar to that of Y791198 that was described in detail by Chizmadia and Brearley (2008). This result is also consistent with the SEM observation (described in chapter 3.4) suggesting relatively low degree of aqueous alteration of QUE97990 in the CM chondrites. On the other hand, crystalline serpentine commonly occurs in host matrix of Murchison (Fig. 6-9-11). As shown in Fig. 6-9, the serpentine crystal shows ribbon-like textures. Moreover, a part of the serpentine crystal show rounded shape (Fig. 6-10).

Clast matrix in Cold Bokkeveld

A magnetite-rich clast in Cold Bokkeveld mainly consists of relatively large phyllosilicates (0.1 to 1 μm in width and from 1 to 3 μm in length) and magnetite with minor amount of iron-sulfide grains. Fig. 6-12 shows a bright field image of framboidal magnetite, in which the crystals are developed with a clear euhedral shape with several hundred nm in diameter, and are arranged in disordered directions. Fig. 6-13 shows that acicular fibrous clusters of coarse phyllosilicates in the clast matrix of Cold Bokkeveld. Such clusters are commonly found in the CI chondrite (e.g. Tomeoka and Buseck, 1988), while tubular assemblage of phyllosilicate is rather common in the CM chondrites. High-resolution TEM image (Fig. 6-14) shows an intergrowth texture of serpentine and

saponite in the clasts matrices. Serpentine and saponite show fibrous and plate-like textures. The existence of saponite in the CM chondrites have not reported so far.

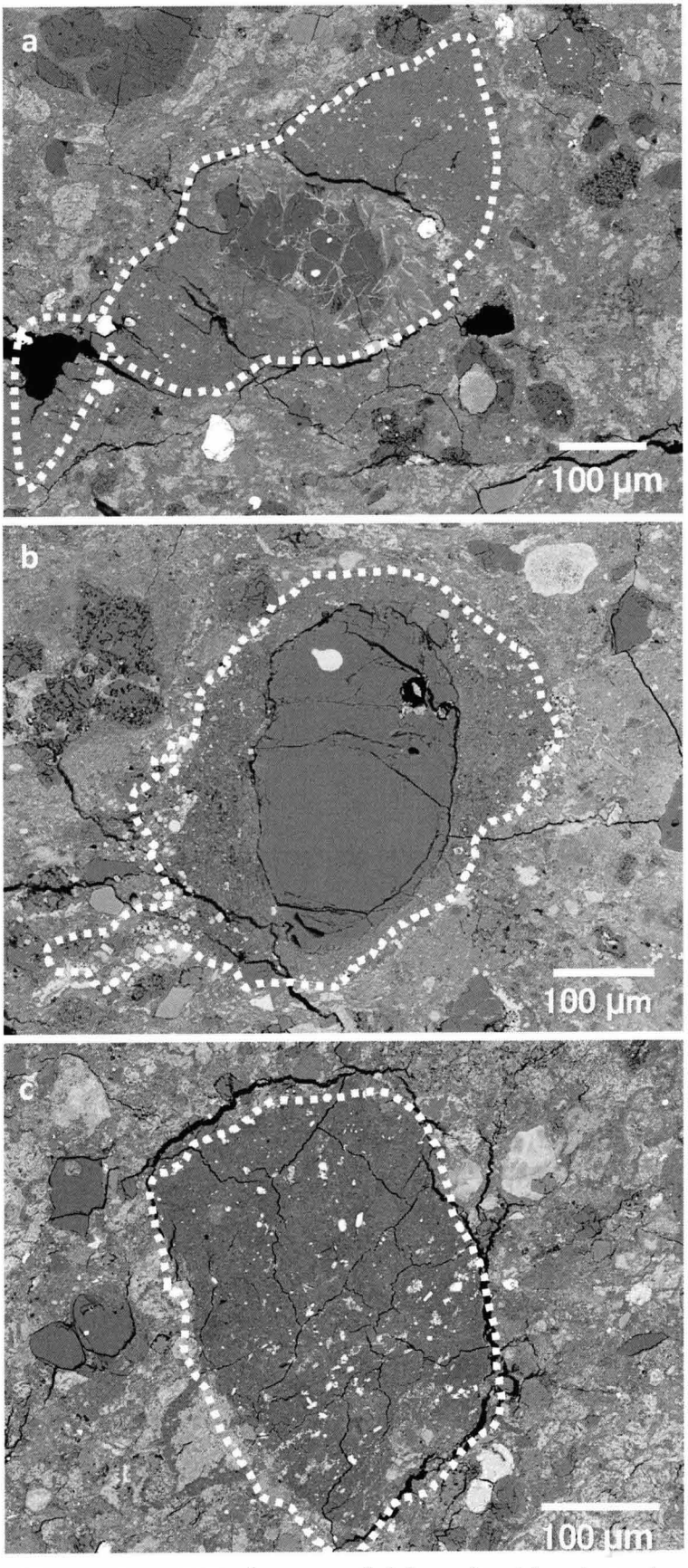

Figure 6-1. BSE images of Magnetite-rich clasts in QUE97990 (a), Murchison (b) and Cold Bokkeveld (c). Magnetite commonly occurs in the clast matrices.

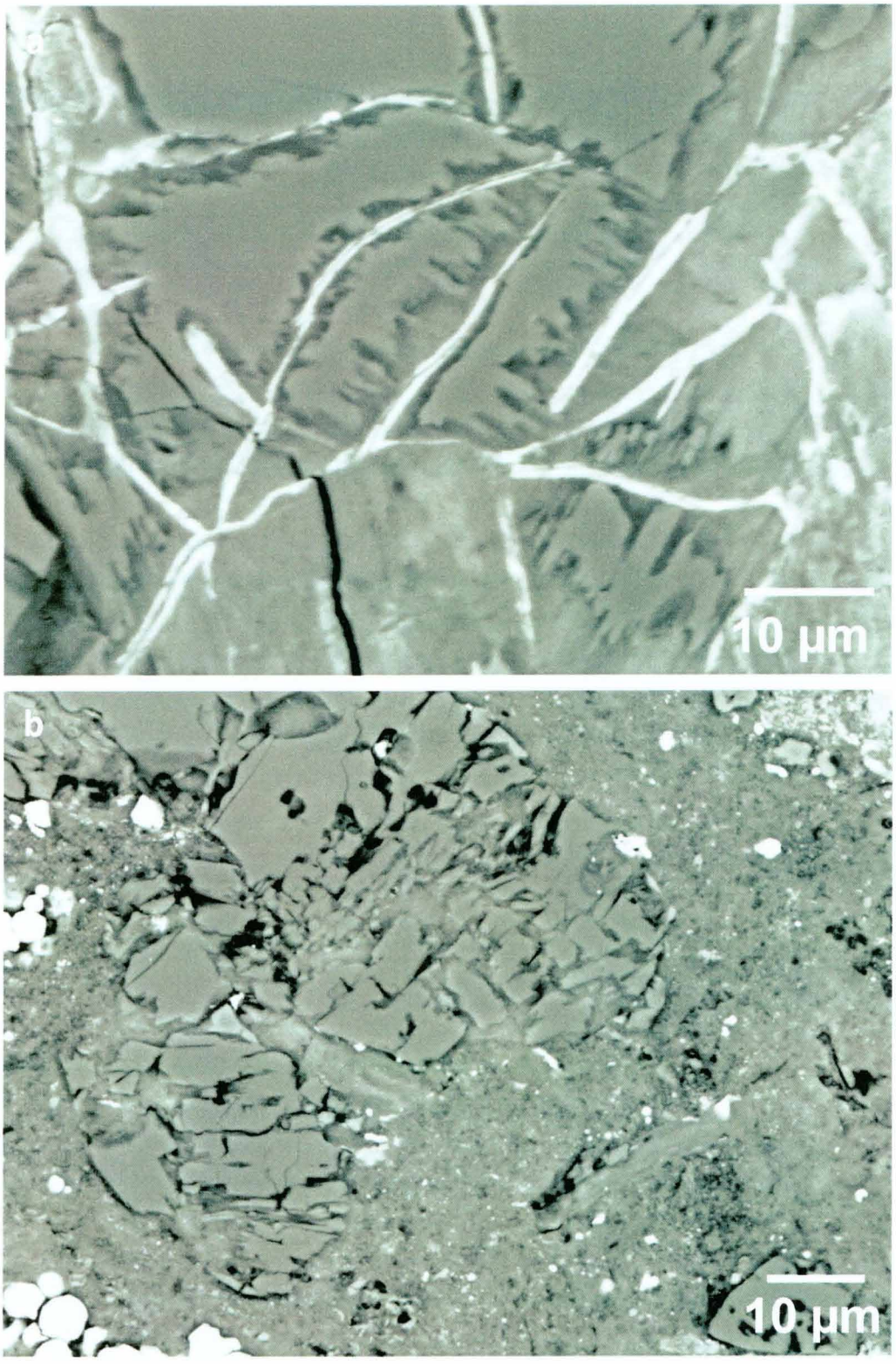

Figure 6-2. BSE images of phenocrysts in the chondrules in the magnetite-rich clasts in QUE97990 (a) and Murchison (b). The phenocrysts of olivine are partly altered by phyllosilicate.

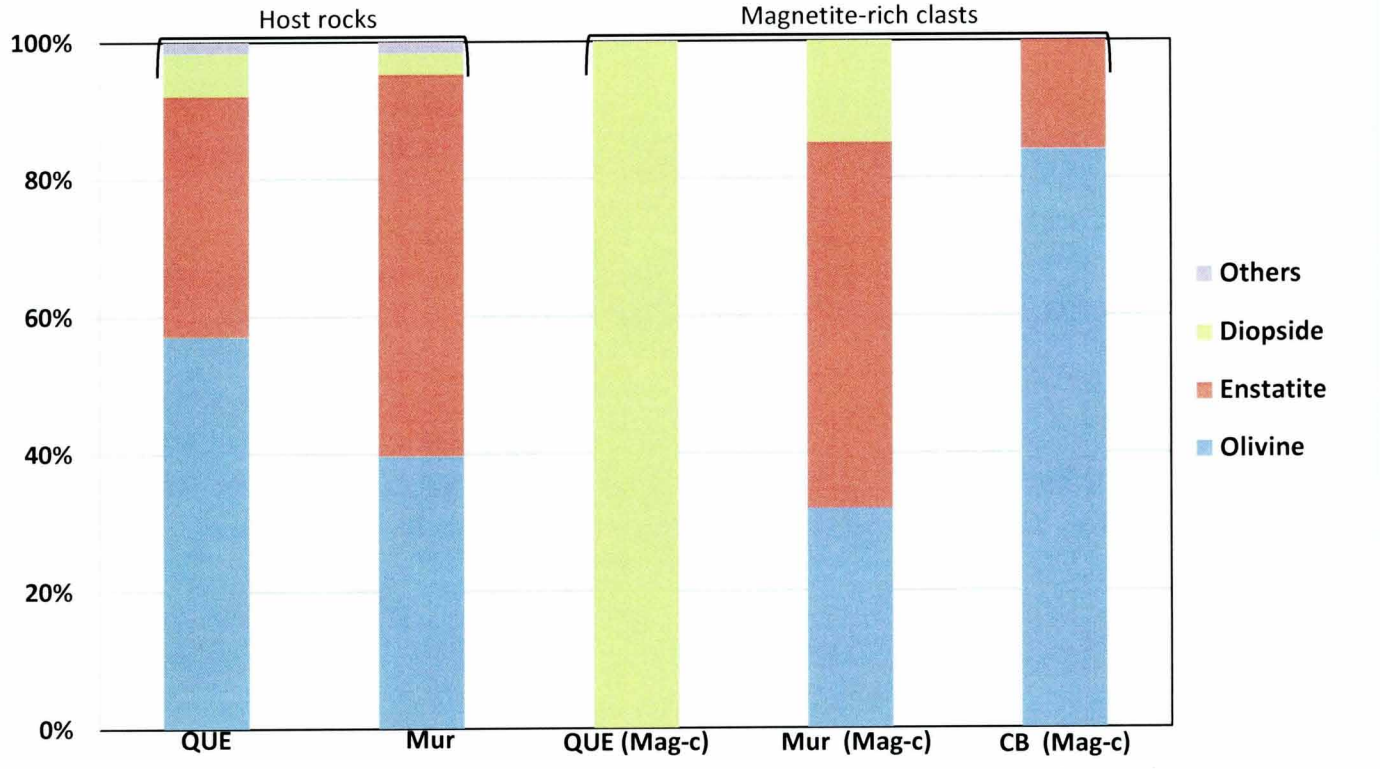

Figure 6-3. Existence ratio of anhydrous silicate minerals in the magnetite-rich clasts and host matrices. Only two grains of diopside as anhydrous silicates are found in the clast matrix of QUE97990. QUE = QUE97990, Mur = Murchison, CB = Cold Bokkeveld, Mag-c = Magnetite-rich clasts

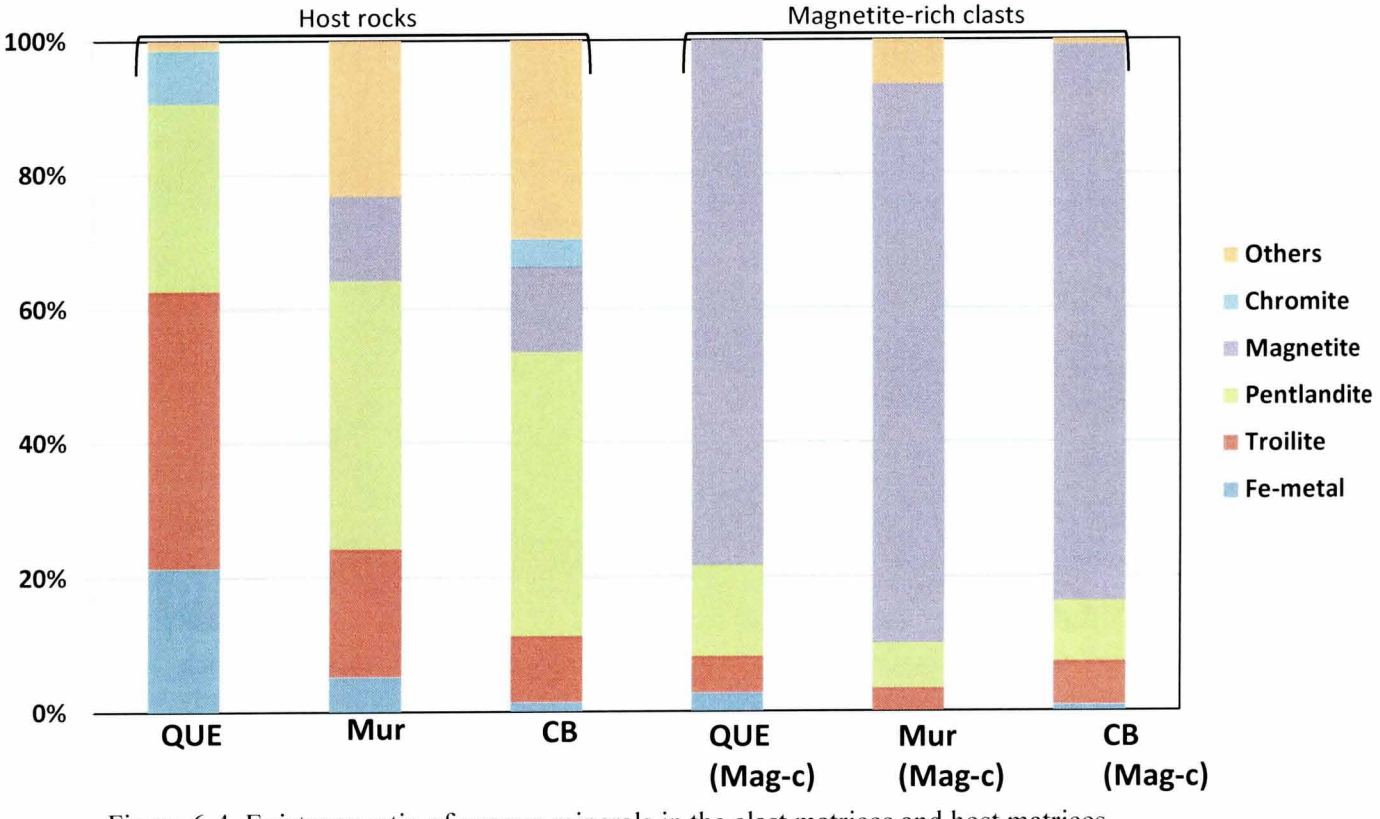

Figure 6-4. Existence ratio of opaque minerals in the clast matrices and host matrices. Magnetite in clast matrices is more abundant than that in host matrices. On the other hand, Fe-sulfide in host matrices is more abundant than that in clast matrices. QUE = QUE97990, Mur = Murchison, CB = Cold Bokkeveld, Mag-c = Magnetite-rich clasts

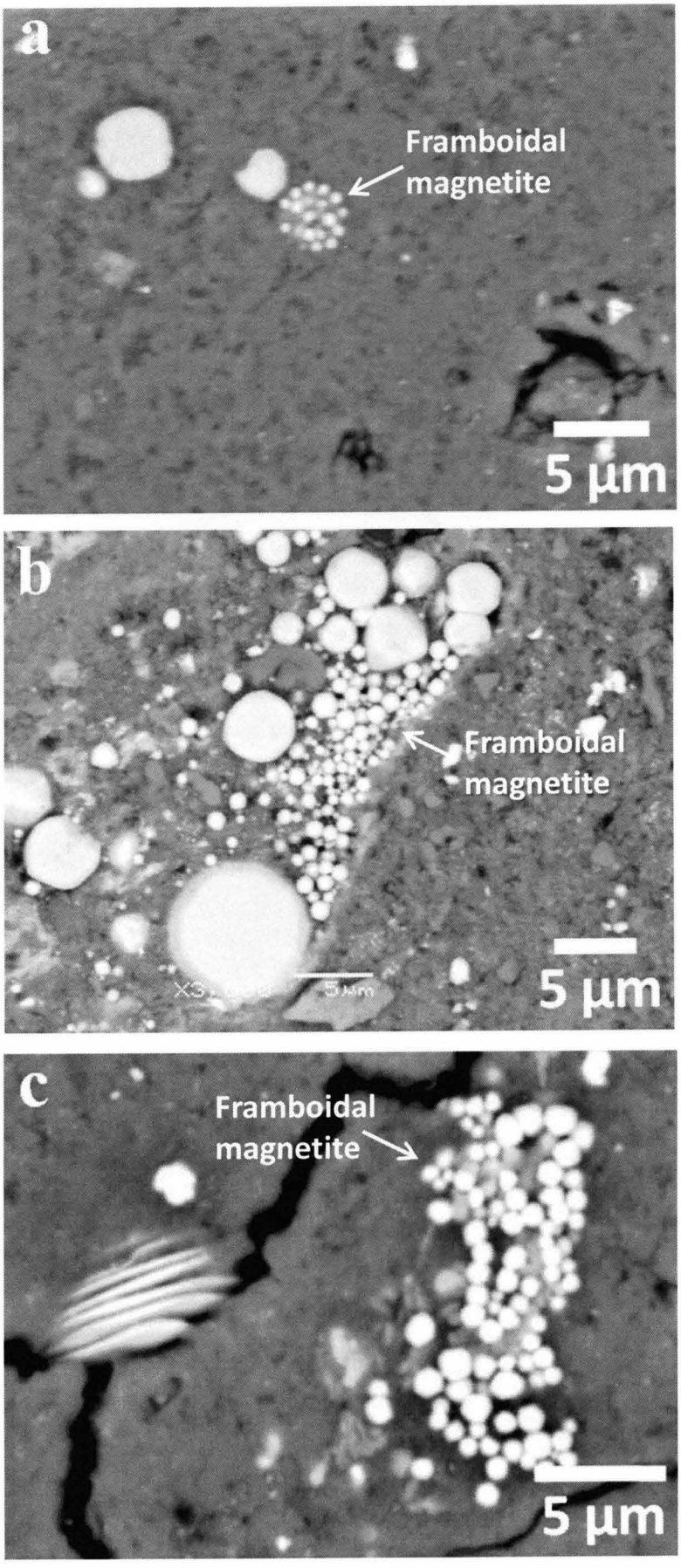

Figure 6-5. BSE image of the matrices in the clasts in QUE97990 (a), Murchison(b) and Cold Bokkeveld (c). The matrices in the clasts mainly consist of phyllosilicate and magnetite. Magnetite commonly shows framboidal texture.

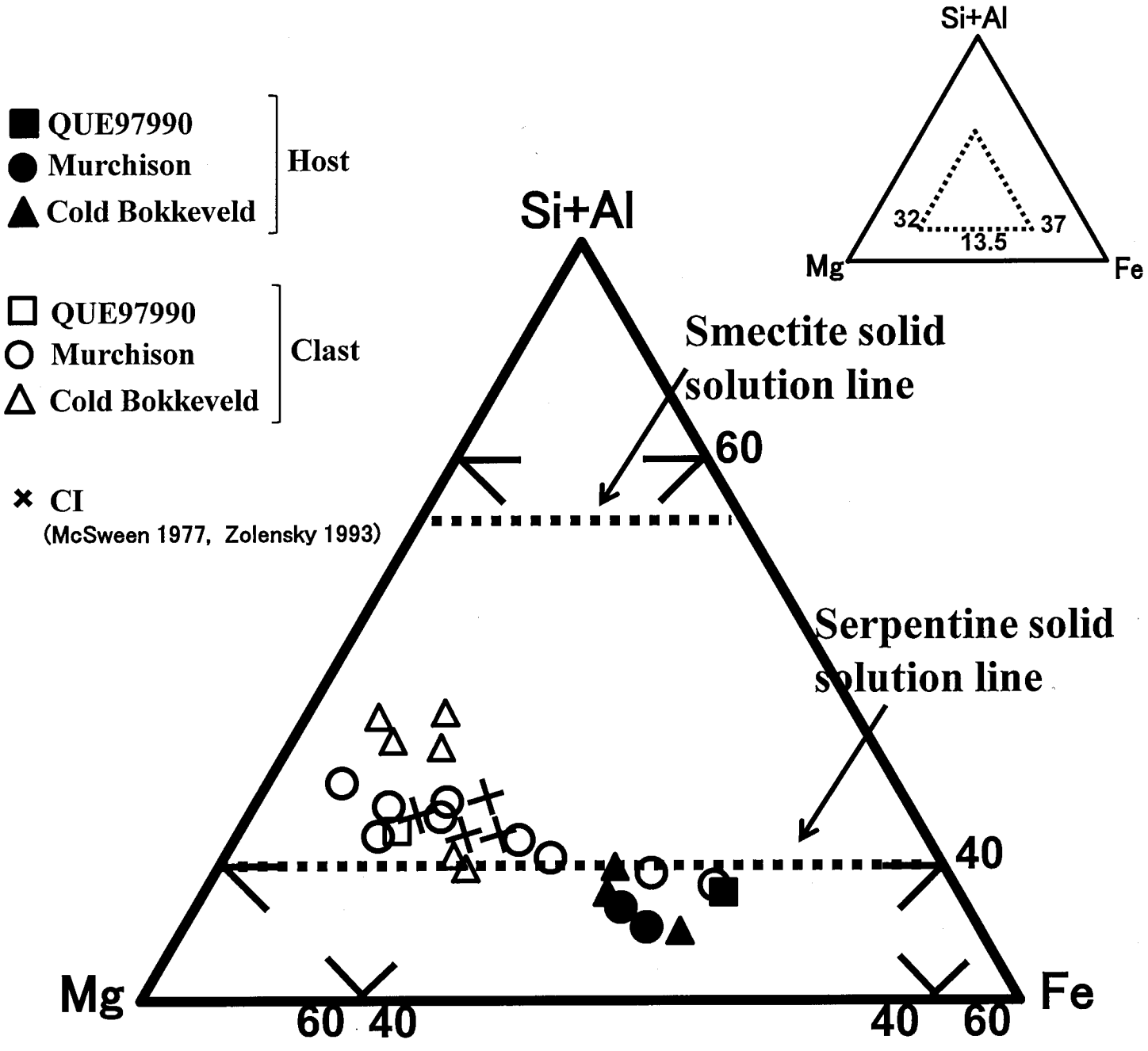

Figure 6-6. Defocused-beam analyses of phyllosilicate-rich matrices in the clasts and host matrices in QUE97990, Murchison and Cold Bokkeveld.

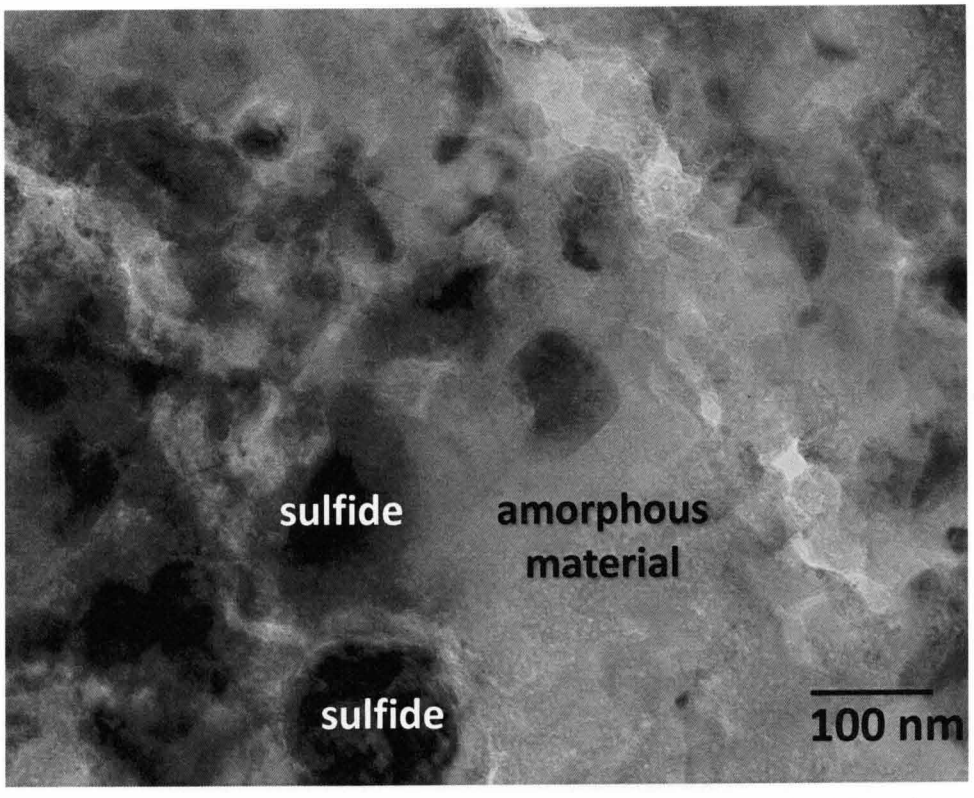

Figure 6-8. TEM image shows that the host matrix in QUE97990 mainly consist of amorphous materials and Fe-sulfide.

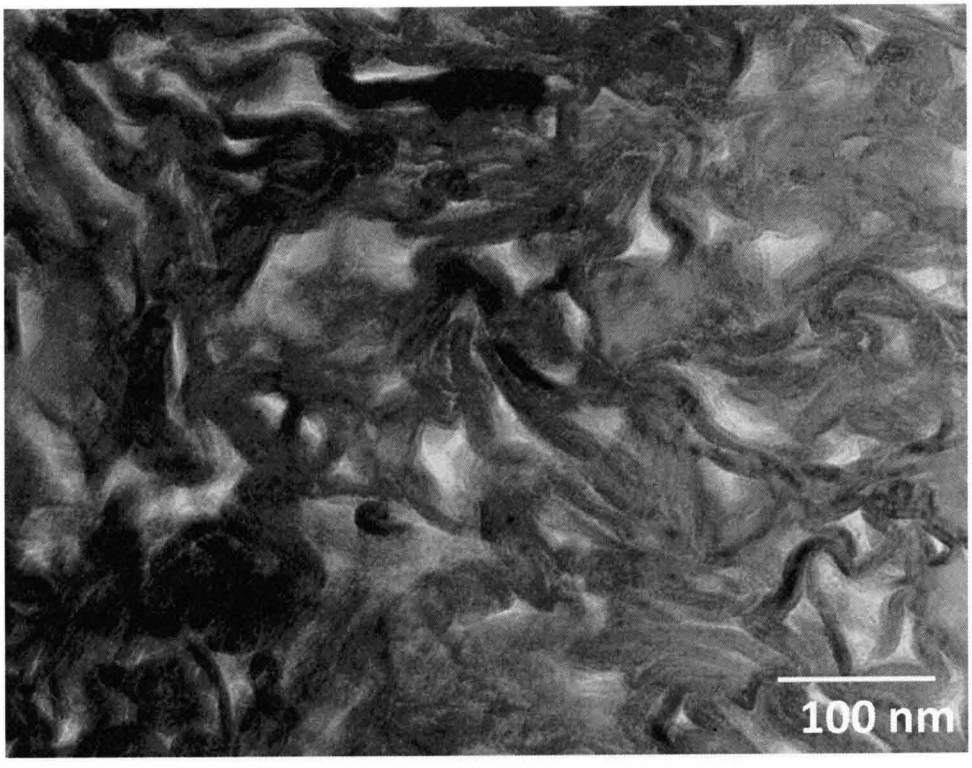

Figure 6-9. TEM image shows the host matrix in Murchison. Mg-Fe serpentine, which shows ribbon-like texture, commonly occur in the host matrix.

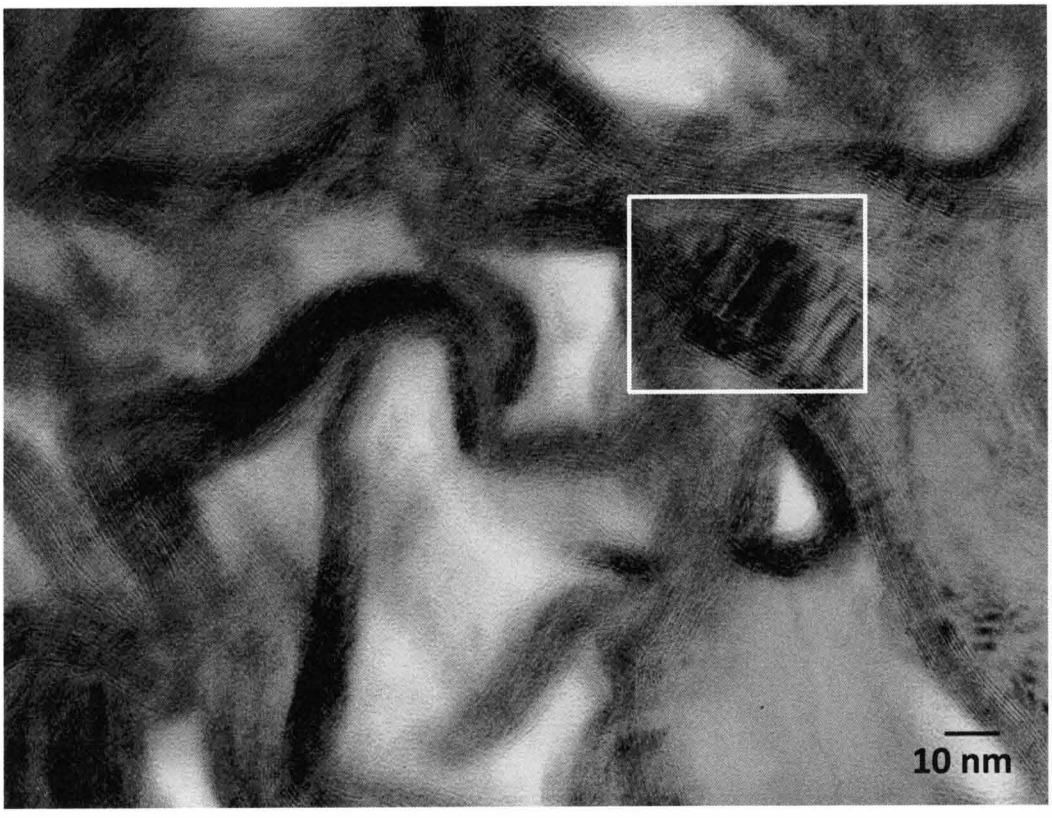

Figure 6-10. TEM image show round shaped serpentine crystal in host matrix of Murchison.

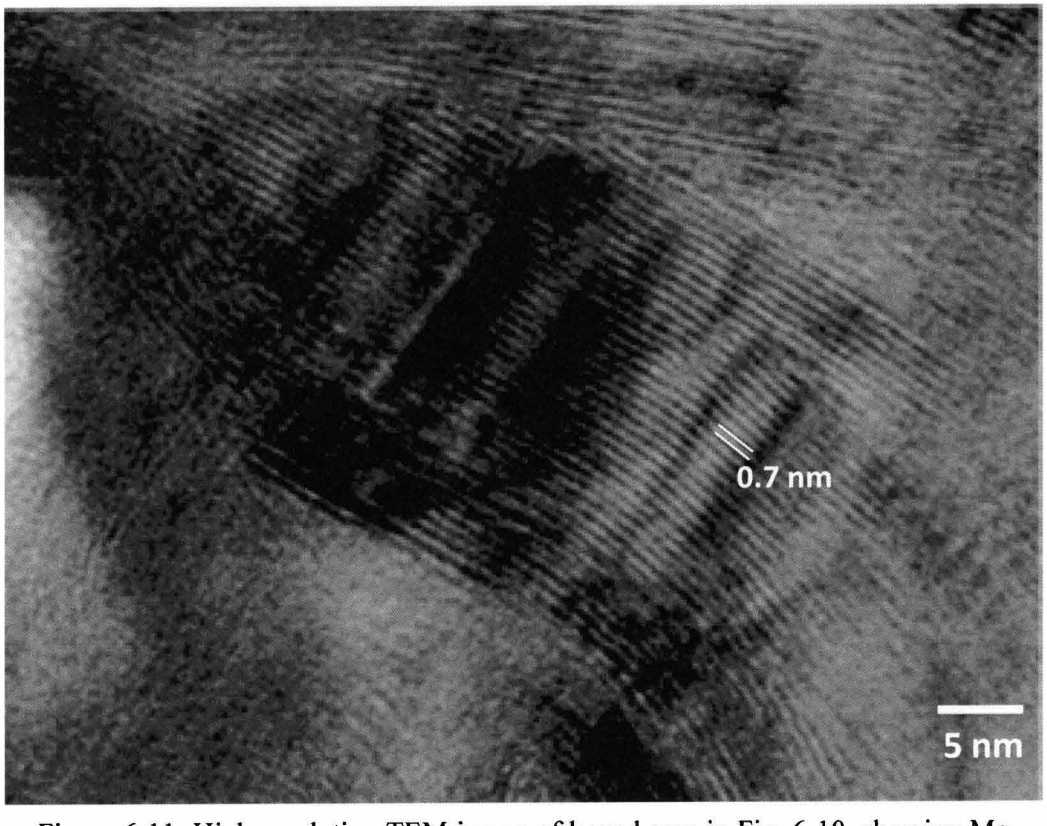

Figure 6-11. High resolution TEM image of boxed area in Fig. 6-10, showing Mg-Fe serpentine crystal. The serpentine show 0.7 nm basal spacing.

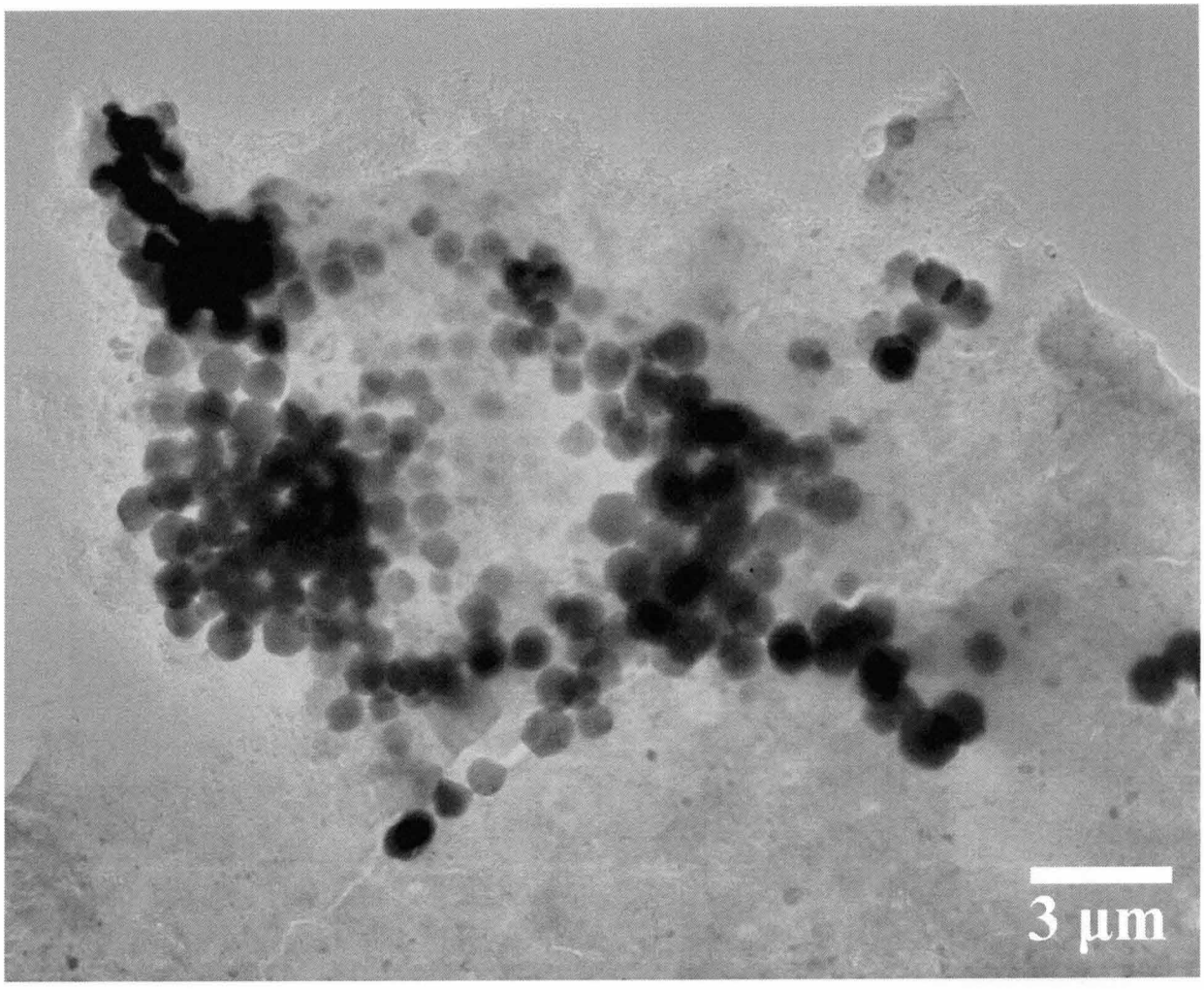

Figure 6-12. TEM image of framboidal magnetite in the clast of Cold Bokkeveld. The framboidal magnetite are developed with a euhedral shape with several hundred nm in diameter and are arranged in disordered directions.

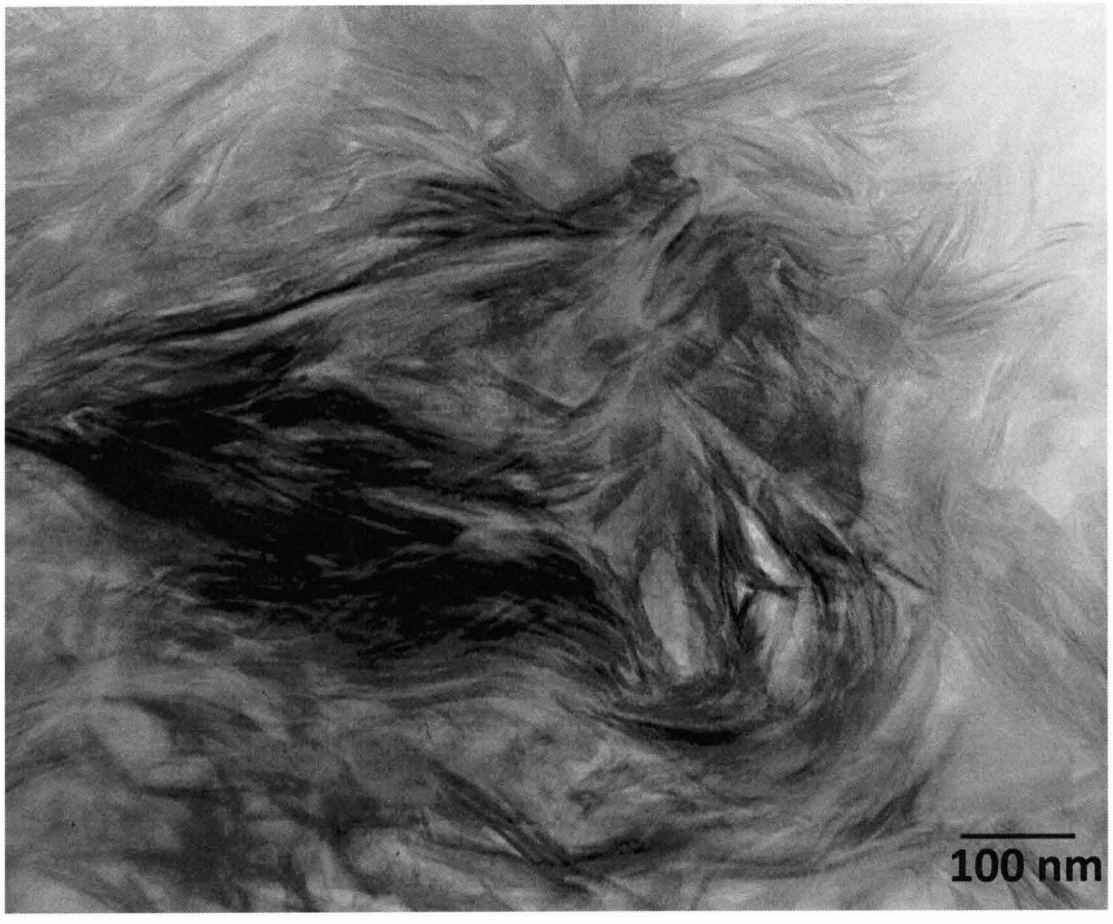

Figure 6-13. TEM image shows that clusters of coarse phyllosilicate in the clast matrix of Cold Bokkeveld.

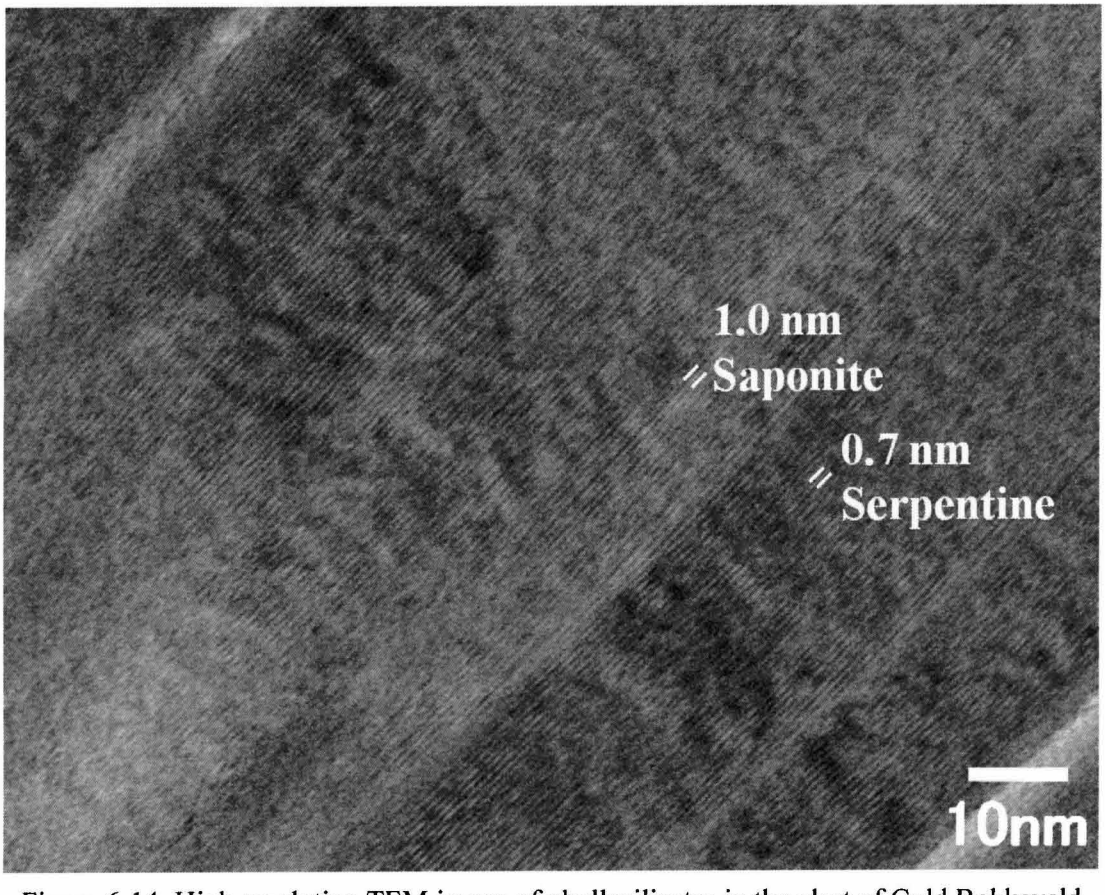

Figure 6-14. High resolution TEM image of phyllosilicates in the clast of Cold Bokkeveld. The phyllosilicates consist of serpentine and saponite.

Chapter 7

Discussion: How conditions did aqueous alteration occur in the magnetite-rich clasts of three CM chondrites?

The thoroughgoing observations revealed that magnetite commonly occurs in the clasts of QUE97990, Murchison and Cold Bokkeveld, while magnetite is almost absent in their host meteorites. PCPs and Fe-sulfide, which are abundant in the host matrices, are rarely found in the clast matrices. The phyllosilicates in the clast matrices of three meteorites are mixture of serpentine and saponite. All clasts in the three meteorites have the common characteristics. These results show that the all observed clasts irrespective of the variation of host meteorites have experienced aqueous alteration on same conditions.

In CI chondrites, magnetite is common and appears with not only a polyhedral morphology, but also framboidal, plaquette, and platelet morphologies. TEM observation directly shows the existence of saponite in the clast matrix. The assemblage of serpentine and saponite commonly occur in CI chondrites. Moreover, the phyllosilicates in the clasts show acicular fibrous clustered texture which do not occur in host matrix. These results show that such characteristics of the clasts are similar to that of CI chondrites rather than that of CM chondrites. Previous studies (e.g. Brearley and Johns, 2005) reported that CI chondrites have experienced aqueous alteration in oxidized conditions. Thus, magnetite-rich clasts also have experienced aqueous alteration in oxidized condition, although alteration in host meteorites have occurred in

reduced condition. These results suggest that CM parent body is extensively heterogeneous conditions (e.g. reduction/oxidation states, temperatures, water/rock ratios). Moreover, precursor materials of the components, which have experienced aqueous alteration on different conditions, were mixed on the parent body by brecciation. Moreover, I will point out the possibility that CM and CI chondrites have single parent body. In general, it is thought that CM and CI chondrites have different parent body. However, my study suggests possibility that differences of characteristics of CM and CI chondrites can be explained by heterogeneous on conditions and brecciation on their parent body. This hypothesis gives us new insight about parent bodies of carbonaceous chondrites.

Conclusion for part Ⅱ

I discovered magnetite-rich clasts in the matrices of QUE97990, Murchison and Cold Bokkeveld. Framboidal magnetite commonly occurs in the clasts. Chemical compositions of the clast matrix are similar to mixing serpentine and saponite. Moreover, saponite is found in the clast in Cold Bokkeveld by TEM observations. These results show that characteristics of the clasts are similarities to CI chondrites rather than CM chondrites. Moreover, oxidized conditions would partly exist on CM parent body. Though, CM parent body are recognized as reduced condition during aqueous alteration, my study give new insights about conditions on CM parent body during aqueous alteration.

Acknowledgment

I would like to acknowledge Professor Kazushige Tomeoka for introducing the planetary material science to me and discussing with me about subject of research. I learned so much about the science about from him and I am fortunate to study as a member of his students. I would like to acknowledgement Professor Masayuki Hyodo for obtaining valuable comments on this thesis. I would like to acknowledgement Assistant Professor Yusuke Seto for obtaining valuable comments and sincere encouragement on writing this thesis writing. I gratefully thank Dr. Naotaka Tomioka and Ichiro Ohnishi for valuable discussion and technical support. I thank all of my colleagues in the Planetary Material Science Laboratory of Kobe University for their useful and enjoyable discussion. Finally, I am grateful to my family for their infinite support. Thank you so much.

Makoto Maeda

Reference

Benedix G. K., Cosarinsky M., and Leshin L. A. (2000) Carbonate petrography along the CM chondrite alteration sequence. *Meteoritics & Planetary Science* 35, 24.

Brearley A. J. (2006) The role of microchemical environments in the alteration of CM carbonaceous chondrites (2006) *Lunar and Planetary Sci.* 37 abstract no. 2074.

Brearley A. J. and Chizmadia L. J. (2005) On the behavior of phosphorus during the aqueous alteration of CM2 carbonaceous chondrites. *Lunar and Planetary Sci.* 36 abstract no. 2176.

Brearley A. J. and Duke C. L. (1998) Aqueous alteration of chondritic meteorites: Insights from experimental low temperature hydrothermal alteration of Allende. *Lunar and Planetary Sci.* 29 abstract no. 1274.

Brearley A. J. and Geiger T. (1991) Mineralogical and chemical studies bearing on the origin of accretionary rims in the Murchison CM2 carbonaceous chondrites. *Meteoritical Sci.* 26, 323.

Brearley A. J. and Geiger T. (1993) Fine-grained chondrule rims in the Murchison CM2 chondrite: Compositional and mineralogical systematics. *Meteoritical Sci.* 28, 328.

Brearley A. J., Hanowski N. P., and Whalen J. F. (1999) Fine-grained rims in CM carbonaceous chondrites: A comparison of rims in Murchison and ALH81002. *Lunar and Planetary Sci.* 30 abstract no. 1460.

Browning L. B. and Bourcier W. L. (1996) Tochilinite: A sensitive indicator of alteration conditions on the CM asteroidal parent body. *Lunar and Planetary Sci.* 27 171.

Browning L. B., McSween H. Y. J., and Zolensky M. E. (1996) Correlated alteration effects in CM carbonaceous chondrites. *Geochem. Cosmochim. Acta* 60, 2621-2633.

Chizmadia L. J. (2005) Fine-grained rims of Y-791198 are texturally, mineralogically and compositionally similar to GEMS-TYPE IDPS. *Lunar and Planetary Sci.* 36 abstract no. 2229.

Chizmadia L. J. and Brearley A. J. (2003) Mineralogy and textural characteristics of fine-grained rims in the Yamato791198 CM2 carbonaceous chondrites: Constraints on the location of aqueous alteration. *Lunar and Planetary Sci.* 34 abstract no. 1419.

Chizmadia L. J. and Brearley A. J. (2004) Formation of Fe-enrichment boundary zones between chondrules and their fine grained rims CM2 chondrite, Y-791198. *67th Annual Meteoritical Society Meeting* abstract no. 5216.

Chizmadia L. J.aand Brearley A. J. (2001) Petrographic studies of fine-grained rims in the Yamato 791198 CM carbonaceous chondrite and comparison to Murchison and ALH81002. *Lunar and Planetary Sci.* 32 abstract no. 1906.

Chizmadia L. J.aand Brearley A. J. (2002) Petrographic study of chondrule mesostasis in the Yamato 791198 CM carbonaceous chondrite and comparison to ALH 81002. *Lunar and Planetary Sci.* 33 abstract no. 2059.

Chizmadia L. J.aand Brearley A. J. (2004) Aqueous alteration of carobonaceous chondrites: New insights from comparative studies of two unbrecciated CM2 chondrites, Y-791198 and ALH81002. *Lunar and Planetary Sci.* 35 abstract no. 1753.

Ciesla F. J., Lauretta D. S., Cohen B. A., and Hood L. H. (2003) A nebular origin for chondritic fine-grained phyllosilicates. *Science* 299, 549-551.

DuFresne E. R. and Anders E. (1962) On the chemical evolution of the carbonaceous chondrites. *Geochem. Cosmochim. Acta* 26, 1085-1114.

Dyl K. A., Manning C. E., and Young E. D. (2006) Modeling aqueous alteration of CM carbonaceous chondrites: Implications for cronstedtite formation by water-rock reaction. *Lunar and Planetary Sci.* 37 abstract no. 2060.

Goreva J. S. and Lauretta D. S. (2006) Early oxidation of phosphorus associated with sulfides in CM chondrites. *Lunar and Planetary Sci.* 37 abstract no. 2422.

Grossman J. N., Alexander, C. M. O' D., Wang J., and Brearley A. J. (2000) Bleached chondrules: Evidence for widespread aqueous processes on the parent asteroids of

ordinary chondrites. *Meteoritics & Planetary Science* 35, 467-486.

Grossman J. N., Alexander, C. M. O' D., Wang J., and Brearley A. J. (2002) Zoned chondrulesin Semarkona: Evidence for high- and low-temperature processing. *Meteoritics & Planetary Science* 37, 49-73.

Greshake A., Krot A. N., Flynn G. J., and Keil K. (2005) Fine-grained dust rims in the Tagish Lake carbonaceous chondrite: Evidence for parent body alteration. *Meteoritics & Planetary Science* 40, 1413-1431.

Hanowski N. P. and Brearley A. J. (1997) Chondrule serpentine as indicators of aqueous alteration in CM carbonaceous chondrites. *Lunar and Planetary Sci.* 28 abstract no. 1371.

Hanowski N. P. and Brearley A. J. (2001) Aqueous alteration of chondrules in the CM carbonaceous chondrite, Allan Hills 81002: Implications for parent body alteration. *Geochem. Cosmochim. Acta* 65, 495-518.

Hua X., Wang J., and Buseck P. R. (2002) Fine-grained rims in the Allan Hills 81002 and Lewis Cliff 90500 CM2 meteorites: Their origin and modification. *Meteoritics & Planetary Science* 37, 229-244.

Jones C. L. and Brearley A. J. (2006) Experomental aqueous alteration of the Allende meteorite under oxidizing conditions: Constraints on asteroidal alteration. *Geochem. Cosmochim. Acta* 70, 1040-1058.

Kerridge J. F., Macdougall J. D., and Marti (1979) Clues to the origin sulfide minerals in CI chondrites. *Earth and Planet. Sci. Lett.*, 43, 359-367

Kozerenko S. V., Organova N. J., Fadeev V. V., Magazina L. O., Kolpakova N. N., and Kopneva L. A. (1996) Tochilinite produced in laboratory. *Lunar and Planetary Sci.* 27 abstract no. 695.

Lauretta D. S., Hua X., and Buseck P. R. (2000) Mineralogy of fine-grained rims in the ALH 81002 CM chondrite. *Geochem. Cosmochim. Acta* 64, 3263-3273.

Lee M. R. (1993) The petrography, mineralogy and origins of calcium sulphate within the Cold Bokkeveld CM carbonaceous chondrite. *Meteoritics* 28, 53-62.

McSween H. Y. J. (1979) Alteration in CM carbonaceous chondrites inferred from mdal and chemical variations in matrix. *Geochem. Cosmochim. Acta* 43, 1761-1770.

McSween H. Y. J. (1987) Matrix compositions in Antarctic and non-Antarctic CM carbonaceous chondrites. *Lunar and Planetary Sci.* 18 abstract no. 631.

McSween H. Y. and Richardson S. N. (1977) The composition of carbonaceous chondrite matrix. *Geochem. Cosmochim. Acta* 51, 2469-2477.

Metzler K. (1995) Aqueous alteration of primary rock on the CM parent body. *Lunar and Planetary Sci.* 26 abstract no. 961.

Metzler K. (2004) Formation of accretionary dust mantles in the solar nebula: Evidence from preirradiated olivines in CM chondrites. *Meteoritics & Planetary Science* 39, 1307-1319.

Metzler K. and Bischoff A. (1987) Accretionary dark rims in CM chondrites. *Meteoritical Sci.* 22, 458.

Metzler K. and Bischoff A. (1989) Accretionary dust mantles in CM chondrites as indicators for process prior to parent body formation. *Lunar and Planetary Sci.* 20 abstract no. 689.

Metzler K. and Bischoff A. (1989) Formation of accretionary dust mantles in the solar nebula as confirmed by noble gas data of CM chondrites. *Meteoritical Sci.* 24, 160.

Metzler K., Bischoff A. and Stoffler D. (1992) Accretionary dust mantles in CM chondrites: Evidence for solar nebula process. *Geochem. Cosmochim. Acta* 56, 2823-2897.

Metzler K., Bischoff A., and Morfill G. (1991) Accretionary dust mantles in CM chondrites: Chemical variations and calculated time scales of formation. *Meteoritical*

Sci. 26, 372.

Metzler K., Bischoff A., and Stoffler D. (1988) Characteristic of accretionary dark rims carbonaceous chondrites. *Lunar and Planetary Sci.* 19 abstract no. 772.

Nazorov M. A., Brandstaetter F., Kurat G., and Ntaflos T. (1998) Chemistry of P-rich suldides in Murchison, Cold Bokkeveld and Nogoya CM chondrites. *Lunar and Planetary Sci.* 29 abstract no. 1628.

Noguchi T. (1995) Petrology and mineralogy of the PCA 91082 chondrite and its comparison with the Yamato-793495 (CR) chondrites. *Proc. NIPR Symp. Antarct. Meteorites*, 8, 32-62, 1995

Sears D. W. G., Benoit P. H., and Jie L. (1993) Two chondrule groups each with distinctive rims in Murchison recognized by cathodoluminescence. *Meteoritical Sci.* 28, 669-675.

Tomeoka K. and Buseck P. R. (1985) Indicator of aqueous alteration in CM carbonaceous chondrites: Microtextures of a layered mineral containing Fe, S, O and Ni. *Geochem. Cosmochim. Acta* 49, 2149-2163.

Tomeoka K. and Buseck P. R. (1988) Matrix mineralogy of the Orgueil CI carbonaceous chondrite.
Geochem. Cosmochim. Acta 52, 1627-1640

Tomeoka K. and Tanimura I. (2000) Phyllosilicate-rich chondrule rims in the Vigarano CV3 chondrite: Evidence for parent-body process. *Geochem. Cosmochim. Acta* 64, 1971-1988.

Trigo-Rodriguez J. M., Rubin A. E., and Wasson J. T. (2006) Non-nebula origin of dark mantles around chondrules and inclusions in CM chondrites. *Geochem. Cosmochim. Acta* 70, 1271-1290.

Velbel M. A. (2001) Compositions of partly altered silicates and replacement serpentine in Nogoya and ALLAN HILLS 81002 (CM2): Implications for scales of elemental redistribution during aqueous alteration. *64th Annual Meteoritical Society Meeting*

abstract no. 3701.

Velbel M. A., Tonui E. K., and Zolensky M. E. (2001) Compositions of partly altered silicates and replacement serpentine in Nogoya and ALLAN HILLS 81002 (CM2): Implications for scales of elemental redistribution during aqueous alteration. *Lunar and Planetary Sci.* 33 abstract no. 1336.

Velbel M. A., Tonui E. K., and Zolensky M. E. (2003) Compositions of partly altered olivine and replacement serpentine in the CM2 chondrites QUE93005 and Nogoya: Implications for scales of elemental redistribution during aqueous alteration. *Lunar and Planetary Sci.* 34 abstract no. 1611.

Weisburg M. K. and Prinz M., Clayton R. N., and Mayeda T. K. (1993) The CR (Renazzo-type) carbonaceous chondrites group and its implications. *Geochem. Cosmochim. Acta* 57, 1567-1586.

Weisburg M. K. and Prinz M., Clayton R. N., and Mayeda T. K., Grady M. M. and Pillinger C. T. (1995) The CR chondrites clan. *Proc. NIPR Symp. Antarct. Meteorites*, 8, 11-32, 1995

(1993) The CR (Renazzo-type) carbonaceous chondrites group and its implications. *Geochem. Cosmochim. Acta* 57, 1567-1586.

Zega T. J. and Buseck P. R. (2003) Fine-grained-rim mineralogy of the Cold Bokkeveld CM chondrite. *Geochem. Cosmochim. Acta* 67, 1711-1721.

Zolensky M. E. and Gooding J. L. (1987) Mineralogical within the matrices of CM carbonaceous chondrites. *Meteoritical Sci.* 22, 544.

Zolensky M., Barret R., and Browning L. (1993) Mineralogy and composition of matrix and chondrule rims in carbonaceous chondrites. *Geochem. Cosmochim. Acta* 57, 3123-3148.